A THESIS

Microwave Spectroscopy : Five Molecular Studies.

Submitted to the University of Glasgow
in part fulfillment of the requirements
for the degree of Doctor of Philosophy
in the Faculty of Science

by

S. A. MACKAY, B.Sc.,

Chemistry Department

October 1971.

ProQuest LLC.
789 East Eisenhower Parkway
P.O. Box 1346
Ann Arbor, MI 48106 – 1346

ACKNOWLEDGEMENT

It is with pleasure that I thank my supervisor, Dr. J. K. Tyler, for his unfailing interest and guidance throughout the course of the work described in this thesis and for his critical reading of the text.

I would like to thank Dr. J. N. Macdonald for his help and for use of his computer programs. I am also indebted to Professor D. W. A. Sharp and Mr. J. C. Fuggle for their help with the preparation of NF_2CN.

I am sincerely grateful to the Science Research Council for a maintenance grant.

SUMMARY

The first chapter of this thesis briefly describes the Stark modulation spectrometer which was used in the studies of microwave spectra described in the following chapters.

The second chapter continues the study of the molecular geometries of the 4-pyrone series of compounds by investigating that of pyran-4-thione. It is shown that pyran-4-thione, like pyran-4-one, is planar in the ground-state. From a comparison of the structures of these two compounds it is believed that the resonance benzoid forms have a greater contribution to the overall structure in the case of pyran-4-thione.

The third chapter is concerned with the spectra of cyclohex-2-en-1-one, for which two of the principal components of the dipole moment have been obtained and the fundamental frequency of the lowest ring bending deformation has been determined as 95 ± 6 cm^{-1}. The observed moments of inertia are in fair agreement with the calculated moments for a structural model for cyclohexenone in which five of the six carbon atoms are coplanar.

The following two chapters deal with two compounds of the cyanamide series, difluorocyanamide and dimethylcyanamide. Although the structure is not accurately determined, limits are placed on the structure of NF_2CN and a study has been made of the ^{14}N-quadrupole coupling in the spectra of the molecule. An account is given of the

interesting spectra of dimethylcyanamide and the satellite spectrum of each transition is discussed in terms of skeletal deformation and torsional vibrations of this two methyl-top molecule. Because of near-degeneracy of the energy levels of dimethylcyanamide, second-order perturbation theory was found insufficient for the calculation of the dipole moment.

In the next section halogen substituent effects on the geometry of the NH_2-group in aniline were viewed by means of the structural determination of the NH_2-group of p-chloroaniline.

The final chapter is devoted to a brief account of chemical syntheses undertaken in the course of this work.

CONTENTS

CHAPTER 1.

THE STARK MODULATION SPECTROMETER

A simplified block diagram of the Stark modulation spectrometer is shown in Fig. 1.

The 'reflex' klystrons used produced nearly monochromatic radiation for a range of frequencies through 10 - 40 GHz. The frequency of the klystron may be varied by distorting the klystron cavity either manually or with a mechanical drive. Small variations in frequency (25 MHz) are produced by varying the potential of the reflector by means of a saw-tooth voltage. The same voltage is applied to the X-plates of the oscilloscope enabling the oscilloscope trace to represent a linear section of the frequency scale along its X-coordinate. The absorption cell is a ten foot long X-band copper waveguide with a brass Stark electrode fitted centrally. The gaseous sample in the cell can be studied at temperatures between -80°C and 60°C. Even with the greatest care, variation can occur in the distance between the Stark electrode and the wide face of the waveguide. This produces different values of field strength along the waveguide and, at high voltage, has the effect of smearing the Stark lobes. The Stark lobes are also smeared at high voltages as a result of a not quite perfect square-wave line shape and this has the effect, when

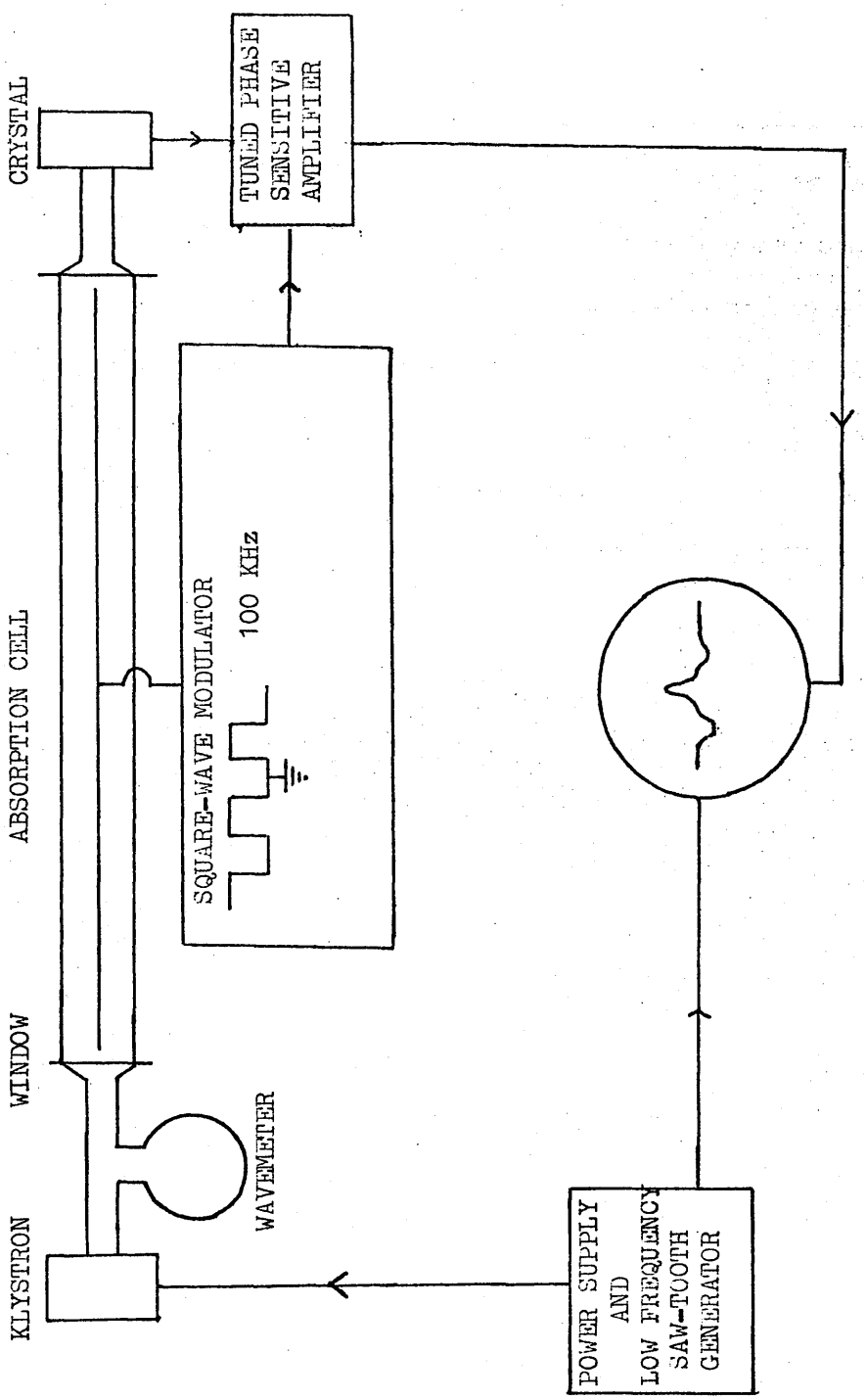

Fig.1. Block diagram of a Stark modulation spectrometer.

measuring a dipole moment without a d.c. bias, of reducing the accuracy when voltages greater than 800 are used. A zero-based square-wave with a modulation frequency of 100 KHz is used to provide the Stark field. The choice of the modulation frequency is determined by the necessity of keeping both crystal noise and broadening of the absorption lines low. Noise power, in excess of thermal noise, is approximately proportional to the square of the crystal current divided by the modulation frequency. If the modulation frequency is too large then the variation of the molecular energy levels with field strength can no longer strictly follow the changes in electric field. At the frequencies usually employed the effect is to increase the line width.

The crystal detector consists of a fine wire in contact with a block of semi-conducting material (silicon or germanium). This system behaves as a rectifier since it presents different impedances in opposite directions. The crystal noise is most important to crystal performance and is given by

$$S' = \frac{CI^2 \Delta\nu}{\nu} \qquad \ldots (1)$$

where C is a constant,

I is the rectified crystal current,

$\Delta\nu$ is the bandwidth,

and ν is the value of the modulation frequency.

The current-voltage characteristic can be generally represented by

$$I = KV^2 \qquad \ldots \quad (2)$$

where K is a constant,

V is the voltage developed across the crystal

and I is the crystal current.

It follows that the output power and the crystal noise are proportional to the square of the crystal current. Therefore, the precise value of the crystal current will not affect the signal-to-noise ratio to a great extent.

The output from the crystal detector is passed to a tuned preamplifier and a tuned amplifier. The noise level is reduced by slow sweep frequencies and narrow bandwidth. Phase-sensitive detection is used for portrayal of the absorption line as shown in Fig. 1 and for production of narrow bandwidths for the amplifier. If a phase-sensitive detector is not used, the signal is fed through the amplifier, rectified and then filtered. The effective bandwidth may then be greater than that associated with the filter.

The approximate frequency of an absorption line can be determined very rapidly by means of resonant-cavity wavemeters. Although wavemeters often produce systematic errors throughout their range of operation, when the systematic error is known line frequencies can be obtained with an error of ± 2 MHz.

For accurate measurement of frequencies, the line frequency is compared with frequencies derived from a quartz crystal-controlled oscillator of 5 MHz. A Micro-Now frequency multiplier chain provides harmonics of 50, 150 and 450 MHz and these are fed onto the wavemeter crystal detector, which provides harmonics spaced by 50 MHz. The harmonics are then mixed with some of the microwave power from the klystron via a directional coupler to produce beat frequencies, which are then fed through a radio receiver. When the beat frequency equals the receiver setting a sharp marker appears on the oscilloscope trace. Two markers separated by twice the receiver-setting are produced from each harmonic and the variable frequency oscillator of the Micro-Now is tuned until one of the markers is set on the line. In order to eliminate the receiver setting both markers are set on the line and to eliminate instrumental time delays the measurements are repeated for forward and backward sweeps of the klystron. The value of the harmonic in use is determined from wavemeter measurements.

The crystal oscillator frequency is measured to ± 0.1 Hz using a Marconi frequency counter calibrated against the 200 KHz transmission of the B.B.C. Droitwich transmitter. Frequency measurements can be made to an accuracy of ± 0.05 — ± 0.1 MHz depending on the quality of the line. The minimum observable line intensity is 5×10^{-9} cm^{-1}.

References.

1. W. Gordy, W. V. Smith and R. F. Trambarulo, "Microwave Spectroscopy", John Wiley & Sons, Inc. (1953).

2. C. H. Townes and A. L. Shawlow, "Microwave Spectroscopy", McGraw-Hill Book Co., Inc. (1955).

3. T. M. Sugden and C. N. Kenney, "Microwave Spectroscopy", D. Van. Nostrand Co. Ltd. (1965).

CHAPTER 2.

THE STRUCTURE AND DIPOLE MOMENT OF PYRAN-4-THIONE

2-1. Introduction.

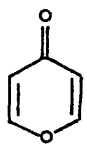

I

pyran-4-one
γ-pyrone

II

thiapyran-4-one
thiapyrone

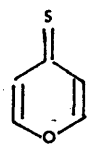

III

pyran-4-thione
thiopyrone

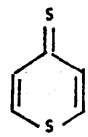

IV

thiapyran-4-thione
thiathiopyrone

The properties of the molecules I → IV are often described in terms of the following canonical forms -

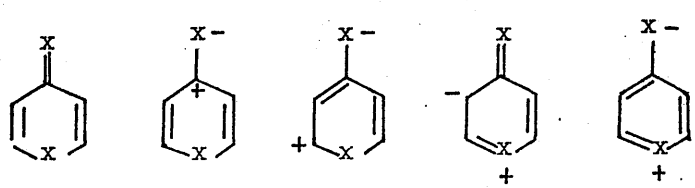

a b c d e

These structures suggest 'aromatic' character and the extent to which the molecules are stabilized has been calculated for 2,6-diphenyl-1,4-thiapyrone as 32.7 Kcal/mole (1). (a) is believed to be the most significant form. An estimate of this can be obtained from dipole

moment calculations. In the case of 2,6-dimethylpyrone the calculated dipole moment for (a) is 1.75 D and for (e) 22 D (1). The observed value of 4D favours (a) rather than (e). In pyran-4-one the absence of addition reactions (1) indicate resonance stabilization of the C = O bond, but in pyran-4-thione the C = S behaves more as a normal thio group (2,3).

The series of compounds I — IV behave in the same way as appropriate acyclic models in their infra-red carbonyl absorption and ultra-violet spectra. At one point only do they differ markedly from those of acyclic models - in the characteristics of the salts which they form with acids. These salts are comparatively stable and are considered to be aromatic. The increased importance of the phenol-like structure for the salts of these molecules follows from a comparison of the Raman spectra of dimethylpyrone and its hydrochloride (4), in which the latter displays the expected shift of the carbonyl band and a lowering of the C = C frequency.

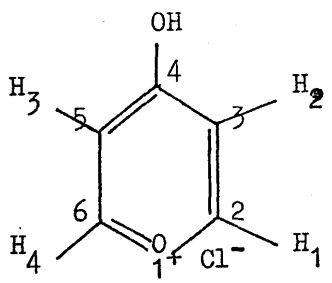

Fig.1. Pyran-4-one hydrochloride, showing the numbering of the ring.

However, the canonical forms are useful in describing the directional attack in the substitution reactions of the four compounds.

Electrophilic substitution takes place at positions 3 and 5 and nucleophilic substitution at positions 2 and 6. The preparation of the isotopic species of pyran-4-one shown below, highlights the interesting chemistry of these molecules (5). Hydrolysis is carried out in slightly acid solution as pyran-4-one is destroyed in basic media.

Nucleophilic 1:4 addition of water to pyran-4-one gives

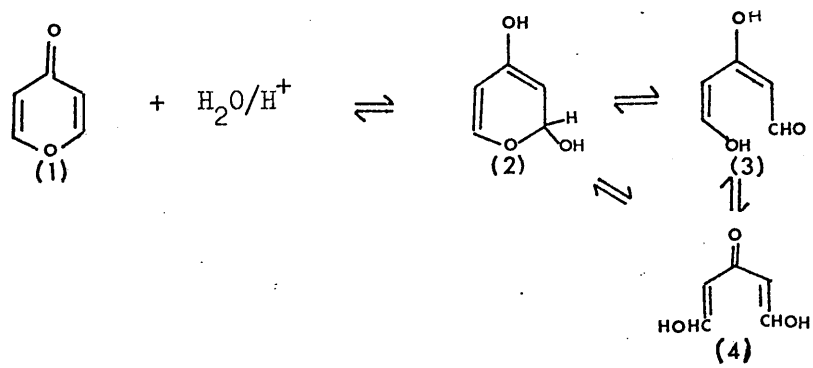

3:5 deuteration could occur by the usual keto-enol equilibria of any of the intermediates (2), (3) or (4). ^{18}O incorporation into the heterocyclic ring implies the intermediacy of (3) or (4). Although the hydrogen atoms in the 2,6 positions are not directly exchangeable they can readily be replaced by deuterium atoms by the following method.

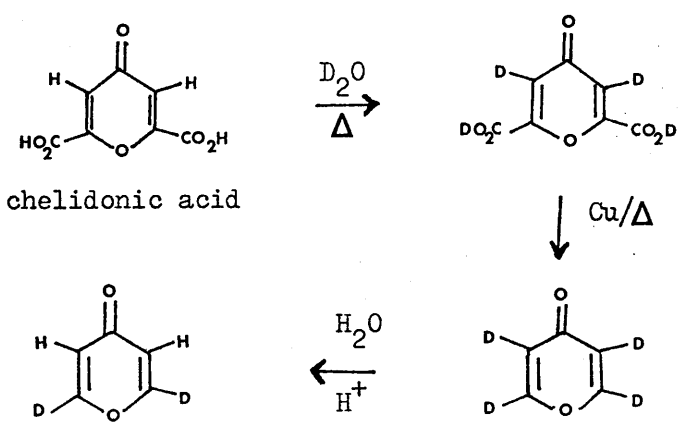

Having prepared these isotopic forms of pyran-4-one they can be converted into the corresponding pyran-4-thione compound by the action of phosphorus pentasulphide in toluene.

The microwave spectra of pyran-4-one and thiapyran-4-one have been studied in relation to the geometry and planarity of their rings (6). This chapter extends the series to include pyran-4-thione and it is concluded that all three compounds are planar.

2-2. Analysis of the Spectra.

Pyran-4-thione is an orange solid (m.p. 48°C) with sufficient vapour pressure to be easily sublimed in vacuum at room temperature or slightly above. When observing spectra, both sample and absorption cell were maintained at room temperature and initially vapour from the sample was continuously streamed through the cell. When optimum conditions for spectral observations were reached, the absorption cell was isolated and a static pressure of sample used.

For the purpose of predicting line frequencies two structural models were considered. The first was based on the structure of 2,6-dimethylpyran-4-thione as determined by X-ray crystallographic methods (7,8), and the second assumed the ring to be the same as that obtained for pyran-4-one from the microwave study (6).

A C - S bond length of 1.66 Å was taken in both cases. The models were planar and therefore μ_a is the only non-zero component of the dipole moment.

Both models predicted that the J = 7 — 8 μ_a R-branch group of transitions should occur in K-band. The second model was of sufficient quality to make the assignment very simple, and lines with the correct characteristics were found approximately 300 MHz higher than the predicted positions. The measured frequencies of the J = 7 → 8 transitions were then used in a least-squares procedure in order to obtain better values of $\frac{A+C}{2}$, $\frac{A-C}{2}$ and κ; thus enabling the prediction and subsequent measurement of other lines. The final values of the constants were obtained using thirty-five measured transition frequencies in a least-squares rigid-rotor procedure.

The isotopic samples prepared and studied were 3,5 d_2- ,2,6 d_2- and ^{18}O- pyran-4-thione. ^{34}S-pyran-4-thione was studied in natural abundance (4%). Using the observed moments of inertia for pyran-4-thione and the model's coordinates for the isotopically substituted atom in the form of Kraitchman's equations (9), the changes in the values of the moments of inertia, ΔI_a, ΔI_b and ΔI_c were found. These were then used with the observed moments of inertia to calculate the transition frequencies. For each isotopic sample the predicted and observed transition frequencies differed by no more than 10 MHz. Refined values of the rotational constants were obtained from a least-squares calculation as above. The results

of these measurements are listed in Table 1.

Each of the observed ground-state transitions was found to be accompanied by a vibrational satellite transition to high frequency. The measured frequencies of the satellite transitions are also given in Table 1. On closer inspection each of these satellite lines were observed to be one of a family of approximately equally spaced vibrational satellite transitions. Only the ground-state spectrum was observed for the ^{34}S-pyran-4-thione sample. Both ground-state lines and vibrational satellite lines ($v = 1,2,3$) showed alterations in intensity characteristic of nuclear spin statistical weight effects.

Since planar pyran-4-thione has C_{2V} symmetry and two pairs of hydrogen atoms that are interchanged by rotation of 180° around the symmetry axis, the ratio of the number of symmetric spin functions to antisymmetric spin functions is 10:6. This is obtained from

$$n_s = \tfrac{1}{2}\left[\prod_{i=1}^{n}(2I_i + 1)\right]\left[\prod_{i=1}^{n}(2I_i + 1) + 1\right]$$

and

$$n_a = \tfrac{1}{2}\left[\prod_{i=1}^{n}(2I_i + 1)\right]\left[\prod_{i=1}^{n}(2I_i + 1) - 1\right]$$

where I is the nuclear spin and the product is over the number of pairs of identical nuclei. The electronic and vibrational ground-states are symmetric and Bose-Einstein statistics are obeyed, hence the symmetric rotational states (those with K_{-1} even) are more

Table. 1.

Transition frequencies and rotational constants for the isotopic samples of pyran-4-thione.

(a) pyran-4-thione.

	v = 0		v = 1	
	observed	$\nu_{obs} - \nu_{calc}$	observed	$\nu_{obs} - \nu_{calc}$ (MHz)
$7_{07} - 6_{06}$	19142.10	+0.05	19170.13	+0.05
$7_{17} - 6_{16}$	18661.38	+0.11	18692.73	+0.06
$7_{16} - 6_{15}$	20970.50	+0.26		
$7_{26} - 6_{25}$	19923.05	+0.02		
$7_{25} - 6_{24}$	20852.66	+0.10		
$7_{35} - 6_{34}$	20195.63	+0.16	20227.88	+0.04
$7_{34} - 6_{33}$	20280.94	+0.02	20314.33	+0.02
$8_{08} - 7_{07}$	21659.72	-0.01		
$8_{18} - 7_{17}$	21262.39	+0.13		
$8_{17} - 7_{16}$	23831.58	+0.15	23864.01	+0.04
$8_{27} - 7_{26}$	22705.71	+0.04		
$8_{26} - 7_{25}$	23981.04	+0.07	24020.40	+0.03
$8_{36} - 7_{35}$	23096.47	-0.09	23133.52	+0.04
$8_{35} - 7_{34}$	23263.78	-0.01	23302.63	-0.01
$8_{45} - 7_{44}$	23076.25	+0.10		
$8_{44} - 7_{43}$	23082.61	-0.27		
$8_{54} - 7_{53}$ / $8_{53} - 7_{52}$	23037.36	-0.05		
$8_{63} - 7_{62}$ / $8_{62} - 7_{61}$	23015.37	-0.13		
$8_{72} - 7_{71}$ / $8_{71} - 7_{70}$	23002.43	-0.16		
$9_{09} - 8_{08}$	24156.24	-0.04		
$9_{19} - 8_{18}$	23846.96	+0.06	23886.84	-0.01
$9_{28} - 8_{27}$	25464.31	-0.02	25503.36	-0.05
$9_{27} - 8_{26}$	27101.51	-0.01	27144.88	+0.01
$9_{37} - 8_{36}$	25994.44	-0.03		
$9_{36} - 8_{35}$	26291.20	+0.03	26335.88	+0.07

(a) pyran-4-thione. (contd.)

	v = 0		v = 1
	observed	Vobs- Vcalc	
$9_{46} - 8_{45}$	25990.45	+0.12	
$9_{55} - 8_{54}$, $9_{54} - 8_{53}$	25937.90	-0.07	
$9_{64} - 8_{63}$, $9_{63} - 8_{62}$	25906.59	-0.12	
$9_{73} - 8_{72}$, $9_{72} - 8_{71}$	25888.12	-0.18	
$9_{82} - 8_{81}$, $9_{81} - 8_{80}$	25876.24	-0.27	
$10_{110} - 9_{19}$	26417.39	+0.05	
$10_{19} - 9_{18}$	29351.73	-0.03	
$10_{29} - 9_{28}$	28197.32	-0.05	
$10_{28} - 9_{27}$	30193.48	-0.03	
$10_{37} - 9_{36}$	29370.00	+0.22	
$\frac{A+C}{2}$	3593.33		3580.61
$\frac{A-C}{2}$	2330.50		2315.43
K	-0.8532228		-0.852332
A	5923.83		5896.05
B	1604.89		1607.10
C	1262.83		1265.18
Ia	85.3386		85.7407
Ib	314.9938		314.5618
Ic	400.3168		399.5722
Δ	-0.0157		-0.7303

Δ = Ic - Ia - Ib.

Ia, Ib, Ic and Δ are in units of a.m.u.Å^2.

(b) ^{18}O pyran-4-thione.

	v = 0		v = 1	
	observed	$\nu_{obs} - \nu_{calc}$	observed	$\nu_{obs} - \nu_{calc}$ (MHz)
$7_{07} - 6_{06}$	18682.77	+0.10	18710.25	-0.02
$7_{16} - 6_{15}$	20392.81	+0.18	20421.52	+0.02
$7_{25} - 6_{24}$	20229.97	+0.08	20263.80	+0.09
$7_{35} - 6_{34}$	19634.59	+0.27	19665.91	+0.06
$7_{34} - 6_{33}$	19705.72	-0.10	19737.99	-0.19
$8_{08} - 7_{07}$	21147.66	-0.03	21179.16	+0.01
$8_{18} - 7_{17}$	20738.03	+0.03	20772.93	+0.04
$8_{17} - 7_{16}$	23188.17	+0.12	23220.27	+0.06
$8_{27} - 7_{26}$	22103.58	+0.03	22137.94	+0.01
$8_{36} - 7_{35}$	22455.07	+0.11	22491.10	+0.16
$8_{35} - 7_{34}$	22595.23	-0.03	22632.83	+0.00
$9_{09} - 8_{08}$	23589.05	-0.06		
$9_{18} - 8_{17}$	25927.07	-0.00	25962.12	-0.00
$9_{28} - 8_{27}$	24795.56	+0.10	24833.83	+0.06
$9_{27} - 8_{26}$	26296.53	-0.02	26339.04	+0.09
$9_{37} - 8_{36}$	25273.74	+0.11		
$9_{36} - 8_{35}$	25523.48	-0.12		
$9_{45} - 8_{44}$	25276.50	-0.20		
$10_{010} - 9_{09}$	26021.74	-0.03	26061.91	-0.05
$10_{110} - 9_{19}$	25774.57	-0.01	25817.85	-0.01
$10_{19} - 9_{18}$	28600.40	-0.22	28638.14	-0.05
$10_{28} - 9_{27}$	29307.45	-0.07	29353.28	-0.14
$10_{37} - 9_{36}$	28497.57	-0.04	28546.37	-0.07
$\frac{A+C}{2}$	3578.07		3565.52	
$\frac{A-C}{2}$	2345.37		2330.53	
K	-0.861939		-0.861121	
A	5923.44		5896.04	
B	1556.50		1558.65	

(b) ^{18}O pyran-4-thione. (contd.)

	v = 0	v = 1
C	1232.70	1234.99
Ia	85.3441	85.7407
Ib	324.7869	324.3389
Ic	410.1020	409.3403
Δ	-0.0290	-0.7393

$\Delta = Ic - Ia - Ib.$

Ia, Ib, Ic and Δ are in units of a.m.u.$\AA^2$.

(c) ^{34}S pyran-4-thione.

$v = 0$

	observed	νobs- νcalc. (MHz)
$8_{08} - 7_{07}$	21131.36	-0.16
$8_{18} - 7_{17}$	20721.44	-0.10
$8_{27} - 7_{26}$	22084.91	+0.15
$9_{09} - 8_{08}$	23571.20	-0.01
$9_{28} - 8_{27}$	24774.55	-0.02
$9_{27} - 8_{26}$	26271.49	-0.20
$10_{110} - 9_{19}$	25754.43	+0.06
$10_{19} - 9_{18}$	28576.91	-0.08
$10_{29} - 9_{28}$	27441.64	+0.32
$11_{011} - 10_{010}$	28433.37	-0.02
$11_{111} - 10_{110}$	28252.46	-0.05
$11_{210} - 10_{29}$	30084.02	+0.04
$11_{29} - 10_{28}$	32252.30	+0.03

$\frac{A+C}{2}$	3577.38
$\frac{A-C}{2}$	2345.63
κ	-0.86219
A	5923.01
B	1555.01
C	1231.75
Ia	85.3504
Ib	325.0987
Ic	410.4175
Δ	-0.0316

Δ = Ic - Ia - Ib.

Ia, Ib, Ic and Δ are in units of a.m.u.$\AA^2$.

(d) 2,6 d_2- pyran-4-thione.

	v = 0		v = 1	
	observed	$\nu_{obs} - \nu_{calc}$	observed	$\nu_{obs} - \nu_{calc}$ (MHz)
$8_{08} - 7_{07}$	20737.47	+0.01		
$8_{18} - 7_{17}$	20403.13	+0.12	20436.38	+0.08
$8_{17} - 7_{16}$	22975.86	+0.11	23006.52	+0.23
$8_{27} - 7_{26}$	21875.54	+0.01	21908.56	-0.11
$8_{26} - 7_{25}$	23276.96	+0.25	23314.37	-0.11
$8_{36} - 7_{35}$	22317.57	+0.08	22352.70	-0.06
$8_{35} - 7_{34}$	22535.20	+0.01	22572.99	+0.03
$8_{44} - 7_{43}$	22313.59	-0.37	22349.56	-0.27
$8_{54} - 7_{53}$ / $8_{53} - 7_{52}$	22259.94	+0.07		
$8_{63} - 7_{62}$ / $8_{62} - 7_{61}$	22234.04	-0.37		
$9_{09} - 8_{08}$	23122.76	+0.05	23156.89	-0.04
$9_{19} - 8_{18}$	22874.58	+0.08	22911.90	+0.14
$9_{18} - 8_{17}$	25631.13	+0.01	25664.02	+0.11
$9_{28} - 8_{27}$	24519.03	+0.30	24555.57	+0.05
$9_{27} - 8_{26}$	26289.65	+0.23	26330.63	-0.05
$9_{36} - 8_{35}$	25496.10	+0.19	25540.04	+0.53
$9_{46} - 8_{45}$	25125.29	+0.15	25165.57	+0.14
$9_{55} - 8_{54}$ / $9_{54} - 8_{53}$	25066.95	+0.30		
$9_{64} - 8_{63}$ / $9_{63} - 8_{62}$	25030.15	-0.14		
$9_{73} - 8_{72}$ / $9_{72} - 8_{71}$	25008.43	-0.47		
$9_{82} - 8_{81}$ / $9_{81} - 8_{80}$	24994.55	-0.65		
$10_{010} - 9_{09}$	25507.66	-0.09	25546.34	-0.11
$10_{110} - 9_{19}$	25332.17	+0.08	25373.39	+0.04
$10_{19} - 9_{18}$	28202.96	-0.07	28237.70	-0.04
$10_{29} - 9_{28}$	27133.51	+0.21	27173.69	+0.07
$10_{38} - 9_{37}$	27898.38	-0.09	27941.67	-0.18
$10_{37} - 9_{36}$	28514.01	+0.07		
$10_{47} - 9_{46}$	27954.59	+0.02		
$10_{46} - 9_{45}$	28005.46	-0.09		

(d) 2,6 d_2- pyran-4-thione. (contd.)

	v = 0	v = 1
$\frac{A+C}{2}$	3307.44	3296.93
$\frac{A-C}{2}$	2097.56	2084.86
κ	-0.83370	-0.8327
A	5405.00	5381.80
B	1558.71	1560.87
C	1209.88	1212.07
Ia	93.5303	93.9335
Ib	324.3262	323.8775
Ic	417.8349	417.0806
Δ	-0.0216	-0.7304

$\Delta = Ic - Ia - Ib.$

Ia, Ib, Ic and Δ are in units of a.m.u.$\AA^2$.

(e) 3,5, d_2- pyran-4-thione.

	v = 0		v = 1	
	observed	νobs- νcalc	observed	νobs- νcalc (MHz)
$7_{16} - 6_{15}$	20735.70	+0.01		
$7_{26} - 6_{25}$	19654.70	+0.05	19682.50	
$7_{25} - 6_{24}$	20822.92	-0.04	20854.52	
$7_{34} - 6_{33}$	20150.35	-0.00	20181.28	
$7_{53} - 6_{52}$	19951.10	-0.09		
$7_{52} - 6_{51}$				
$8_{08} - 7_{07}$	21120.93	+0.03	21149.82	
$8_{18} - 7_{17}$	20813.47	+0.07	20845.56	
$8_{27} - 7_{26}$	22377.87	-0.10	22409.18	
$8_{26} - 7_{25}$	23937.61	+0.13	23972.58	
$8_{35} - 7_{34}$	23153.44	+0.03	23189.55	
$9_{09} - 8_{08}$	23548.95	-0.00	23582.09	
$9_{19} - 8_{18}$	23328.43	+0.03	23364.40	
$9_{28} - 8_{27}$	25070.36	-0.00		
$9_{37} - 8_{36}$	25743.83	+0.05		
$9_{36} - 8_{35}$	26217.70	-0.06		
$10_{46} - 9_{45}$	25770.27	-0.04		
$10_{010} - 9_{09}$	25980.15	-0.06	26017.88	
$10_{110} - 9_{19}$	25829.22	+0.01	25869.14	
$\frac{A+C}{2}$	3282.09		3271.69	
$\frac{A-C}{2}$	2049.11		2036.57	
K	-0.819025		-0.817996	
A	5331.20		5308.26	
B	1603.82		1605.79	
C	1232.98		1235.13	
Ia	94.8249		95.2348	
Ib	315.2050		314.8180	
Ic	410.0082		409.2952	
Δ	-0.0218		-0.7575	

Δ = Ic - Ia - Ib. Ia, Ib, Ic and Δ are in units of a.m.u.$Å^2$.

populated than the antisymmetric by the ratio 10 : 6. For the excited vibrational states, the vibrational wavefunction alternates in symmetry, so that the nuclear spin factor also alternates. Table 2 shows the population ratios for the isotopic samples in the ground- and first excited-state.

Table 2.

Relative intensities of the transitions of pyran-4-thione.

			v = 0		v = 1	
	n_s : n_a	K_{-1} even	K_{-1} odd	K_{-1} even	K_{-1} odd
pyran-4-thione	10 : 6	10	6	6	10
2,6 d_2- "	7 : 5	7	5	5	7
3,5 d_2- "	7 : 5	7	5	5	7

This analysis of the relative intensities for pyran-4-thione is in good agreement with that observed experimentally, and justifies the assumption of the planarity of the molecule.

Table 3.

The inertial defects of pyran-4-thione (a.m.u.Å^2).

	Δ
v = 0	-0.0157
v = 1	-0.7303

For a planar molecule the inertial defect, $\Delta = I_c - I_a - I_b$, is approximately zero. The value of Δ given in Table 3 for the ground-state of pyran-4-thione confirms the planarity of the molecule in the ground state. It can also be seen in Table 3 that the first

excited-state of the vibrational mode has a large negative value of Δ. This value indicates that the vibration involves predominantly out-of-plane displacements. Since this is the lowest frequency vibration it would make the largest negative contribution to Δ even in the ground-state and explains the negative value of Δ = -0.0157 a.m.u.$\mathring{A}^2$ for the ground-state of pyran-4-thione.

2-3. Stark Effect and the Measurement of the Dipole Moment.

The perturbations of the energy levels, which arise from the interaction of the permanent dipole moment of a molecule with a uniform electric field, produce changes in the spectrum called Stark Effects (10, 11). For an asymmetric rotor, and providing no accidental degeneracies occur, these perturbations are second order with respect to the dipole moment and the applied field (12). The correction to the energy levels is the usual second order perturbation result and is given by :-

$$\Delta E_n^{(2)} = \sum_{n'} \frac{\left| \int \psi_n^* \left| E \sum_g \phi_{z_g} \mu_g \right| \psi_{n'} \, d\tau \right|^2}{E_n^o - E_{n'}^o} \qquad \ldots(1)$$

where n represents all the quantum numbers describing the state ψ,

E_n^o is the energy of the undisturbed state,

$E_{n'}^o$ is the energy of any other state unperturbed by the electric field E,

ϕ_{z_g} is the direction cosine between the space fixed z-axis defined by the electric field and the component of μ along the principal axis g

and $\left| \int \psi_n^* \left| E \sum_g \phi_{z_g} \mu_g \right| \psi_{n'} \, d\tau \right|$ is E multiplied by the z-component of the dipole moment matrix element defined by n;n', and can be represented by $\left| \mu_{n;n'} \right|$.

The dipole moment matrix elements for an asymmetric rotor are tabulated as reduced Stark coefficients (3) and, resulting from an evaluation of transition intensities, as line strengths, $^{g}S_{J_T \, ; \, J_{T'}}$ (13, 14).

$$\left| \mu_{J_{\nearrow T},M \; ; \; J-1_{\nearrow T'},M} \right|^2 = \mu_g^2 \frac{(J^2 - M^2)}{J(4J^2 - 1)} \, {}^{g}S_{J_T \; ; \; J-1_{T'}}$$

$$\left| \mu_{J_{\nearrow T},M \; ; \; J_{\nearrow T'},M} \right|^2 = \mu_g^2 \frac{M^2}{J(J+1)(2J+1)} \, {}^{g}S_{J_T, \; J_{T'}} \qquad \ldots(2)$$

$$\left| \mu_{J_{\nearrow T},M \; ; \; J+1_{\nearrow T'},M} \right|^2 = \mu_g^2 \frac{(J+1)^2 - M^2}{(J+1)(2J+1)(2J+3)} \, {}^{g}S_{J_T, J+1_{T'}}$$

where n is expanded in terms of the quantum numbers for the asymmetric rotor energy levels.

Combining equations (1) and (2) gives the Stark perturbation to the energy levels, in the case of no degeneracy, as :-

$$\Delta E^{(2)}_{J_T M} = \sum_{g=a,b,c.} \frac{\mu_g^2 E^2}{2J+1} \sum_{T'}{}' \left[\frac{J^2 - M^2}{J(2J-1)} \frac{g_{S_{J_T},\, J-1_{T'}}}{E^o_{J_T} - E^o_{J-1_{T'}}} + \right.$$

$$\left. \frac{M^2}{J(J+1)} \frac{g_{S_{J_T},\, J_{T'}}}{E^o_{J_T} - E^o_{J_{T'}}} + \frac{(J+1)^2 - M^2}{(J+1)(2J+3)} \frac{g_{S_{J_T},\, J+1_{T'}}}{E^o_{J_T} - E^o_{J+1_{T'}}} \right] \quad \ldots(3)$$

Each component of the dipole moment along the directions of the principal axes, a, b, c, can be treated separately. Since (3) depends only on M^2, and $\Delta M = 0$, the application of an electric field removes the spacial M degeneracy to give pairs of degenerate levels, with the exception of $M = 0$ which is nondegenerate. Therefore, an R-branch line $J \rightarrow J + 1$, will split into $(J + 1)$ M-components.

The dipole moment (μ_a) of pyran-4-thione was determined by measuring two of the Stark components of the $4_{04} - 3_{03}$ transition (15). These were well defined, and their frequency separations from the unsplit zero-field line ($\Delta\nu$) were measured at various values of the applied voltage (V). The graphs of $\Delta\nu$ against V^2 were straight lines and verify the quadratic nature of the Stark shifts. The

spectrometer was then calibrated against the J = 1 - 2 transition of OCS, taking the dipole moment of OCS as 0.7124 D (16). The calibration determines the electrode-to-cell spacing in order to define the proportionality constant (C) between the electric field strength and the applied voltage.

The Stark coefficients, with the appropriate value of M, were calculated for μ_a^2 from equation (3) and the Stark shifts could then be written as :

$4_{04} - 3_{03}$ M = 0 $-0.3255\ \mu_a^2 = -4.8123$

$\mu_a = 3.845$ D

and $4_{04} - 3_{03}$ M = 1 $-0.1996\ \mu_a^2 = -2.9545$

$\mu_a = 3.847$ D

The value of the dipole moment is therefore $\mu = \mu_a = 3.85 \pm 0.02$ D. This value may be compared with the dipole moment of pyran-4-one (3.70 D) (6). The values of the dipole moments of the series of compounds, determined in solution, are as follows (17) -

pyran-4-one	3.72 D
1-thiapyrone	3.96 D
pyran-4-thione	4.08 D
1-thia-4-thiopyrone	4.41 D.

2-4. Structure and Discussion.

The principal moments of inertia of all isotopic species of pyran-4-thione are collected in Table 4.

Table 4.

Ground-state moments of inertia of pyran-4-thione (a.m.u.Å^2).

	I_a	I_b	I_c	Δ
pyran-4-thione	85.3386	314.9938	400.3168	-0.0157
^{18}O- "	85.3441	324.7896	410.1020	-0.0290
^{34}S- "	85.3504	325.0987	410.4175	-0.0316
2,6d_2- "	93.5303	324.3262	417.8349	-0.0216
3,5d_2- "	94.8249	315.2050	410.0082	-0.0218

A total of eight independent moments of inertia are available for determination of the ten parameters describing this structure of the molecule (C_{2V} symmetry). Therefore, two structural assumptions must be made. The structural calculation was carried out using Kraitchmann's "substitution" method (9) (and for further discussion (18, 19)).

This method uses the isotope shifts in the moments of inertia to determine the structural parameters. The isotopic substitution of a single atom in a rigid molecule yields the coordinates of that atom in the principal axis system of the original molecule. Kraitchmann's equations for a planar asymmetric top are :-

$$x^2 = \frac{\Delta I_Y}{\mu}\left[\frac{I_{X'} - I_Y}{I_X - I_Y}\right] \qquad \ldots(4)$$

$$y^2 = \frac{\Delta I_X}{\mu}\left[\frac{I_{Y'} - I_X}{I_Y - I_X}\right]$$

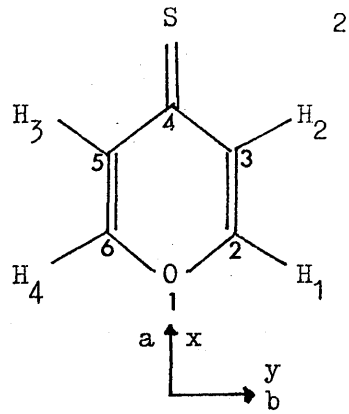

where $\mu = \frac{M.\Delta m}{M + \Delta m}$ is the reduced mass and the primes refer to the substituted molecule. The coordinates obtained from equations (4) and Table 4 are (in Å.) :-

	x	y
O_1	-2.2298	0
S	2.2698	0
H_1	-2.1723	2.0172
H_2	0.3268	2.1707

For an error of $\pm$0.005 a.m.u.Å^2 in the moments of inertia the calculated error in the coordinates is $\pm$0.003Å.

The x and y coordinates of atom C_2 and the y coordinate of atom C_3 in pyran-4-thione were calculated using the values of 1.360 Å for $r(O_1 - C_2)$ and 1.080 Å for $r(C_2 - H_1)$ which were obtained from the microwave study of pyran-4-one. The following diagram shows the notation used for the method of calculation of these coordinates.

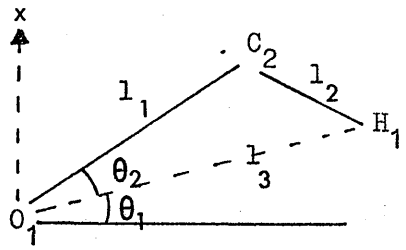

$$\theta_1 = \tan^{-1} \frac{x_H - x_0}{y_H - y_0}$$

where x_H, y_H = substitution coordinates of H_1

x_0, y_0 = " " of O_1

and $$\theta_2 = \cos^{-1} \frac{l_1^2 + l_3^2 - l_2^2}{2l_1 l_3}$$

where l_1, l_2, l_3 = values of the bond lengths as shown in the diagram above.

Therefore $y_{C_2} = l_1 \cos(\theta_1 + \theta_2)$

and $x_{C_2} = x_0 - l_1 \sin(\theta_1 + \theta_2)$.

For the other off-axis carbon atom,

$$y_{C_3} = \left[\frac{I_a - \sum' my^2}{2m_C} \right]^{\frac{1}{2}}$$

where I_a = principal moment of inertia about the a(x)-axis of pyran-4-thione,

m_C = atomic mass of carbon,

and $\sum' my^2$ = summation of my^2 for the atoms of pyran-4-thione excluding C_3 and C_5.

The error in the bond lengths of pyran-4-one were estimated to be $\pm$0.008 Å. The calculation of the structure of pyran-4-one involved four isotopic modifications and the structural assumptions r(C = O) = 1.220 Å and r(C - H_2) = 1.080 Å. The expected value for r(C - O) is 1.34 $\pm$ 0.02 Å (20).

The values obtained from the calculation shown above, for the following coordinates of pyran-4-thione, relative to the principal axes of the molecule, were :-

$$x_{C_2} = -1.5172 \text{ Å} \qquad y_{C_2} = 1.1584 \text{ Å}$$

$$y_{C_3} = 1.2146 \text{ Å}$$

A change of $\pm$ 0.01 Å in the value of either of the assumed parameters produces an error of $\pm$ 0.008 Å in the coordinates.

In order to calculate the positions of the remaining carbon atoms the first and second moment equations were used to fit the structure to the value of I_b. The first and second moment equations

$$\Sigma mx = 0$$

and $\Sigma mx^2 = I_b$ give

$$\text{and} \qquad \begin{aligned} \Sigma' mx + 2m_C \cdot x_{C_3} + m_C \cdot x_{C_4} &= 0 \\ \Sigma' mx^2 + 2m_C \cdot x_{C_3}^2 + m_C \cdot x_{C_4}^2 &= I_b \end{aligned} \qquad \ldots(5)$$

where Σ' refers to the summation of the atoms of the molecule excluding C_3 and C_4.

Equations (5) gave

$$x_{C_4} = 0.6366 \text{ Å}$$

and $$x_{C_3} = -0.1838 \text{ Å}$$

The near-axis coordinate, x_{C_3}, is not defined, by this method of calculation, as accurately as a coordinate of larger magnitude (9).

The coordinates of the atoms of the molecule, relative to the principal axes, are collected in Table 5.

Table 5.

The coordinates of the atoms of pyran-4-thione relative to the principal axes and for comparison, the coordinates of pyran-4-thione obtained from those of pyran-4-one (6) by a shift of origin.

	x	y	x (from pyran-4-one)	y (from pyran-4-one) (Å)
O_1	-2.2298	0	-2.2359	0
C_2	-1.5172	1.1584	-1.5300	1.1627
C_3	-0.1838	1.2146	-0.1875	1.2251
C_4	0.6366	0	0.6259	0
C_5	-0.1838	-1.2146	-0.1875	-1.2251
C_6	-1.5172	-1.1584	-1.5300	-1.1627
S	2.2698	0		
H_1	-2.1723	2.0172	-2.1891	2.0152
H_2	0.3268	2.1707	0.3125	2.1823
H_3	0.3268	-2.1707	0.3125	-2.1823
H_4	-2.1723	-2.0172	-2.1891	-2.0152

(centre of mass of pyran-4-thione relative to that of pyran-4-one 0.4554,0)

The error on each coordinate, except those determined directly by isotopic substitution, depends on the structural assumptions and the method of calculation leading from the assumptions.

pyran-4-thione $I_a = 85.3386$ a.m.u.Å^2,

pyran-4-one $I_a = 86.2809$ a.m.u.Å^2.

The difference in the values of I_a indicates that the ring of pyran-4-thione is narrower than that of pyran-4-one. The ring is not significantly longer as the $C_4 - O_1$ distance in pyran-4-thione equals 2.866 Å and in pyran-4-one equals 2.862 Å.

In order to investigate further the narrowing of the pyran-4-thione ring, the Kraitchman substitution coordinates of the hydrogen atoms were compaired between the two molecules. Using the hydrogen coordinates of Table 5 the following differences were obtained.

$$x_{H_1}(S) - x_{H_1}(0) = 0.017 \text{ Å}$$

$$x_{H_2}(S) - x_{H_2}(0) = 0.014 \text{ Å}$$

$$y_{H_1}(S) - y_{H_1}(0) = 0.002 \text{ Å}$$

$$y_{H_2}(S) - y_{H_2}(0) = -0.012 \text{ Å}$$

S represents pyran-4-thione and

0 " pyran-4-one.

The directions of the above positional changes of the hydrogen atoms are shown in Fig.2.

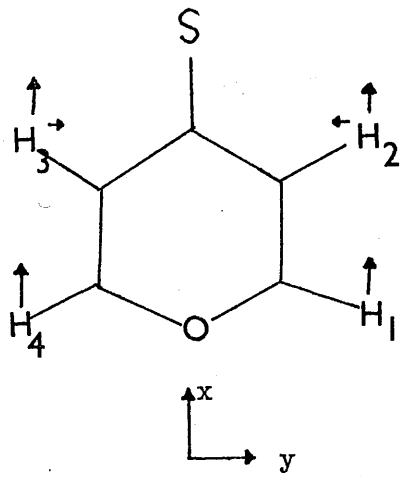

Fig.2. The directions of the change in the positions of the hydrogen atoms of pyran-4-thione with respect to the corresponding positions in pyran-4-one.

From the above, it can be seen that the narrowing of the pyran-4-thione ring results mainly from changes in the upper portion of the ring.

To test the validity of assuming the C - O bond length as 1.360 Å, structures were calculated for two different values of r(C - O) as shown in Table 6. The values of 1.350 Å and 1.370 Å were chosen since these represent extreme values of this bond length with respect to the estimated standard deviation of 0.008 Å.

The situation of the double bond (C = C) in pyran-4-thione can be compared to that found in enone and diene systems. In acrolein and butadiene (21), for example, the values of r_s(C = C) were found to be 1.345 Å and 1.337 Å respectively and of r_s(C - C), 1.470 Å and 1.476 Å respectively. Therefore, from Table 6 the value of 1.360 Å for $r(C_2 - O_1)$ is a reasonable assumption because in order to produce a

Table 6.

Some structural parameters of pyran-4-thione using different values of $r(C_2 - O_1)$.

$C_2 - O_1$	1.350 Å	1.360 Å	1.370 Å
$C_4 - S$	1.6624 Å	1.6332 Å	1.6072 Å
$C_3 - C_4$	1.4423 Å	1.4657 Å	1.4876 Å
$C_2 = C_3$	1.3669 Å	1.3346 Å	1.3045 Å
$C_3 - H_2$	1.0677 Å	1.0839 Å	1.0997 Å
$C_2 - H_1$	1.080 Å	1.080 Å	1.080 Å
$\angle C_2O_1C_6$	117° 8'	116° 48'	116° 30'
$\angle C_3C_4C_5$	115° 40'	111° 56'	108° 38'

value of $r(C_3 - C_4)$ of 1.470 Å the value of $r(C_2 - O_1)$ would have to be greater than 1.360 Å and to produce a value of $r(C_2 = C_3)$ of 1.335 Å the assumed value of $r(C_2 - O_1)$ would have to be decreased.

As mentioned previously the dipole moment of pyran-4-thione is larger than that of pyran-4-one and this would indicate an increased contribution to conjugation in the former molecule. This, in turn, would be expected to result in a reduction in the length of the $C_2 - O_1$ and $C_3 - C_4$ bonds in pyran-4-thione with respect to pyran-4-one. Any effect on the length of the $C_2 = C_3$ would be expected to be small. The effect of increased conjugation can not be disregarded since, if anything, the value of 1.360 Å for $r(C_2 - O_1)$ is slightly large, as is

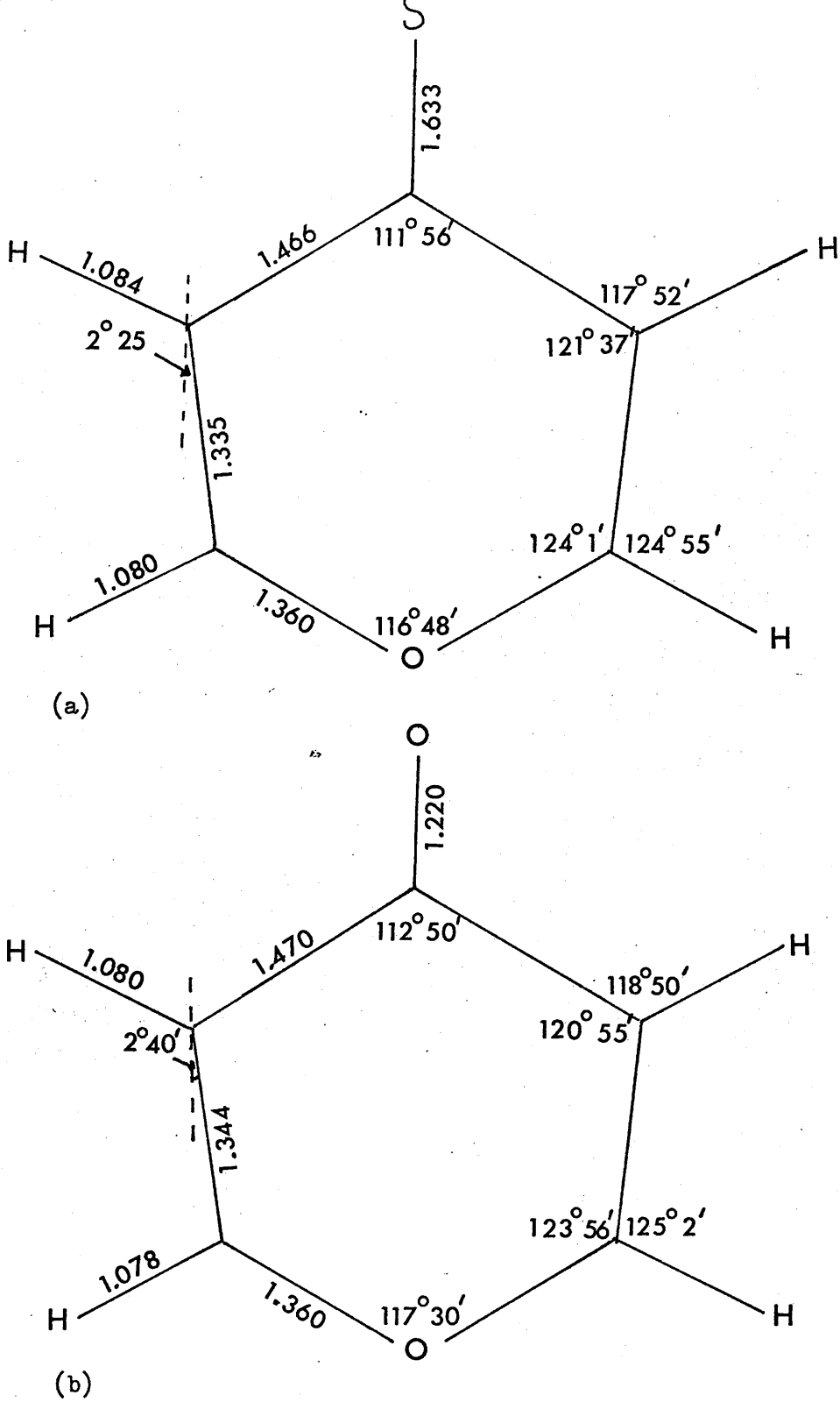

Fig.3. (a) Structure of pyran-4-thione (Å),
(b) structure of pyran-4-one (Å).

indicated from the relative values of the bond lengths in Table 6. Fig.3. shows the calculated structures of pyran-4-thione and pyran-4-one. If it were assumed that $r(C_2 = C_3)$ has the same value in both molecules, then from Table 6 it can be seen that the effect on the bond lengths $C_2 - O_1$ and $C_3 - C_4$ would be in accordance with the greater participation of the thio-group over the keto-group in the resonance conjugation.

The bond angles of the planar structure (Fig.3) suggest the presence of angle-strain in the molecule as a result of the incorporation of the oxygen atom in the plane. Evidence for this angle-strain is obtained from the angular distortion of the $C_2 - C_3$ bond from the direction of the a-axis. This strain could be relieved by a deviation from planarity as shown.

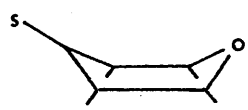

This, however, would result in a reduction of conjugation within the molecule.

References.

1. Elderfield, "Heterocyclic Compounds" Vol. 1, P.370 - 376, John Wiley & Sons, inc.

2. Elderfield, "Heterocyclic Compounds" Vol. 1, P.382, John Wiley & Sons, inc.

3. (a) L. Lorenz and H. Sternitzke, Z. Electrochem., 40, 501 (1934).
(b) F. Arndt, G. T. O. Martin and J. R. Partington, J. Chem. Soc., 1, 602 (1935).

4. L. Kahovec and K. W. F. Kohlrausch, Ber., 75, 627 (1942).

5. P. Beak and G. A. Carls, J. Org. Chem., 29, 2678 (1964).

6. J. N. Macdonald, Ph. D. Thesis, University of Glasgow (1969).

7. J. Toussaint, Bull. Soc. Chim. Belges., 65, 216 (1956).

8. J. Toussaint, Acta. Cryst., 7, 648 (1954).

9. J. Kraitchman, Am. J. Phys., 21, 17 (1953).

10. C. H. Townes and A. L. Schawlow, "Microwave Spectroscopy", McGraw-Hill Book Co., Inc. (1955).

11. W. G. Penney, Phil. Mag., 11, 602 (1931).

12. S. Golden and E. B. Wilson, Jr., J. Chem. Phys., 16, 669 (1948).

13. G. W. King, R. M. Hainer and P. C. Cross, J. Chem. Phys., 12, 210 (1944).

14. Tables of Line Strengths, National Bureau of Standards, Monograph 70 Vol. II (1964).

15. S. A. Manley, B.Sc. Thesis, University of Glasgow (1968).

16. S. A. Marshall and J. Weber, Phys. Rev., 105, 1502 (1957).

17. M. Rolla, M. Sanesi and G. Traverso, Ann. Chim. (Rome), 42, 673 (1952).

18. C. C. Costain, J. Chem. Phys., 29, 864 (1958).

19. L. Pierce, J. Mol. Spec., 3, 575 (1959).

20. D. R. Lide, Jr., Tetrahedron, 17, 125 (1962).

21. E. A. Cherniak and C. C. Costain, J. Chem. Phys., 45, 104 (1966).

CHAPTER 3.

THE MICROWAVE SPECTRUM OF CYCLOHEX-2-EN-1-ONE

3-1. Introduction.

Cyclohexenone is a well-known molecule which is often found as a constituent ring in larger molecules of chemical and biological interest, for example in androgen-type steroids. The results presented in the report which follows show clearly that the molecule is non-planar.

Some of the possible conformations for cyclohexenone are shown

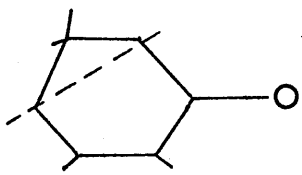

envelope-form
(a)

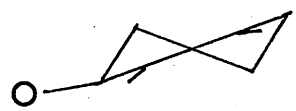

half-chair-form
(b)

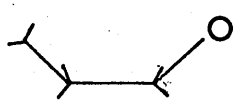

boat-form
(c)

The boat-form (c) is considered unfavourable because it involves the steric interactions of two pairs of eclipsed hydrogen atoms, whereas forms (a) and (b) have no eclipsed hydrogen atoms. The conformation (a), unlike (b), allows for the coplanarity of the double bonds and thereby

favours resonance. As yet, insufficient microwave data is available to determine the true geometry of the ring. However, it is shown that the observed moments of inertia can be interpreted in terms of a structure with the form (a).

Support for this structure can be found from the planarity of the heavy atom frame in cyclopent-2-en-1-one (1). The tendency of the conjugated 2-en and carbonyl double bonds to keep the heavy atoms coplanar is obviously strong enough to overcome the torque necessary to fix the two methylenic groups in an unfavourable eclipsed position. The acyclic en-one, trans-acrolein (2) is certainly planar and therefore if there is little angle-strain in the ring, the cyclohexenone molecule should adopt a conformation to favour conjugation of the double bonds.

Only μ_a-type transitions have been observed and μ_a and μ_c components of the dipole moment for the ground vibrational state have been determined from Stark effect measurements as 3.75 ± 0.02D and 0.31 ± 0.01D. No precise value of the μ_b component was obtained from the transitions studied.

Much attention has been focused in recent years on the vibrational satellites accompanying the ground-state spectra of ring compounds. An investigation of the relative intensities of the ground- and excited-state lines of the lowest vibrational mode of cyclohexenone shows that the vibrational energy levels can be represented by

$$E_v = (95 \pm 6)\ (v + \tfrac{1}{2})\ \text{cm}^{-1}.$$

3-2. Observed Spectrum.

The sample of cyclohexenone was supplied by Kodak Ltd., and the infra-red spectrum indicated that no further purification was necessary. The sample (b.pt 170 at 760m.m. pressure) and the sample cell were maintained at room temperature. From initial estimates of the structure of cyclohexenone it was apparent that a-type transitions should predominate, although the possibility of b-type and c-type transitions was not excluded. Subsequently, only a-type transitions were observed. Concentrating on R-branch transitions, in the frequency range 20 - 27 GHz a strong feature of the spectrum was a pair of transitions centred at 26,160 MHz and separated by 60 MHz. On the basis of Stark effect splittings the higher frequency transition was assigned to a $K_{-1} = 0$ line and the other to a $K_{-1} = 1$ line. A similar pair of transitions were observed with a central frequency of 22,630 MHz. In order to characterize the J values of these transitions a planar structural model was calculated using the bond length values obtained from the microwave study of acrolein (2). When assignments of two further transitions had been made, the transition frequencies observed thus far were used in a least-squares procedure, as outlined in the previous chapter, allowing the successful prediction and measurement of the spectrum. Each of the observed ground-state transitions was found to be accompanied by many satellites, the most prominent of which formed a progression of satellite lines of regularly decreasing intensities. Fig. 1 shows a typical transition. These satellite lines exhibited the same Stark effects as the ground-state

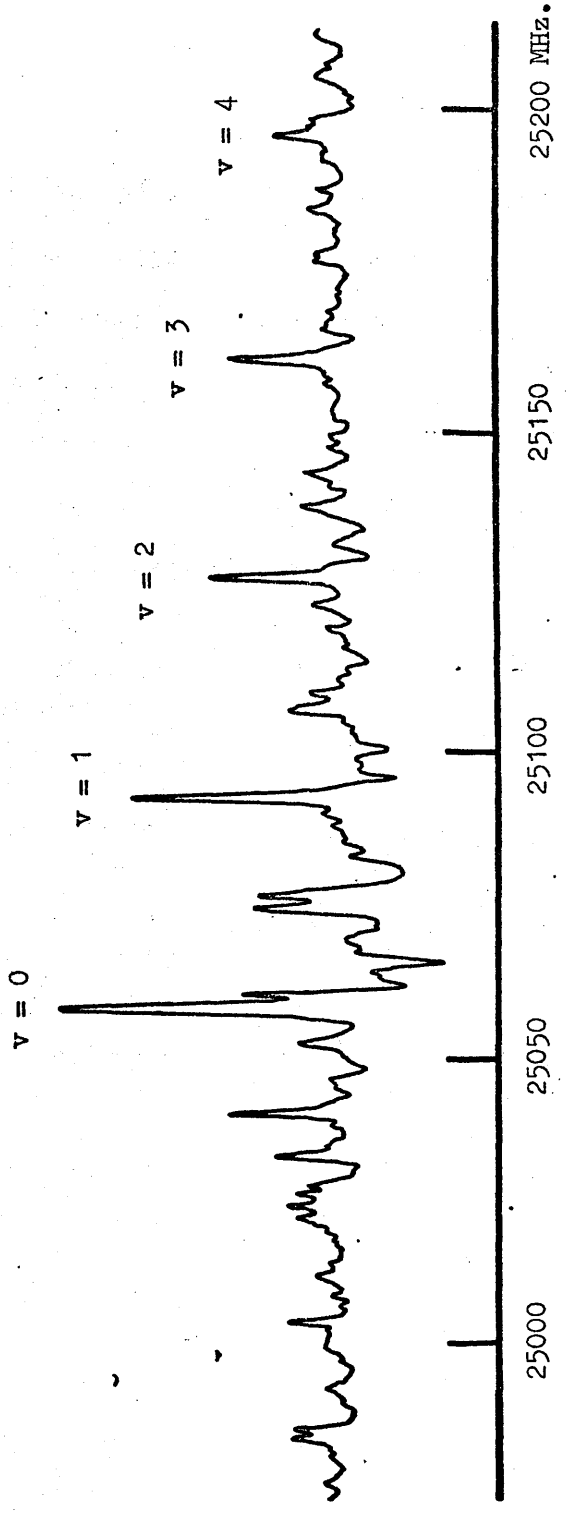

Fig.1. The $6_{25} - 5_{24}$ transition of cyclohex-2-en-1-one.

lines, and the frequencies of each set of spectral lines could be fitted by conventional rigid-rotor expressions. The measured frequencies of the observed lines are shown in Table 1. The rotational constants, moments of inertia and pseudo-inertial defects (Δ), calculated from these measurements, are also given in Table 1.

The Δ's increase in a negative sense from $v = 0$ to $v = 4$, implying that the vibration is not in the ab plane of the molecule. The differences between the measured and calculated frequencies, even for transitions between $J = 6 \leftarrow 7$ and high K_{-1}, have an average value of 0.07 MHz and indicate that the effect of centrifugal distortion is small.

For a planar heavy atom configuration the main contribution to the inertial defect (Δ) would come from the six methylenic hydrogen atoms. For C - H bond lengths of 1.09 Å and tetrahedral HCH angles

$$\Delta \approx -2 \sum_i m_i c_i^2 \approx -9.5 \text{ a.m.u.Å}^2$$

where c_i is the out-of-plane coordinate of the i th atom. The observed value of -17.24 a.m.u.Å^2 clearly indicates that at least one other atom is contributing to this quantity. A structure for cyclohexenone, with oxygen and five of the carbon atoms coplanar and one carbon atom C(5) deviating from this plane, is shown in Fig.2. The validity of this model was checked by a calculation of the moments of inertia for the structural parameters shown in Fig.2. The bond length and bond angle values of the conjugated region were taken directly from the r_s structure obtained for acrolein (1), and the

Table 1.

Observed transition frequencies and calculated rotational constants of cyclohex-2-en-1-one.

	v = 0		v = 1		v = 2	
	observed	$\nu_{obs} - \nu_{calc}$	observed	$\nu_{obs} - \nu_{calc}$	observed	$\nu_{obs} - \nu_{calc}$ (MHz)
$4_{04} - 3_{03}$	15820.98	+0.08				
$4_{14} - 3_{13}$	15350.79	+0.03	15375.02	+0.06		
$4_{13} - 3_{12}$	18347.46	+0.11	18371.09	-0.07		
$4_{23} - 3_{22}$	17069.47	+0.11	17094.97	-0.05		
$4_{22} - 3_{21}$	18451.56	+0.05				
$5_{05} - 4_{04}$	19268.34	+0.08	19294.02	-0.00		
$5_{15} - 4_{14}$	18994.48	+0.10	19024.00	+0.10		
$5_{14} - 4_{13}$	22455.10	+0.02	22480.84	+0.07	22506.33	-0.00
$5_{24} - 4_{23}$	21123.57	+0.06	21154.31	+0.19		
$5_{23} - 4_{22}$	23340.06	+0.07	23377.78	+0.09	23415.16	+0.01
$5_{32} - 4_{31}$	22355.54	-0.05	22396.29	+0.01	22436.79	+0.09
$6_{06} - 5_{05}$	22716.41	-0.01	22748.91	+0.01	22781.26	+0.03
$6_{16} - 5_{15}$	22580.40	-0.08	22615.47	-0.01	22650.25	-0.05
$6_{15} - 5_{14}$	26218.58	-0.02	26244.83	+0.13	26270.77	+0.09
$6_{25} - 5_{24}$	25053.61	+0.08	25088.52	+0.05	25123.26	+0.04
$6_{24} - 5_{23}$	28047.79	-0.16	28088.42	+0.00	28128.58	-0.06
					27411.63	+0.10
$7_{33} - 6_{32}$	26192.35	-0.04	26231.74	+0.03	26270.77	-0.06
$7_{07} - 6_{06}$	26131.19	+0.00	26171.81	-0.10	26212.46	+0.03
$7_{17} - 6_{16}$	29701.51	-0.01	29729.42	-0.25		
$7_{16} - 6_{15}$	28860.73	-0.23	28899.88	-0.02	28938.78	+0.14
$7_{26} - 6_{25}$	30493.96	+0.07	30539.00	+0.06	30583.47	-0.26
$7_{35} - 6_{34}$	30863.13	+0.10	30913.81	+0.10		
$7_{44} - 6_{43}$	31167.11	-0.07	31223.38	-0.26		
$7_{43} - 6_{42}$						

Table 1. (contd.)

	v = 3		v = 4	
	observed	$\nu_{obs} - \nu_{calc}$	observed	$\nu_{obs} - \nu_{calc}$
$4_{04} - 3_{03}$				
$4_{14} - 3_{13}$				
$4_{13} - 3_{12}$				
$4_{23} - 3_{22}$				
$4_{22} - 3_{21}$				
$5_{05} - 4_{04}$				
$5_{15} - 4_{14}$	22531.43	-0.23	22556.75	+0.03
$5_{14} - 4_{13}$				
$5_{24} - 4_{23}$	23452.28	+0.06	23489.03	+0.12
$5_{23} - 4_{22}$				
$5_{32} - 4_{31}$	22813.85	+0.30	22845.76	+0.06
$6_{06} - 5_{05}$	22684.98	-0.12		
$6_{16} - 5_{15}$	26296.48	+0.00		
$6_{15} - 5_{14}$	25157.74	-0.05	25192.19	+0.10
$6_{25} - 5_{24}$	28168.35	-0.08	28207.58	-0.21
$6_{24} - 5_{23}$	26360.96	-0.02	26400.68	+0.06
$6_{34} - 5_{33}$	27462.37	-0.05		
$6_{33} - 5_{32}$	26309.81	-0.14		
$7_{07} - 6_{06}$	26252.83	-0.11	26293.15	-0.11
$7_{17} - 6_{16}$				
$7_{16} - 6_{15}$	28977.35	+0.15	29015.48	+0.00
$7_{26} - 6_{25}$	30628.43	+0.24		
$7_{35} - 6_{34}$				
$7_{44} - 6_{43}$				
$7_{43} - 6_{42}$				

Table 1. (contd.)

	v = 0	v = 1	v = 2	v = 3	v = 4
$\frac{A+C}{2}$	3264.36	3259.33	3254.35	3249.34	3244.32
$\frac{A-C}{2}$	1506.07	1497.90	1489.80	1481.67	1473.53
κ	-0.47883	-0.47573	-0.47262	-0.46951	-0.46638
A	4770.43	4757.23	4744.15	4731.01	4717.85
B	2543.20	2546.73	2550.23	2553.69	2557.09
C	1758.29	1761.42	1764.54	1767.67	1770.78
Ia	105.9719	106.2658	106.5587	106.8548	107.1527
Ib	198.7774	198.5022	198.2294	197.9613	197.6975
Ic	287.5133	287.0013	286.4937	285.9872	285.4842
Δ	-17.2360	-17.7667	-18.2944	-18.8289	-19.3660

$\Delta = Ic - Ia - Ib.$

Ia, Ib, Ic and Δ are in units of a.m.u.Å^2.

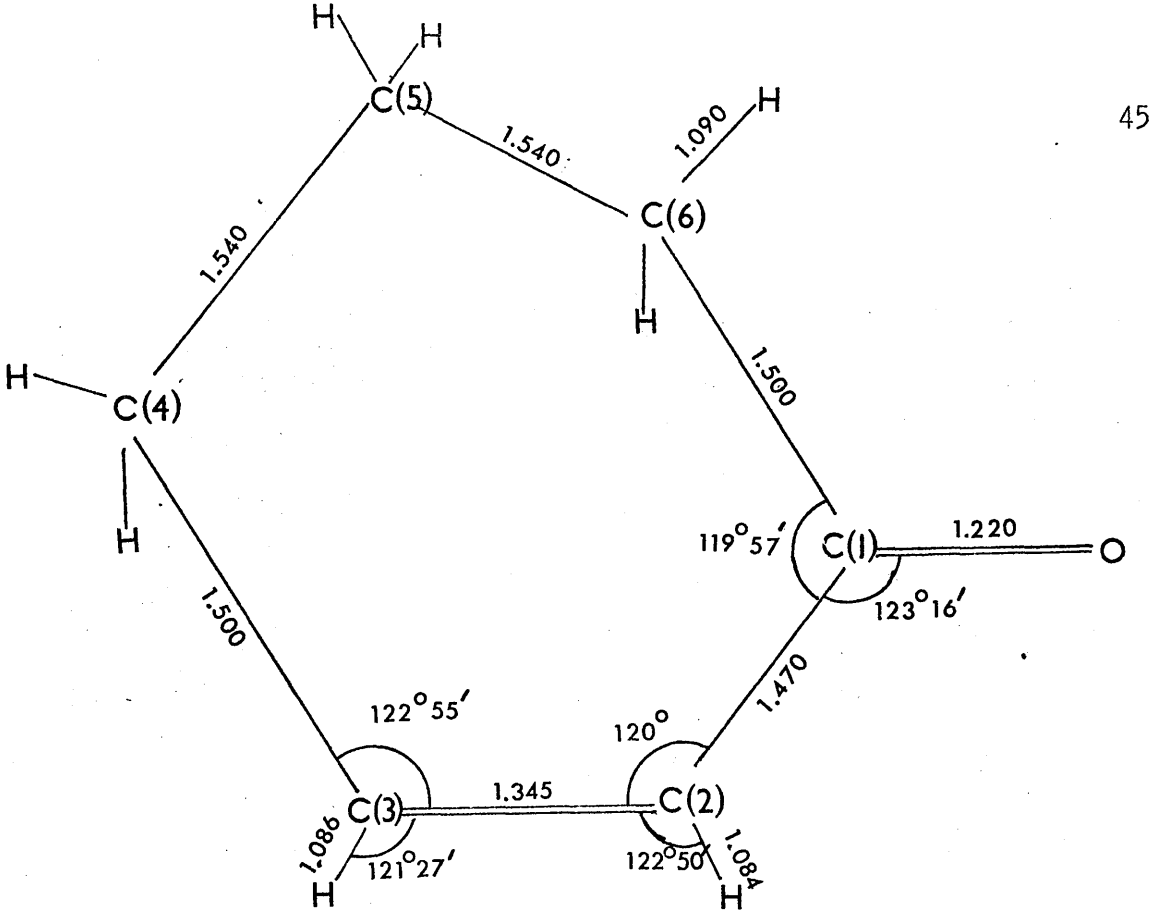

Fig.2. A model for cyclohexenone (Å).

configurations of C(4), C(5) and C(6) were taken as approximately tetrahedral. The calculated and observed moments of inertia are given in Table 2. The values are in reasonable agreement and the calculated pseudo-inertial defect implies the correct degree of non-planarity.

Table 2.

Observed and calculated moments of inertia (a.m.u.Å^2).

	OBS.	CALC.
I_a	105.97	105.40
I_b	198.78	194.15
I_c	287.51	280.92
Δ	-17.24	-18.63

3-3. Ring-bending Vibration.

Further information was sought concerning the potential function for the vibration mentioned earlier. For a strain-free ring with no torsional barrier, the potential function will be parabolic in form. A barrier to torsion about the single bonds in the ring would result in a pairing, to some extent, of the vibrational energy levels with a consequent alternating variation in the differences between the rotational constants for adjacent vibrational states. The rotational constants, when plotted against the vibrational quantum number (Fig.3), show no evidence of this behaviour and therefore the vibrational potential function appears to have a single minimum. The relative intensities of the vibrational states were examined in order to determine the dependence of the energy levels on vibrational amplitude. For a purely quadratic potential function, the vibrational energy levels are evenly spaced. A quartic term causes the energy levels to diverge with increasing values of v.

The relative intensities were obtained by comparing the peak heights of the ground-state and excited-state lines of certain of the transitions, under the same operating conditions. The signals from the stronger transitions were attenuated until they were reduced to approximately the same height as the weakest line. This was achieved by an attenuator calibrated in decibels (range 0 - 70 d.b.) placed between the preamplifier and the main amplifier. Care was taken to

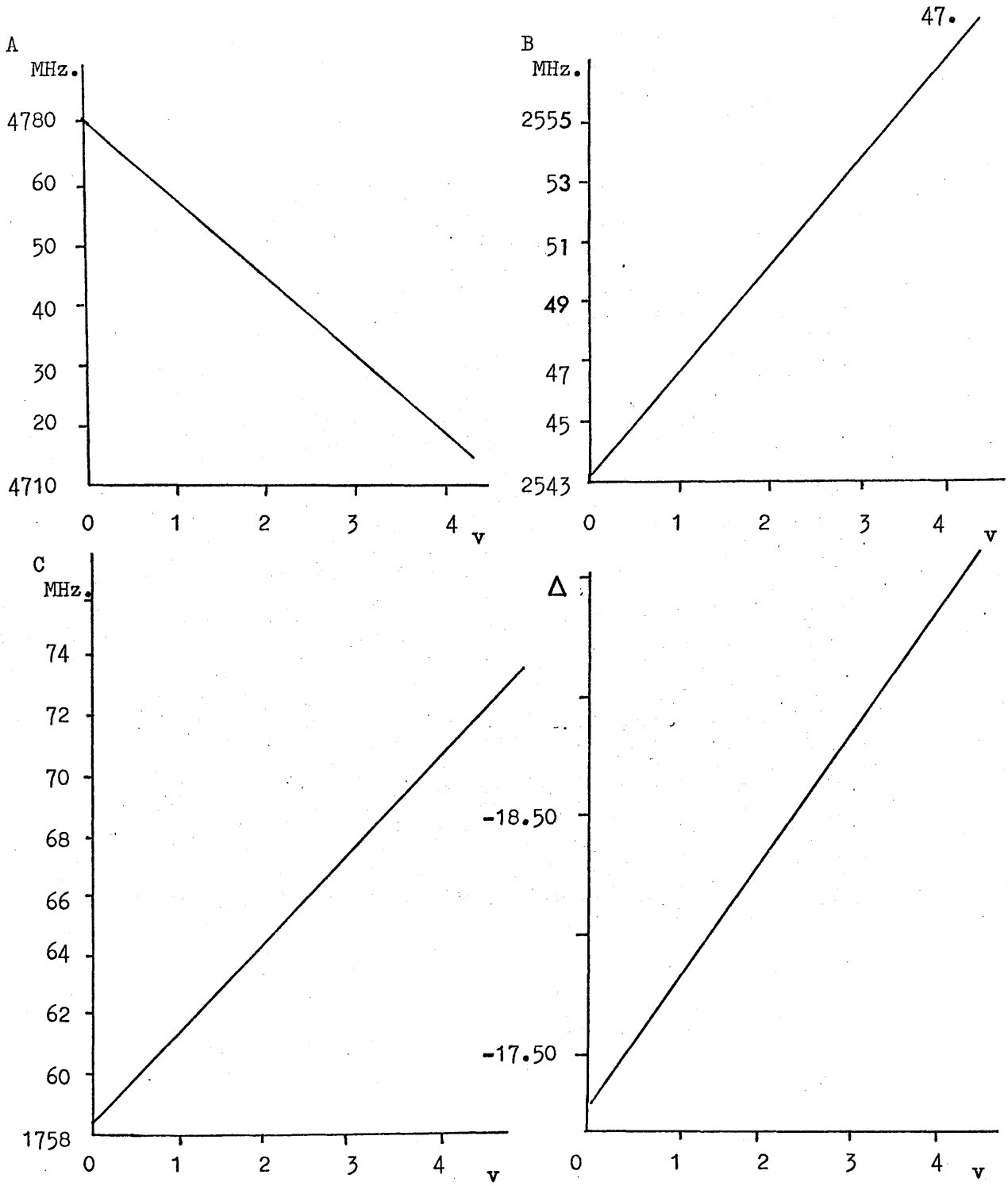

Fig.3. Variation of rotational constants with vibrational quantum number.

maintain constant power at the detector and constant pressure in the cell. A suitable Stark voltage was used for each transition and the results obtained are shown as

	Attenuation (d.b.).			
	v = 0	v = 1	v = 2	v = 3
$5_{14} - 4_{13}$	0	-4.0		
$5_{23} - 4_{22}$	0	-4.5		
$6_{06} - 5_{05}$	0	-4.5	-8.0	
$6_{16} - 5_{15}$	0	-3.5	-6.5	
$6_{25} - 5_{24}$	0	-4.5	-8.5	
$6_{24} - 5_{23}$	0	-3.5	-8.0	-12.0
$7_{34} - 6_{33}$	0	-3.0	-8.5	-10.0
$7_{26} - 6_{25}$	0	-4.5	-9.0	-12.0
(error on each measurement $\pm$ 1.5 d.b.)				
Average	0	-4.0 $\pm$0.8	-8.1 $\pm$0.8	-11.3 $\pm$ 1.0
$\bar{\nu}$ cm^{-1}	0	96.0 $\pm$20.0	194.5 $\pm$20.0	271.3 $\pm$20.0
$\bar{\nu}/v$ cm^{-1}		96	97	90

Using the Boltzmann distribution of population,

$$N_1/N_0 = V_1/V_0 = e^{-\Delta Ehc/kT}$$

and the relationship,

$$1 \text{ decibel} = 20 \log V_1/V_0,$$

the energies of the successive vibrational states $\bar{\nu}$ were calculated in cm^{-1} from

$$\bar{\nu} = 2.303 \frac{kT}{hc} \frac{(d.b.)}{20},$$

where $\log V_1/V_0$ = log input voltage/output voltage,

(d.b.) = number of decibels,

k = Boltzmann's constant,

T = temperature, $300^{\circ}K$,

h = Planck's constant,

c = velocity of light

If there were an energy barrier in the potential function, the resulting pairing of the vibrational energy levels should be apparent in the relative intensity data. Within the rather limited experimental accuracy no such pairing was evident and the values of the vibrational energy levels can be represented by

$$E_v = (95 \pm 6)\ (v + \tfrac{1}{2})\ cm^{-1}$$

and could be said to correspond to a quadratic potential function.

3-4. Measurement of the Dipole Moment.

For the quantitative measurement of the Stark splittings, the spectrometer was calibrated using the J = 1 — 2 transition of OCS, taking its dipole moment as 0.7124 D (3). The value obtained for the cell constant C was 1.099 MHz^2 $volts^{-2}$ $debye^{-2}$. The Stark shifts of the transitions $5_{15} - 4_{14}$, $5_{24} - 4_{23}$ and $5_{23} - 4_{22}$ were measured and found to be second order, as was expected. Since a full account of the measurement and analysis of the Stark splittings has been given in Chapter 2 it will not be repeated here.

The expressions for the dipole moment components of the transitions studied were determined as

$$
\begin{array}{lcl}
 & M & \\
5_{15} - 4_{14} & 2 & 0.1087\,\mu_a^2 + 0.1591\,\mu_b^2 + 14.8244\,\mu_c^2 = 2.9487 \\
 & 3 & 0.3507\,\mu_a^2 + 0.4507\,\mu_b^2 + 33.3491\,\mu_c^2 = 8.1184 \\
5_{24} - 4_{23} & 1 & 0.3173\,\mu_a^2 - 0.0119\,\mu_b^2 + 0.0785\,\mu_c^2 = 4.4663 \\
5_{23} - 4_{22} & 3 & -2.6815\,\mu_a^2 - 1.0430\,\mu_b^2 + 0.0148\,\mu_c^2 = -37.5657
\end{array}
\qquad \ldots(1)
$$

The large coefficients of the terms in μ_c^2 for the $5_{15} - 4_{14}$ transition show that the Stark splittings of this transition are strongly μ_c dependent, whereas the coefficients of the terms in μ_b^2 show that there is no Stark equation in which μ_b enters prominently. Equations (1) were therefore solved graphically

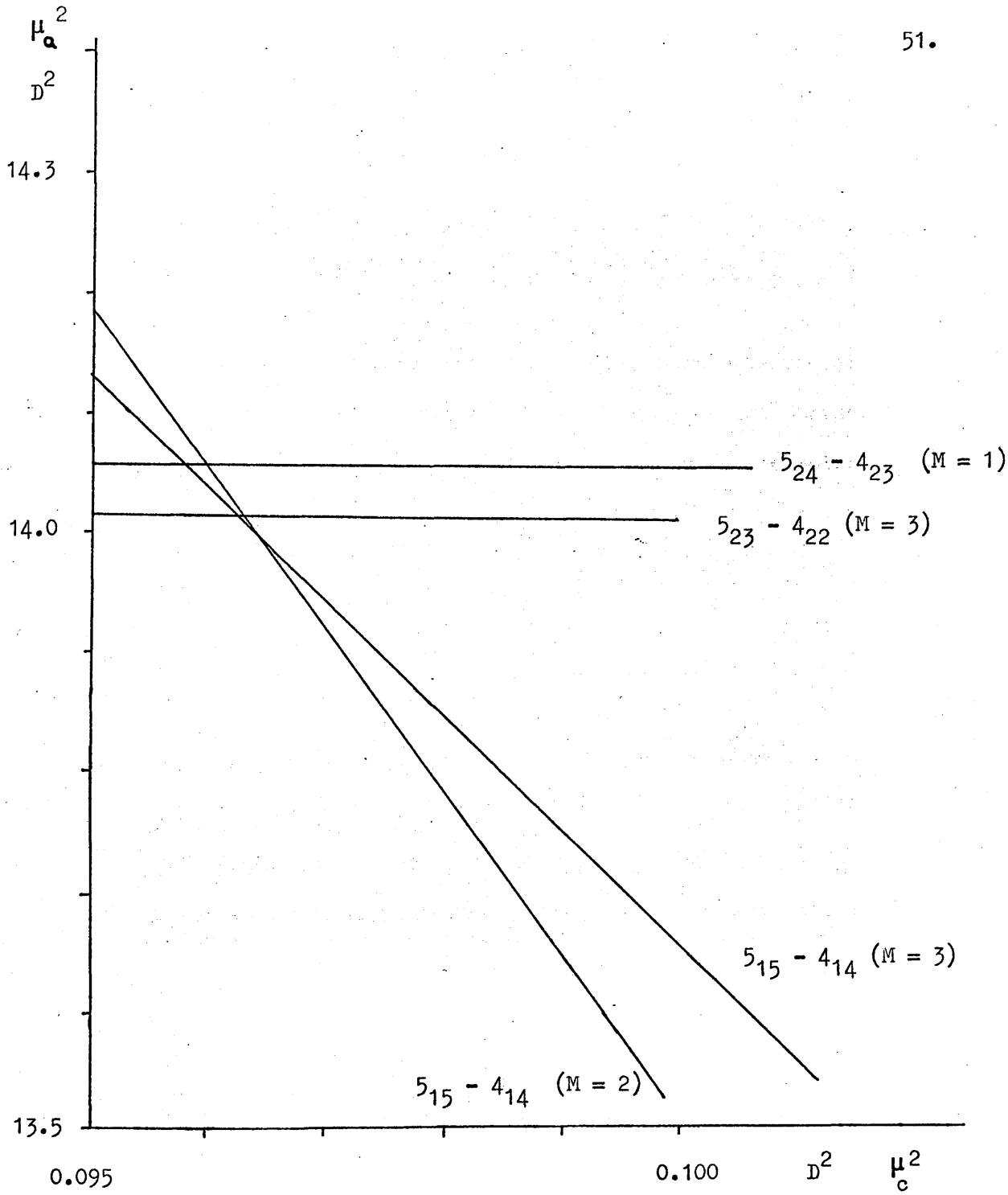

Fig.4. Dipole moment plot for cyclohexenone.

(Fig.4) for μ_a^2 and μ_c^2.

$$\mu_a^2 = 14.026\ D^2 \qquad \mu_a = 3.75 \pm 0.02\ D$$

$$\mu_c^2 = 0.096\ D^2 \qquad \mu_c = 0.31 \pm 0.01\ D$$

The total dipole moment in benzene solution has been measured as 3.62 ± 0.05 D (4). The non-zero value of μ_c provides further evidence for the non-coplanarity of the heavy atoms of the molecule.

References.

1. D. Chadwick, A. C. Legon and D. J. Millen, Chem. Comm., 1130 (1969).

2. E. A. Cherniak and C. C. Costain, J. Chem. Phys.,45, 104 (1966).

3. S. A. Marshall and J. Weber, Phys. Rev.,105, 1502 (1957).

4. D. J. Bertelli and T. G. Andrews, Jr, Tetrahedron Letters, 4467 (1967).

CHAPTER 4.

THE MICROWAVE SPECTRUM AND ^{14}NITROGEN - QUADRUPOLE COUPLING IN DIFLUOROCYANAMIDE.

4-1. Introduction.

The microwave spectrum of NF_2CN has been studied and an approximate structure has been calculated to fit the moments of inertia. The ^{14}N-quadrupole fine structure has been resolved and the analysis yielded the following values of the constants for NF_2CN.

amino N_1 : $\chi_{aa} = 1 \pm 0.2$ MHz $\chi_{bb} = 5.5 \pm 0.2$ MHz

cyanide N_2 : $\chi_{aa} = -4 \pm 0.4$ MHz $\chi_{bb} = 2 \pm 0.4$ MHz

The dipole moment was determined, with component values of $\mu_a = 1.03 \pm 0.01$ D and $\mu_c = 0.34 \pm 0.01$ D and a total dipole moment value of 1.09 D. The uncertainty in the position of the lone pair in this molecule causes a problem in accounting for the dipole moment value in terms of simple models and in accounting for the quadrupole coupling constants in terms of resonance structures.

The structure of NF_2CN has been determined by the method of isotopic substitution by R. H. Schwendeman, P. Lee and Prof. K. Cohn and awaits publication.

4-2. Spectrum of Difluorocyanamide.

Difluorocyanamide is a white solid at -196° and a colourless liquid below its melting point, -61°. It was prepared by elemental fluorination of an aqueous cyanamide solution by a method described in Chapter 7 and similar to that of Meyers and Frank (1). The latter authors characterized the compound as $F_2N - C \equiv N$ from the mass spectrum. Colthup (2) has carried out a complete infrared study and vibrational analysis and has eliminated the possibilities of a carbodiimide structure, $- N = C = N -$, an isocyanodifluoro amine structure, $F_2N - \overset{+}{N} \equiv \overset{-}{C}$ and a difluoro diazo structure, $F_2N = \overset{+}{N} = \overset{-}{C}\overset{+}{N}$, for the compound. Only the cyanamide form was observed in the microwave spectrum.

The infrared spectrum of the prepared sample corresponded closely to that observed by Colthup (2). The sample was stored in a glass bulb at room temperature and over a period of several months there was no evidence of decomposition. The spectrum was observable at room temperature, but the resultant gain in intensity merited a study of the spectrum with the cell at dry ice temperature.

The model chosen to help in the analysis of the spectrum was non-planar, incorporating the bond lengths and bond angles from the microwave study of cyanamide (3) and an r(N - F) value of 1.371 Å from nitrogen trifluoride (4). The planar structure $X_2\overset{+}{N} = C = \overset{-}{N}$, which is considered to be an important contributing species to the structure of cyanamide (3) (X is H) and which tends to make the molecule

planar, is expected to be of less importance in the fluorine analogue.

The μ_a R-branch transition frequencies, calculated by means of the model, indicated a search for the J = 2 —3 group of transitions between 20 and 23 GHz and the J = 3 — 4 group between 28 and 31 GHz. The spectrum was assigned in the region of the more intense J = 3 — 4 transitions, by a similar method to that described in earlier chapters.

Impurity lines were observed for N_2O, COF_2, F_2O, HCN, FCN and ClCN, with the transitions of the latter three molecules being very strong indeed, even with the cell at room temperature. H_2O and NH_3 were removed from the cell by means of the Lewis acid BF_3. The occurence of FCN and ClCN has to be explained, as neither of these impurities were present in the infrared spectrum of the sample and were not quoted as present in the crude product by Meyers and Frank. With the cell and sample closed to the pumps, a small dose of the sample was introduced to the cell and the initially strong difluorocyanamide transition was observed to lose some of its intensity as time passed. Likewise, a transition of FCN and ClCN were observed to increase in intensity with time. Therefore, it would appear that the difluorocyanamide was decomposing and that FCN and ClCN were being formed in the cell. The most probable source of chlorine would be para-chloro-aniline, which was the sample last studied in the cell. The fluorinating agents WF_6 and MoF_6 were introduced to the cell in an attempt to fluorinate para-chloro-aniline and rid the cell of chlorine. This proved to be

unsuccessful and ClCN and FCN were present in the spectrum, in undiminishing intensity, throughout the study of difluorocyanamide. It should be mentioned that the presence of FCN was not checked in the spectrum before admission of the fluorinating agents to the cell. From the above it would appear that there is a very simple pathway to FCN (5).

From the vibrational analysis carried out by Colthup (2), the vibrations with fundamental frequency less than 500 cm^{-1} are given as

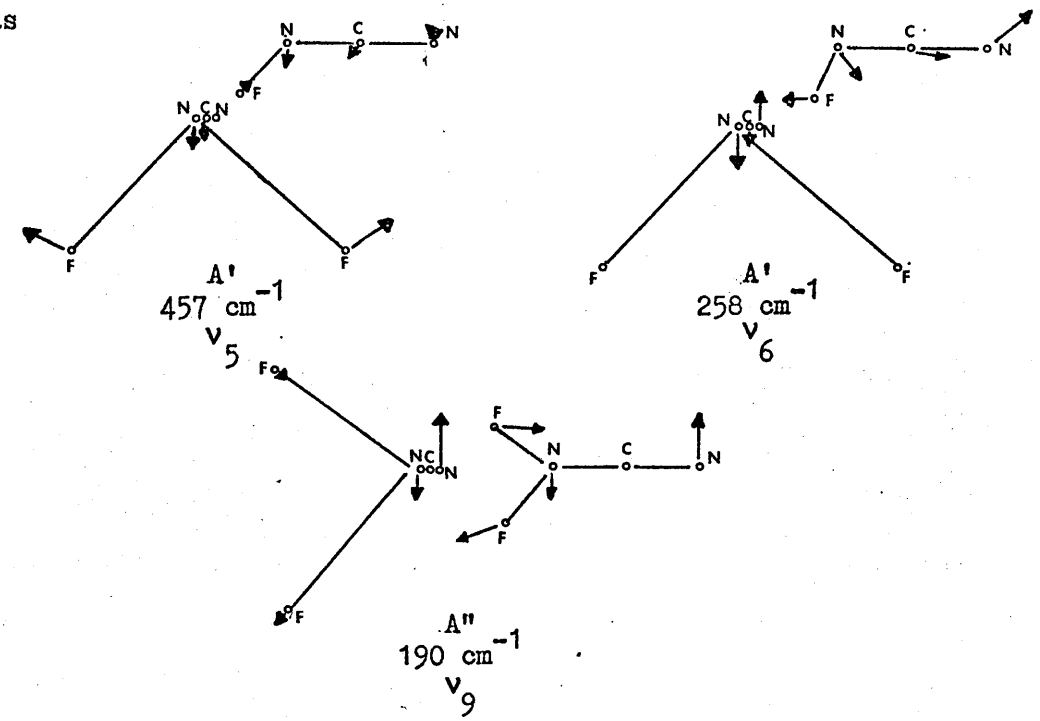

The expected intensities ofthe vibrational satellite lines accompanying each ground state transition can be calculated from the fundamental frequency of the vibration and the Boltzmann equation. The intensities relative to the ground state at room temperature

and at -80°C are given in Table 1.

Table 1.

Relative intensities at 195°K and 300°K of ground- and excited-state transitions with fundamental frequency ω cm^{-1}.

	T = 195°K	T = 300°K
ω cm^{-1}	Rel. Int.	Rel. Int.
0	1	1
100	0.48	0.62
200	0.23	0.38
300	0.11	0.24
400	0.05	0.15
500	0.02	0.09

From Table 1 the rotational transitions in the first vibrational excited-state of ν_5 will not be readily observable. This is borne out experimentally as only two vibrational satellite transitions, accompanying each ground-state transition, were identified. The above analysis of the relative intensities of the vibrational satellite transitions is in fair agreement with the qualitative intensities observed experimentally. Fig.1 shows the ground- and first excited-state of ν_9 of the $5_{05} - 4_{04}$ transition. The measured frequencies of the observed lines are shown in Table 2. The rotational constants calculated from these measurements are also $_g$belonging to ν_9 and the weaker satellites to ν_6 (2). $_{\text{ted as}}$

belonging to ν_9 and the weaker satellites to ν_6 (2).

Although only four transitions were measured for the second excited-state of ν_9, the rotational constants obtained (Table 2)

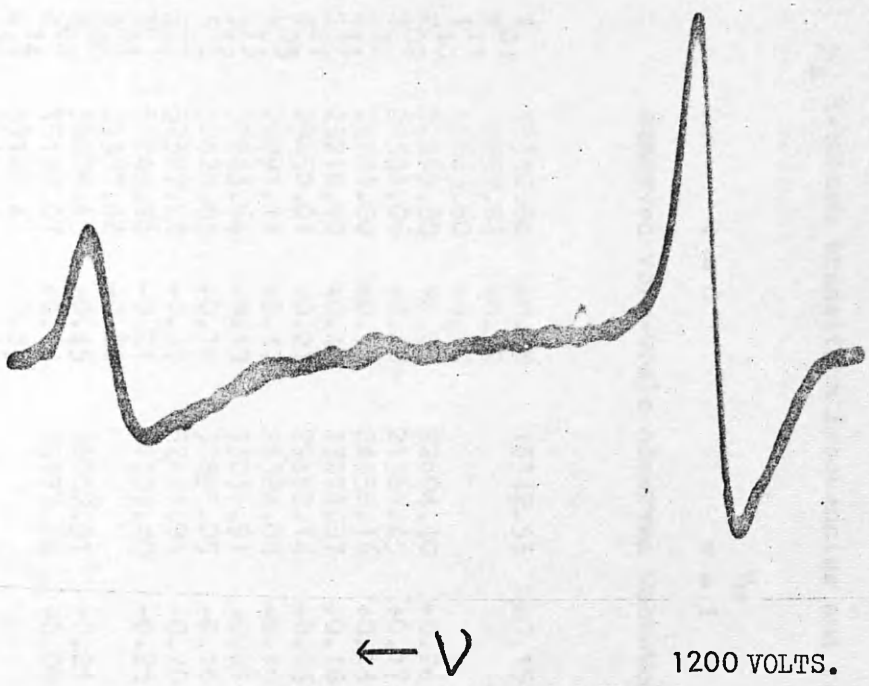

Fig.1. The ground- and first excited-state of ν_9 in the $5_{05} - 4_{04}$ transition of NF_2CN.

Table 2.

μ_a R-branch transition frequencies and rotational constants for NF_2CN.

	ν = 0		ν_9 v = 1		ν_9 v = 2		ν_6 v = 1	
	observed	Vobs-Vcalc	observed	Vobs-Vcalc	observed	Vobs-Vcalc	observed	Vobs-Vcalc (MHz)
$2_{02} - 1_{01}$	15310.84	+0.28	15342.53	+0.15			15356.40	+0.11
$2_{12} - 1_{11}$	14292.83	+0.39						
$2_{11} - 1_{10}$	16663.60	+0.70						
$3_{03} - 2_{02}$	22569.30	+0.29	22604.40	+0.26			22638.52	+0.31
$3_{13} - 2_{12}$	21341.06	+0.40	21369.43	+0.17	21397.43	+0.17	21406.89	+0.10
$3_{12} - 2_{11}$	24881.80	+0.34	24958.16	+0.13	25033.70	+0.17	24952.14	+0.10
$3_{22} - 2_{21}$	23216.90	+0.40	23272.87	+0.18			23284.82	+0.19
$4_{04} - 3_{03}$	29452.01	-0.21	29482.14	-0.03			29544.81	-0.16
$4_{14} - 3_{13}$	28291.11	+0.37	28324.08	+0.15			28379.18	+0.06
$4_{13} - 3_{12}$	32943.64	+0.19	33036.91	-0.01			33038.01	-0.01
$4_{23} - 3_{22}$	30824.83	+0.10	30895.05	-0.16	30964.32	-0.25	30915.60	-0.20
$4_{22} - 3_{21}$	32327.22	+0.47	32441.91	-0.20			32416.03	+0.12
$4_{32} - 3_{31}$	31249.26	-0.21	31333.40	-0.23			31339.44	-0.43
$4_{31} - 3_{30}$	31337.42	-0.28					31425.81	
$5_{05} - 4_{04}$	36039.13	-0.45	36062.91	-0.21	36085.67	-0.00		
$5_{15} - 4_{14}$	35138.07	+0.14	35173.24	-0.09				
$5_{33} - 4_{32}$	39128.47	-0.83						
$5_{32} - 4_{31}$	39428.64	-0.61						

Table 2. (contd.)

		ν_9	ν_9	ν_6
	v = 0	v = 1	v = 2	v = 1
$\frac{A+C}{2}$	6704.73	6690.59	6676.66	6729.28
$\frac{A-C}{2}$	3427.93	3412.55	3397.45	3441.85
κ	-0.65424	-0.64792	-0.6416	-0.65522
A	10132.66	10103.14	10074.10	10171.13
B	4462.03	4479.53	4496.81	4474.11
C	3276.80	3278.03	3279.21	3287.43
Ia	49.8913	50.0370	50.1812	49.7026
Ib	113.2961	112.8536	112.4199	112.9904
Ic	154.2758	154.2177	154.1626	153.7767
Δ	-8.9115	-8.6729	-8.4385	-8.9162

$\Delta = Ic - Ia - Ib.$

Ia, Ib, Ic and Δ are in units of a.m.u.Å^2.

indicate that the vibration is closely harmonic as shown.

	Δ_A	Δ_B	Δ_C	$\Delta(\Delta)$
$\{v = 0\} - \{v = 1\}$	29.52	-17.50	-1.23	0.2386
$\{v = 1\} - \{v = 2\}$	29.04	-17.28	-1.18	0.2344

4-3. Determination of the Dipole Moment.

A simpler and more efficient experimental method than that previously described was adopted for the measurement of the dipole moment of difluorocyanamide. This method involved the application of a small modulation voltage clamped onto a variable, precisely known D.C. voltage, which was supplied by a Fluke 415B power supply. The modulation voltage, required to resolve the Stark component about to be measured, was selected. The zero field line was first measured and then the D.C. voltage was varied. The change in the pattern of the transition on application of a D.C. field is represented in Fig.2. For each D.C. voltage V, the frequency of the component corresponding to the D.C. voltage alone was measured. To keep the Stark lobe well defined, it was sometimes necessary to reduce the

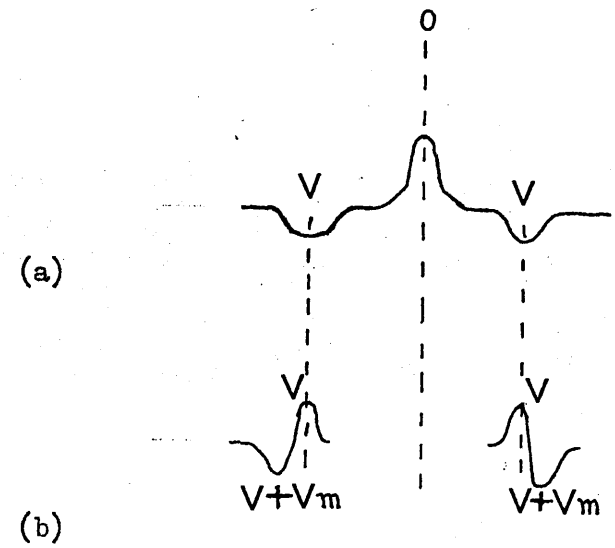

Fig.2. The Stark components of the $2_{02} - 1_{01}$ transition. (a) shows the usual Stark modulation pattern for a modulation voltage V and (b) shows the pattern produced when a D.C. voltage V and a small modulation voltage Vm is applied. As V is varied the distance from the zero field line 0 varies.

modulation voltage at high values of D.C. voltage.

The Stark components of the $2_{02} - 1_{01}$ and $3_{03} - 2_{02}$ ground-state transitions were studied for the determination of the dipole moment. The graphs of V^2 against frequency displacement were linear, thus verifying the expected quadratic nature of the Stark effect. The measured frequency shifts and voltages are shown in Table 3. The cell was calibrated by similar measurements of the Stark lobes of the J = 1 — 2 transition of OCS assuming its dipole moment as 0.7124 D (6). A cell constant C of 1.0743 MHz^2 $volts^{-2}$ $debye^{-2}$ was obtained.

The Stark perturbation coefficients were calculated as

Table 3.

The frequency shifts $\Delta\nu$ (MHz) at voltages V for the Stark components of the $2_{02} - 1_{01}$ and $3_{03} - 2_{02}$ transitions.

$2_{02} - 1_{01}$	M = 0	M = 0	
	$\Delta\nu$	$\Delta\nu$	$V^2 \times 10^{-4}$
	1.73	1.86	9
	3.33	3.46	16
	5.30	5.42	25
	7.64	7.91	36
	10.42	10.81	49
	13.67	14.36	64

$3_{03} - 2_{02}$	M = 0	M = 1	M = 2	
	$\Delta\nu$	$\Delta\nu$	$\Delta\nu$	$V^2 \times 10^{-4}$
			3.20	36
			4.47	49
	2.66	0.47	5.96	64
	3.38	0.61	7.65	81
	4.12	0.73	9.42	100
	5.05	0.88	11.38	121
	5.98	1.06		144
	7.02			169

described in Chapter 2 and are shown on the L.H.S. of equations (1). The expressions for the Stark effect displacements for the transitions studied were determined as

$2_{02} - 1_{01}$

$$M = 0 \qquad -1.9712\ \mu_a^2 + 0.9340\ \mu_c^2 = -1.9864$$

$$M = 1 \qquad +1.5922\ \mu_a^2 + 3.0895\ \mu_c^2 = +2.0255$$

$3_{03} - 2_{02}$

$$M = 0 \qquad -0.3536\ \mu_a^2 - 0.0554\ \mu_c^2 = -0.3863 \qquad \ldots(1)$$

$M = 1 \qquad -0.1157\ \mu_a^2 + 0.4964\ \mu_c^2 = -0.0687$

$M = 2 \qquad +0.5980\ \mu_a^2 + 2.1491\ \mu_c^2 = +0.8741$

Equations (1) were solved for μ_a^2 and μ_c^2, by means of the graph shown in Fig.3. The values were -

$$\mu_a = 1.03 \pm 0.01\ D \qquad \mu_c = 0.34 \pm 0.01\ D$$

$$\mu = 1.09\ D$$

The values for the dipole moment may be compared with those of the following molecules

	μ	μ_a	μ_b	μ_c	Ref.
NH_3	1.47				7
NF_2H	1.92		1.26	1.44	8
NF_2CH_3	2.57		2.54	0.44	9
NF_3	0.23				10
NH_2CN		4.34		0.86	11
NF_2CN	1.09	1.03		0.34	-

In each of these ammonia derivatives the presence of the lone-pair of electrons is expected to make a large contribution to the net dipole moment. The very low value observed for NF_3 is usually explained by a cancellation between the three N - F bond moments and the lone-pair moment. Therefore, because of the three electronegative substituents present in NF_2CN, its dipole moment is expected to be much reduced from that of NH_2CN, as was found. However, it is difficult to estimate dipole moments quantitatively in polyatomic

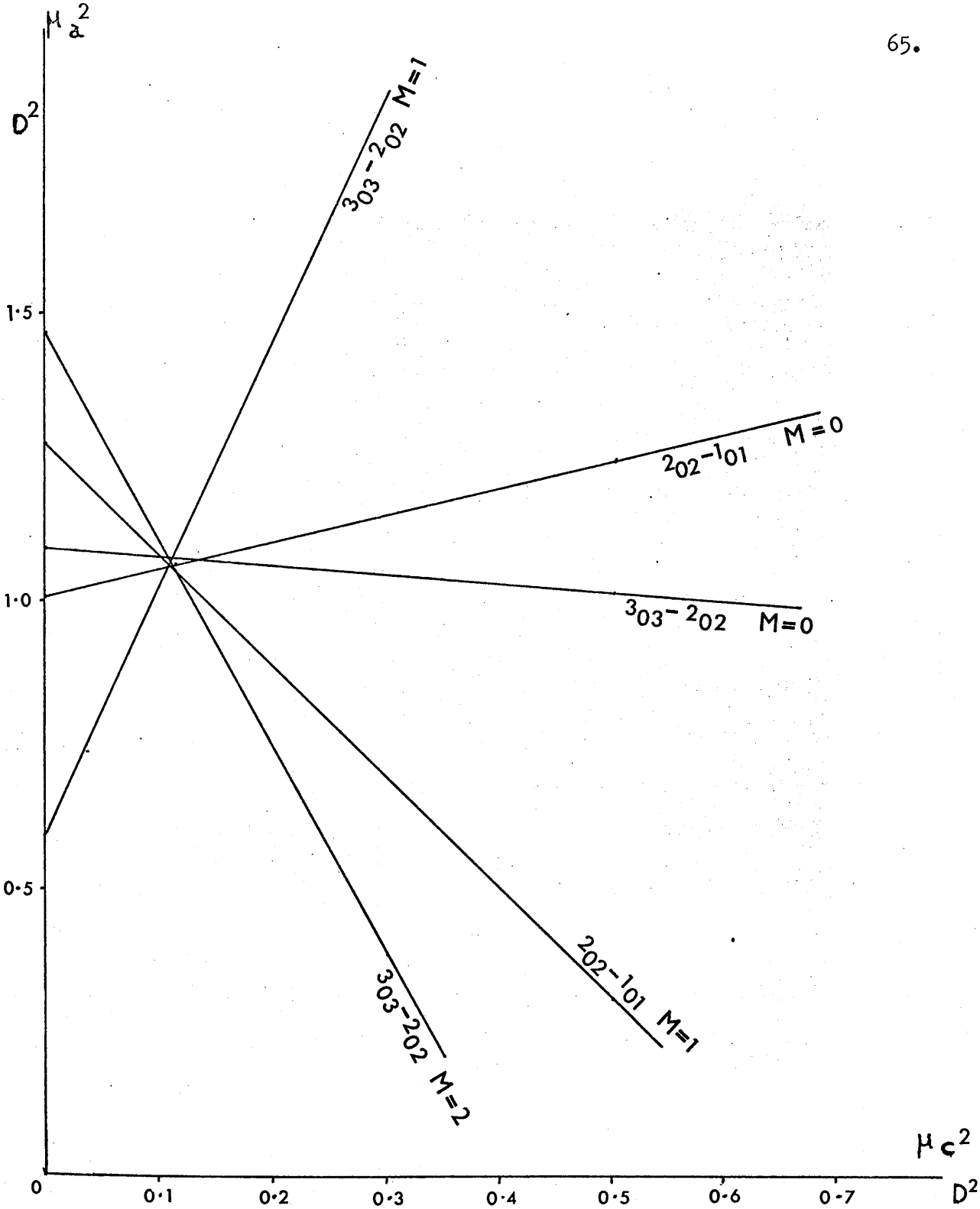

Fig.3. Dipole moment plot of equations (1) for NF_2CN.

molecules, since the electric dipole moment is determined by the charge distribution over the entire molecule and the changes in the dipole moment values of the above molecules, relative to one another, are not easily discussed.

4-4. Calculated Structure for NF_2CN.

Since only the rotational constants for the normal isotopic species have been determined, it is impossible to derive a completely unambiguous structure for NF_2CN. Nevertheless, by comparing the structures of NF_3 and NF_2H with the possible structures of NF_2CN, certain tentative conclusions may be reached. The F - F distance in NF_2CN is given by

$$2Z_F = \left(\frac{I_a + I_c - I_b}{M_F} \right)^{\frac{1}{2}}$$

where Z_F is the Z-coordinate of the fluorine atom and M_F is the atomic mass of fluorine. Hence the F - F distance was found to be 2.187 Å, and in Table 4 this result is compared with several others. Since the F - F distance in NF_2CN is very similar to that in NF_2H and

NF_2CH_3, it would seem that NF_2CN compares with the difluoro- compounds rather than NF_3

Table 4.

F - F distances in some related molecules (Å).

	F - F	Refs.
NF_3	2.134	4
NF_2H	2.190	8
NF_2NF_2	2.216	12
NF_2CH_3	2.181	9
NF_2CN	2.187	this work

The effect of nitrile substitution on the other bond lengths cannot as yet be determined exactly, but reasonable limits for the values of the bond lengths can be found in the following way. Assuming that NCN is linear, there are five parameters required to define the structure of the molecule. The structural assumptions made in the analysis were that r(C ≡ N) has a value of 1.159 Å (5,13) and that r(N - F) has a value of 1.400 Å as in NF_2H (Table 6). The value of r(N - C) was then varied until the calculated moments of inertia were the same as the observed moments. The calculation was then repeated using the value of 1.371 Å for r(N - F) taken from the microwave structure of NF_3 (Table 6). The two structures obtained for NF_2CN are shown in Table 5. The actual value of r(N - F) in NF_2CN is expected to be between the two values chosen, probably closer to the value of 1.400 Å obtained from NF_2H since, as mentioned earlier, NF_2CN probably resembles difluoro- compounds more

Table 5.

Structural parameters of NF_2CN.

amino nitrogen is N_1 ; cyanide nitrogen is N_2.

	Structure I	Structure II
assumed :		
$r(N_1 - F)$	1.400 Å	1.371 Å
$r(C - N_2)$	1.159 Å	1.159 Å
calculated :		
$r(N_1 - C)$	1.348 Å,	1.409 Å
$\angle FNF$	102° 42,	105° 48'
Φ	59° 21,	62° 36,
$\angle CNF$	108° 34	103° 16

moments of inertia :	calc.	calc.	obs.(a.m.u.Å^2)
I_a	49.910	49.914	49.910
I_b	113.299	113.299	113.299
I_c	154.271	154.267	154.271

ϕ is the angle between the HN_1H bisector and the $C - N_1$ bond extended. $(F_2N_1 - C \equiv N_2)$.

Table 6.

The microwave structures of NF_2H (8) and NF_3 (4).

NF_2H :

$r(N - F)$	1.400 Å,
$\angle FNF$	102° 54,
$\angle FNH$	98° 12

NF_3 :

$r(N - F)$	1.371 Å,
$\angle FNF$	102° 9'.

closely than NF_3. Also it has been observed in NF and CF compounds that successive fluorination leads to a successive shortening of N - F and C - F bonds respectively. Examples of this contraction on fluorination are given in Tables 6 and 7.

Table 7.

Parameters for several series of compounds containing fluorine (Å).

	C - F	C - H	C - C	Ref.
CH_3F	1.384	1.109		14
CH_2F_2	1.358	1.092		15
CHF_3	1.332	1.098		16
CH_3CH_3		1.094	1.534	17
CH_3CH_2F	1.398	1.095*	1.505	18
CH_3CF_3	1.348		1.492	19
CH_3CN				13
CF_3CN	1.335		1.461	19

* refers to the C - H bond in $-\overset{H}{\underset{H}{C}}-F$

It can also be seen from Table 7 that the attachment of fluorine atoms to a carbon atom reduces the bond lengths of other bonds to that carbon atom. It might, therefore, be expected that the value of $r(N_1 - C)$ in NF_2CN should be the same, or shorter, than that obtained in NH_2CN. (The bond length of N_1 - C was found to be 1.346 Å in NH_2CN (3)). This would again imply that the structure of NF_2CN is closer to that of Structure I rather than Structure II.

The value of 1.159 Å chosen for r(C ≡ N) in NF_2CN was obtained from the values of that bond found in X - CN (where X = H, CH_3, F, Cl, Br, I(5,13)). This assumes that the triple bond length is little affected by the wide variations in the nature of the attached groups. However, the accurate determination of the value of 1.153 Å for r(C ≡ N) in CF_3CN (19), raises the possibility that the value of r(C ≡ N) in NF_2CN may be shorter than 1.159 Å. Another example of a short triple bond was obtained in trifluoro-methyl acetylene (20), where the value of r(C ≡ C) was found to be 1.201 Å which is somewhat shorter than that found in methyl acetylene itself (14). However, difluorination may not result in a shortening of the nitrile bond from its characteristic value.

The angle ϕ of approximately 60° calculated for NF_2CN, is considerably larger, as expected, than the value of $37^\circ\ 58'$ obtained for NH_2CN (3).

4-5. ^{14}N- Quadrupole Coupling Constants.

In the case of NF_2CN, where there are two non-equivalent nitrogen quadrupolar nuclei, the analysis of the quadrupole fine structure was carried out using the first-order nuclear quadrupole coupling theory of Bardeen and Townes (21,22). Both nuclei were expected to display comparable couplings with the rotational motion of the molecule and all calculated splittings were obtained from the full secular determinants for each level of the transition. The determinants were solved by means of a computer program written by Macdonald (23). Since $I_1 = I_2 = 1$ the largest secular determinant was a 3 x 3.

Rough estimates were made of the magnitude and signs of the coupling constants for both nitrogen nuclei. The C - N_2 bond direction deviates by approximately 17° from the a- principal axis of the molecule and it was assumed that χ_{aa} ($= eQ \frac{\partial^2 V}{\partial \phi_a^2}$) for the cyanide ^{14}N, was equal to the coupling constant along the C - N_2 bond and that the field at the nitrogen was symmetric about the triple bond, that is $\chi_{bb} = \chi_{cc}$. A survey of cyanide molecules indicated a probable value of -4 MHz for χ_{aa}. For the amino ^{14}N a value of -8 MHz was assumed for the coupling constant in the direction of the lone pair, which was assumed to be in the direction of the c-axis of the molecule. Therefore, χ_{cc} = -8 MHz. The value of χ_{bb} of +6 MHz was that obtained for χ_{aa} in NF_2H (8). The estimated constants

were

amino ^{14}N : $\chi_{aa} = +2$ MHz $\chi_{bb} = +6$ MHz

cyanide ^{14}N : $\chi_{aa} = -4$ MHz $\chi_{bb} = +2$ MHz.

The quadrupole fine structure was measured for μ_a- and μ_c- type Q-branch transitions of sufficient intensity to provide a good signal-to-noise ratio. Using a computer program by Beaudet for the rigid-rotor asymmetric top, and the values of the rotational constants and dipole moment components, the μ_a- and μ_c- type frequencies, line strengths and relative intensities were calculated for the transitions of NF_2CN in the range 10 - 40 GHz. The relative intensity of a transition of an asymmetric top (24) is essentially, in the absence of nuclear spin effects

$$\text{Rel. Int.} = {}^{g}S_{J_T\, J_{T'}}\ e^{-W/kT}\ \nu^2 \left|\mu_g\right|^2$$

where $e^{-W/kT}$ is the Boltzmann factor,

ν is the frequency in MHz,

μ_g is the dipole moment coupling the transition,

W is the energy of the lower J level,

and S is the line strength of the transition $J_T - J_{T'}$.

Transitions with a calculated relative intensity less than 1.2 were considered too weak for accurate measurement. In order to obtain a closer prediction of the positions of the high J Q-branch transitions, the A rotational constant was altered to make some

allowance for centrifugal distortion effects. Having assigned the $6_{15}\leftarrow 6_{16}$, $7_{16}\leftarrow 7_{17}$, $8_{26}\leftarrow 8_{27}$ and $9_{27}\leftarrow 9_{28}$ transitions, the values of $\nu/\Delta E(K)$ $\left(=\frac{A-C}{2}\right)$ were plotted against a range of K for each transition. Since transitions within a series (for example $J_{1(J-1)} \leftarrow J_{1J}$) were found to give almost identical lines, a graph was drawn using only the $6_{15}\leftarrow 6_{16}$ and $8_{26}\leftarrow 8_{27}$ transitions. The frequency ν of both transitions were taken as their line centre, as each transition was observed as a doublet. The values of $\frac{A-C}{2}$ and K at the point of intersection were used to obtain a different value for A and the line frequencies were recalculated ($\nu^{(2)}$ in Table 8). The ground-state Q-branch transitions for which quadrupole splittings have been measured are

μ_a-type : 5_{14}-5_{15}, 6_{15}-6_{16}, 7_{16}-7_{17}, 8_{17}-8_{18}, 8_{26}-8_{27}, 9_{27}-9_{28}, 10_{28}-10_{29}, 10_{37}-10_{38}.

μ_c-type : 7_{35}-7_{25}, 9_{46}-9_{36}, 10_{47}-10_{37}.

The observed and calculated frequencies of the centres of these transitions are given in Table 8.

The similarity of the patterns observed for the Q-branch transitions was expected, since $\Delta F = 0$, $\Delta F_1 = 0$, $\Delta F_2 = 0$ components are the most intense, and they become relatively more intense as J increases. Thus, at high J all the Q-branch lines have a similar pattern and differ mainly in their spread. At very high J for transitions of the same series, the spread of the quadrupole patterns

Table 8.

The observed frequencies of the line centres of the Q-branch transitions compared with their calculated values.

	$\nu_{obs.}$	$\nu^{(1)}_{calc.}$	$\nu^{(2)}_{calc.}$
$5_{14}-5_{15}$ *	17374.17	17375.31	17373.89
$6_{15}-6_{16}$	23726.76	23729.16	23726.74
$7_{16}-7_{17}$	30469.43	30473.76	30469.79
$8_{17}-8_{18}$	37260.37	37267.49	37261.15
$8_{26}-8_{27}$	20162.53	20160.71	20162.84
$9_{27}-9_{28}$	27164.22	27163.71	27165.19
$10_{28}-10_{29}$	34659.33	34661.46	34661.51
$10_{37}-10_{38}$	14726.79	14745.80	14752.04
$7_{35}-7_{25}$	21844.23	21866.44	21849.37
$9_{35}-9_{25}$	35479.72	35517.46	35491.48
$10_{47}-10_{37}$	31471.45	31511.89	31485.47

Rotational constants :

A	10132.66	10129.4
B	4462.03	4462.03
C	3276.80	3276.80
$\frac{A-C}{2}$	3427.93	3426.3
$\frac{A+C}{2}$	6704.73	6703.1
κ	-0.65424	-0.6541

$\nu^{(1)}_{(2)}$ transition frequencies calculated using Beaudet's program, " " " " the values of $\frac{A-C}{2}$ and κ obtained from a μ_a Q-branch graph.

* the centre of this triplet transition was taken as the centre of the two outermost component lines.

become the same. For NF_2CN the J values studied were not high enough to observe this "steady state". Fig.4 shows two Q-branch transitions, each split into doublets by the quadrupole hyperfine interaction.

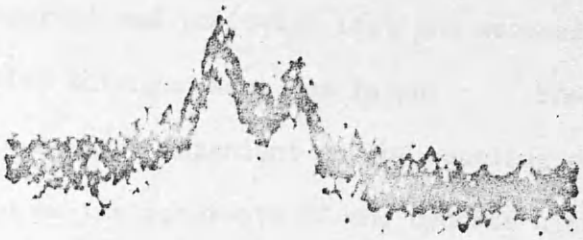

(a) $8_{17} \leftarrow 8_{18}$.

(b) $10_{28} \leftarrow 10_{29}$.

$\leftarrow \nu$

Fig.4. Quadrupole hyperfine splitting of two ground-state transitions of NF_2CN.

The assumed values, given above, produced doublet splittings fairly close to those observed and indicated that the assumed values for χ_{aa} and χ_{bb} of the amino nitrogen were too large. The Q-branch doublet splitting proved to be more dependent on the coupling constants of the amino nitrogen than on the constants of the cyanide nitrogen. With zero coupling constants for the cyanide nitrogen the Q-branch splittings only changed by 0.03 MHz.

As the 1_{01}-0_{00} transition was too weak for a frequency measurement, the fine structure pattern of the 2_{02}-1_{01} line was measured. The remaining J = 1 - 2 R-branch transitions were also too weak for a study of their hyperfine structure. R-branch transitions give patterns which change irregularly with slight changes in the coupling constants and rotational parameters and therefore should define the coupling constants more closely than the Q-branch transitions. The selection rules are $\Delta F = 0 \pm 1$, $\Delta F_1 = 0 \pm 1$, $\Delta F_2 = 0 \pm 1$. The number and type of lines within the pattern of the 2_{02}-1_{01} transition can be obtained from the qualitative correlation diagrams for the 1_{01} and the 2_{02} levels (Fig.5). Using these diagrams, F_1 and F_2 values can be readily assigned to the quadrupole coupling energies calculated by the computer program. The left-hand ordinate in the diagram represents the case where $\chi_{aa}(1)$ is positive and $\chi_{aa}(2)$ is zero, while the right-hand ordinate represents the case where $\chi_{aa}(1)$ is zero and $\chi_{aa}(2)$ is a negative quantity. The approximate relative intensities for the hyperfine components were obtained as described in Townes and Schawlow(25).

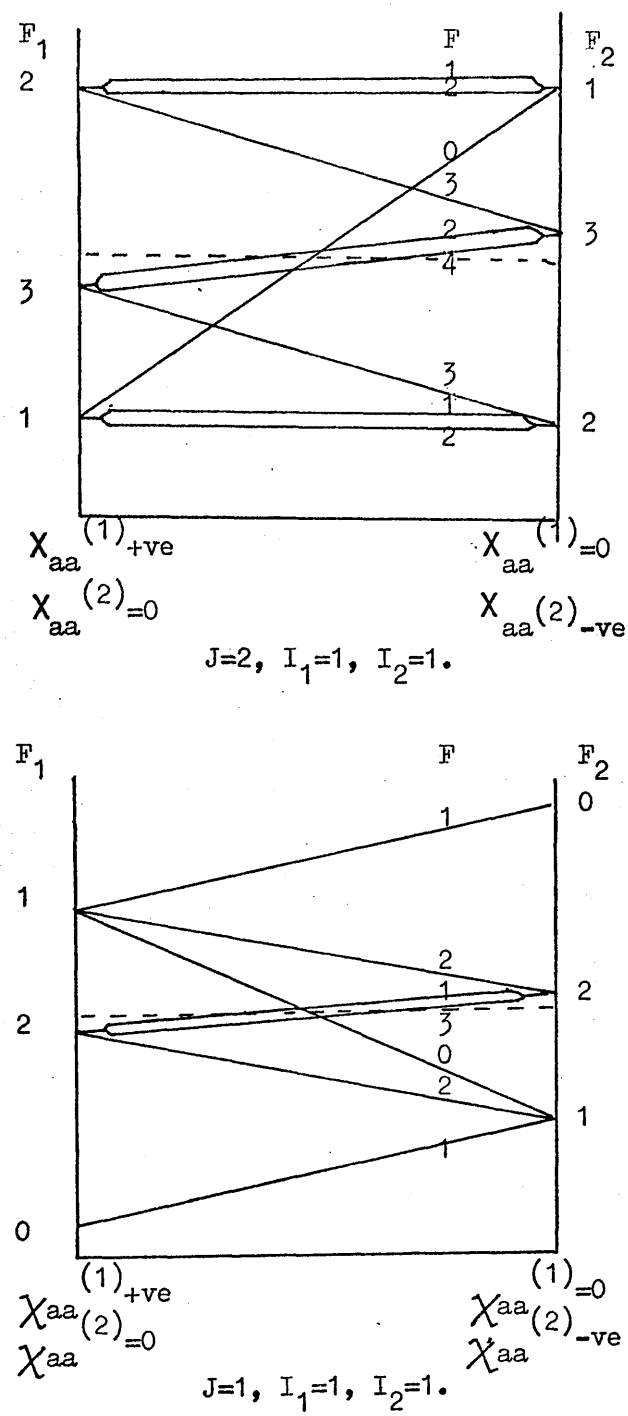

Fig.5. Qualitative correlation diagram for the 1_{01} and 2_{02} levels of NF_2CN.

Coupling constants were fitted by an iterative procedure, the calculated intensities and fine structure splittings being compared with the observed quadrupole pattern. The final set of coupling constants were obtained from the 2_{02}-1_{01} transition and the observed Q-branch transitions and have the following values

N_1 : χ_{aa} = 1.0 ± 0.2 MHz χ_{bb} = 5.5 ± 0.2 MHz,

N_2 : χ_{aa} = -4.0 ± 0.4 MHz χ_{bb} = 2.0 ± 0.4 MHz.

For the final set of coupling constants the calculated and observed fine structure patterns for the 2_{02}-1_{01} transition are given in Fig.6. The calculated line shape was obtained from triangular-shaped component lines each of the same width at half intensity. These are then added together to produce the final line shape. The measured and calculated splittings for the transitions studied are given in Table 9. The observed quadrupole splittings for the 2_{02}-1_{01} transition can be compared with the calculated hyperfine structure for the cases of only one nuclei coupling with the rotational motion (Fig.7). Fig.7. shows that for this transition the cyanide nitrogen determines the overall spread of the component lines.

As mentioned earlier the amino nitrogen is responsible for the doublet structure found in the Q-branch spectrum of NF_2CN. However, in the case of NH_2CN the Q-branch spectrum showed quartet structure. Thus, the asymmetry of the field gradient around the C - N_2 bond in NH_2CN causes a small splitting of each member of the doublet and hence,

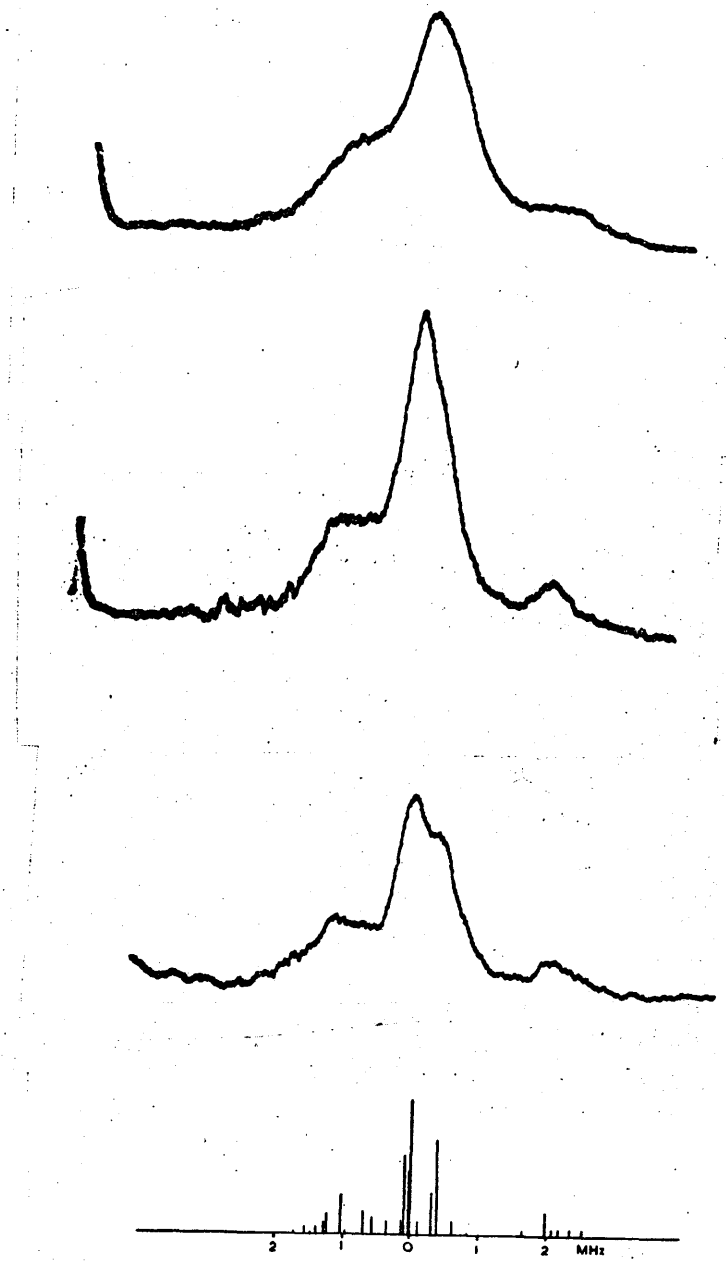

Fig.6. Hyperfine structure of the 2_{02}-1_{01} transition of NF_2CN. Upper curves show experimental observations as sample pressure in the cell is reduced and bottom part of figure shows the theoretical structure.

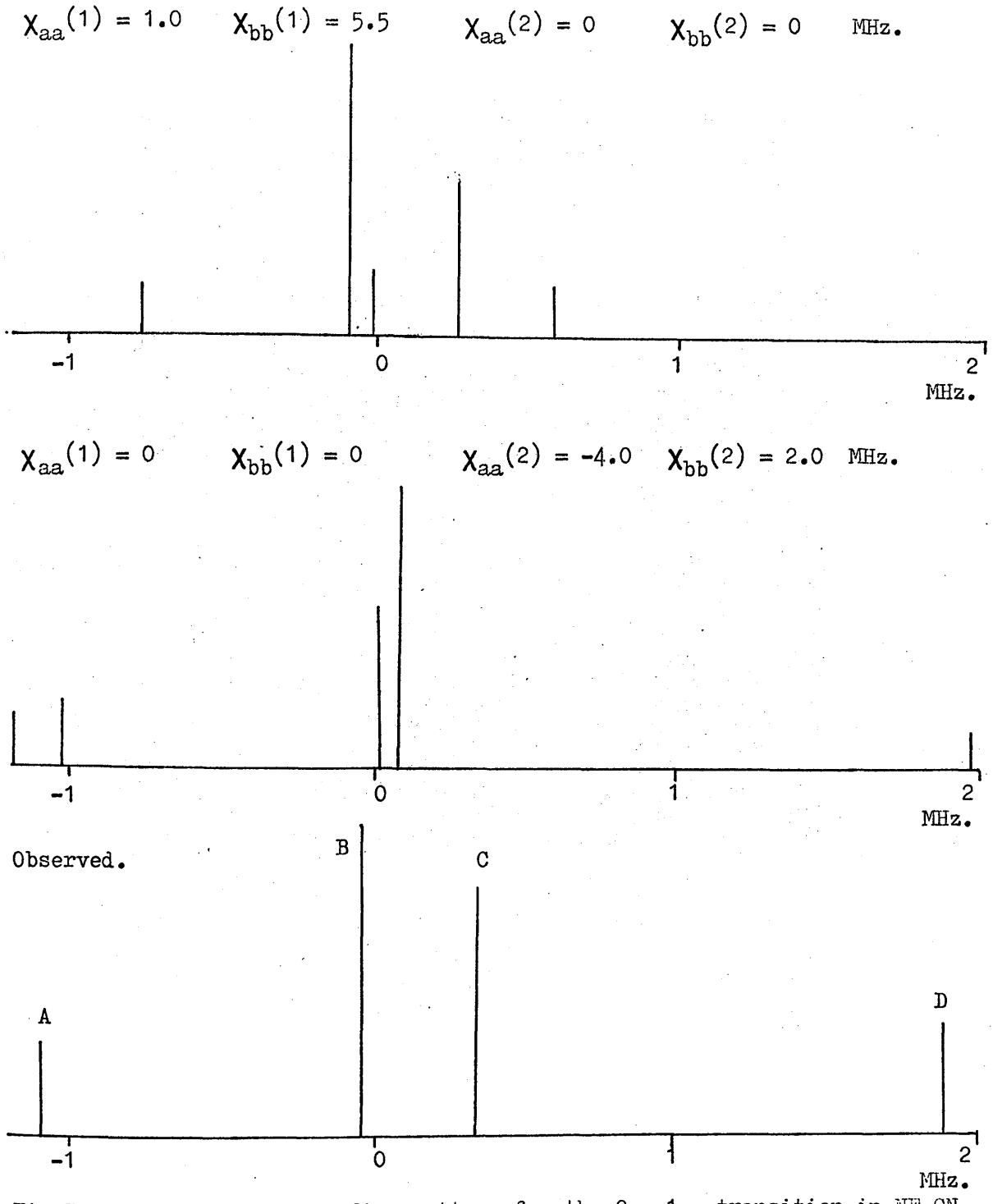

Fig.7. The observed hyperfine pattern for the 2_{02}-1_{01} transition in NF_2CN and the theoretical patterns for the two hypothetical cases of only one nucleus coupling with the rotational motion.

Table 9.

Observed and calculated ^{14}N-quadrupole splittings for NF_2CN (MHz).

Amino N : χ_{aa} = 1.0 MHz χ_{bb} = 5.5 MHz

Cyanide N : χ_{aa} = -4.0 MHz χ_{bb} = 2.0 MHz.

	Peak	$\Delta\nu_{obs.}$	$\Delta\nu_{calc.}$	$\Delta(\Delta\nu)$
$5_{14} - 5_{15}$ *		4.06	3.76	0.30
		0.69	0.75	-0.06
$6_{15} - 6_{16}$		4.01	3.95	0.06
$7_{16} - 7_{17}$		3.60	3.57	0.03
$8_{17} - 8_{18}$		2.98	3.14	-0.16
$8_{26} - 8_{27}$		3.11	2.96	0.15
$9_{27} - 9_{28}$		2.91	3.04	-0.13
$10_{28} - 10_{29}$		2.75	2.72	0.03
$10_{37} - 10_{38}$		2.13	2.11	0.02
$7_{35} - 7_{25}$		1.75	1.70	0.05
$9_{46} - 9_{36}$		1.25	1.25	0.00
$10_{47} - 10_{37}$		1.38	1.50	-0.12
$2_{02} - 1_{01}$	A	1.04	1.11	-0.07
	B	0.38	0.39	-0.01
	C	1.57	1.66	-0.09
	D			

* observed as a triplet
spacings are between peaks in the direction of increasing frequency.

from the appearance of the Q-branch spectrum of NF_2CN, a marked asymmetry of the field gradient around the C - N_2 bond would not be expected. The NH_2CN quadrupole coupling constants are (3).

N_1 : χ_{aa} = 3.05 MHz χ_{bb} = 1.85 MHz

N_2 : χ_{aa} = -3.30 MHz χ_{bb} = 2.86 MHz

and, particularly in the case of the amino nitrogen these show a marked dissimilarity from the coupling constants of NF_2CN.

A comparison of χ_{cc} for NF_2CN with the coupling constant in the direction of the lone-pair in related symmetric top molecules indicates the correct order of magnitude for the field gradient in the direction of the lone-pair.

	χ(MHz)	
NF_2CN	-6.5	
NH_3	-4.1	
$N(CH_3)_3$	-5.5	
NF_3	-7.1	Ref.(26).

References.

1. M. D. Meyers and S. Frank, Inorg. Chem., 5, 1455 (1966).

2. N. B. Colthup, Spectrochim. Acta., 23A, 2167 (1967).

3. J. N. Macdonald, D. Taylor, J. K. Tyler and J. Sheridan, J. Mol. Spec., 26, 285 (1968).

4. J. Sheridan and W. J. Gordy, Phys. Rev., 79, 513 (1950).

5. J. K. Tyler and J. Sheridan, Trans. of Farad. Soc., 59, 2661 (1963).

6. S. A. Marshall and J. Weber, Phys Rev., 105, 1502 (1957).

7. D. K. Coles, W. E. Good, J. K. Bragg and A. H. Sharbaugh, Phys. Rev., 82, 877 (1951).

8. D. R. Lide, Jr., J. Chem. Phys., 38, 456 (1963).

9. L. Pierce, R. G. Hayes and J. F. Beecher, J. Chem. Phys., 46, 4352 (1967).

10. (a) S. N. Ghosh, R. Trambarulo and W. J. Gordy, J. Chem. Phys., 21, 308 (1953) ; Phys. Rev., 87, 172A (1952).
(b) P. Kisluik, J. Chem. Phys., 22, 86 (1954).

11. (a) J. K. Tyler, Ph.D. Thesis, University of Birmingham (1960).
(b) J. N. Macdonald, Ph.D. Thesis, University of Glasgow (1969).

12. D. R. Lide, Jr. and D. E. Mann, J. Chem. Phys., 31, 1129 (1959).

13. L. F. Thomas, E. I. Sherrard and J. Sheridan, Trans. of Farad. Soc., 51, 619 (1955).

14. C. C. Costain, J. Chem. Phys., 29, 864 (1958).

15. D. R. Lide, Jr., J. Am. Chem. Soc., 74, 3548 (1952).

16. S. N. Ghosh, R. Trambarulo and W. Gordy, J. Chem. Phys., 20, 605 (1952).

17. D. E. Shaw, D. W. lepard and H. L. Welsh, J. Chem. Phys., 42, 3736 (1965).

18. L. Nygaard, Spectrochem. Acta., 22, 1261 (1966).

19. L. F. Thomas, J. S. Heeks and J. Sheridan, Z. Electrochem. 61, 935 (1957).

20. J. N. Shoolery, R. G. Shulman, W. E. Sheehan, V. Shomaker and D. M. Yost, J. Chem. Phys., 19, 1364 (1951).

21. J. Bardeen and C. H. Townes, Phys. Rev., 73, 97 (1948).

22. C. H. Townes and A. L. Shawlow, "Microwave Spectroscopy", McGraw-Hill Book Co., P.165.

23. J. N. Macdonald, Ph.D. Thesis, University of Glasgow (1969).

24. C. H. Townes and A. L. Schawlow, "Microwave Spectroscopy", McGraw-Hill Book Co., P.92 -102.

25. C. H. Townes and A. L. Schawlow, "Microwave Spectroscopy", McGraw-Hill Book Co., P.172.

26. "Microwave Spectral Tables, Polyatomic Molecules Without Internal Rotation", National Bureau of Standards, Monograph 70, Vol IV.

CHAPTER 5.

DIMETHYLCYANAMIDE : A PRELIMINARY STUDY OF THE MICROWAVE SPECTRUM.

5-1. Introduction.

In recent years the barriers to internal rotation of methyl groups in a large variety of molecules have been measured by microwave spectroscopy. However, one class of molecules has proved difficult to study, namely the high barrier non-planar two equivalent top case. In these molecules higher torsional states than the ground-state must be studied in order to determine the barrier to internal rotation of two methyl tops.

Since the values of the barrier heights in other non-planar two methyl top molecules proved to be high, the value in dimethylcyanamide was also expected to be high. However, in certain one top molecules, lower values of barrier height than expected were determined. These lower values have previously been accounted for by the presence of resonance forms of the molecule. In the two examples of planar molecules, given below, the resonance form tended to make the structure more linear. Planar molecules are associated with lower values of the barrier height to internal rotation than non-planar molecules and, in turn, linear molecules are associated with lower barrier height values than ~~linear~~ planar molecules. The following molecules show two examples of lower than expected barrier height values.

		V_3(cal/mole)	Ref.
N-methyl methylenimine	$CH_3 - N = CH_2$	1970	1
methyl isocyanate	$CH_3 - N = C = O$	50	2
propylene	$CH_3 - CH = CH_2$	1980	3
methyl ketene	$CH_3 - CH = C = O$	1200	4

In methyl isocyanate the resonance forms are

$$CH_3 \diagup N = C = O \quad \longleftrightarrow \quad CH_3 - \overset{+}{N} \equiv C - \overset{-}{O}$$

The structures of dimethylcyanamide and cyanamide can be represented by the resonance forms

$$X_2N - C \equiv N \quad \longleftrightarrow \quad X_2\overset{+}{N} = C = \overset{-}{N}$$

I II

where X = hydrogen atom or methyl group.

The contribution of form II to the structure of cyanamide has, in the main, accounted for the observed quadrupole structure. It can be estimated that the contribution from resonance form II to the structure of dimethylcyanamide should be as much as, or greater than, its contribution in cyanamide, using the fact that methyl groups can act as electron donors. It was hoped that a contribution from the planar resonance form II would produce a lowering of the barrier height for internal rotation of the methyl groups and thereby enable

torsional splittings of the ground-state transitions to be observed. If no splitting is observed in the ground-state then higher torsional states must be studied to determine the barrier and this involves a more complicated approach which could not be undertaken here. The study of higher torsional states involves the analysis of much weaker lines than the ground-state transitions.

If the lone-pair is localised on the nitrogen its configuration would be approximately tetrahedral. From rough calculations of the moments of inertia and by a comparison of these with the observed moments it was estimated that the configuration of the nitrogen is very like that in cyanamide, showing a reduction from tetrahedral towards a planar configuration. Only a-type dipole transitions were observed and the c-type dipole moment was calculated as zero. The geometry of the molecule must be such as to produce a zero dipole moment along the c-axis. The dipole moment was calculated as $\mu = \mu_a = 4.71 \pm 0.1$ D.

5-2. Nature of Spectra of $(CH_3)_2NCN$ and $(CD_3)_2NCN$.

Dimethylcyanamide was prepared by refluxing sodium cyanamide and methyl iodide in ethanol (as described in Chapter 7). During distillation the dimethylcyanamide was collected as several consecutive samples and the infrared spectra of these were found to compare well with those reported by Davies and Jones (5). Examination of these spectra also indicated the presence of ethanol and this was observed to decrease in the higher boiling fractions. The n.m.r. spectrum of the purest sample in CCl_4 consisted of one peak at $\delta = 2.9$ P.P.M. The deuterated sample was prepared as above using CD_3I previously prepared from CD_3OD (Chapter 7).

Dimethylcyanamide melts at -42°C and boils at 163°C. All measurements were made with the sample at room temperature as it was not possible to observe lines much below this temperature. The sample decomposed slowly at room temperature and the rate of decomposition was observed to increase with rise in temperature. The decomposition products were not identified. To avoid, or at least retard, possible decomposition of the sample it was stored at dry ice temperatures in a blackened tube. The deuterated sample was studied under the same conditions.

Models were constructed for both $(CH_3)_2NCN$ and $(CD_3)_2NCN$ in order to predict the μ_a R-branch transitions. The models were based on the cyanamide microwave structure (6) in which the protons were

replaced with idealised methyl groups and with a methyl-N distance of 1.47 Å (7). Based on these predictions, and on the observed Stark effects, the ground-state a-type lines were assigned. In both samples each R-branch transition was surrounded, for a spread of 100-200 MHz, by many weaker satellites. Ethanol transitions were also observed. The ground-state transitions were broad ($\sim$3 - 4 MHz at half-intensity) and some structure could be observed on several of the lines, although none were resolved sufficiently for measurement. There are two nitrogen quadrupolar nuclei and the spread of the quadrupole structure is estimated as less than 2 MHz for the J = 3 - 2 and 4 - 3 transitions studied. The spread of the quadrupole structure of NH_2CN for the $1_{01} - 0_{00}$ transition is approximately 4 MHz, and of NF_2CN for the $2_{02} - 1_{01}$ transition approximately 3 MHz. In dimethylcyanamide there were several strong satellites accompanying each ground-state transition and to low frequency of the ground-state lines there were a number of weaker lines. Many of the latter are probably due to molecules in excited torsional states. It was hoped to assign some of the stronger satellites to higher excited-states of vibrational deformation modes of the molecule. For the heavier deuterated sample the internal rotation splittings of all the torsional states are reduced from that of the normal sample. It was hoped that this would give the spectrum of the deuterated species a simpler appearance. This was observed to be the case. There were more stronger satellites observed accompanying the ground-state transitions

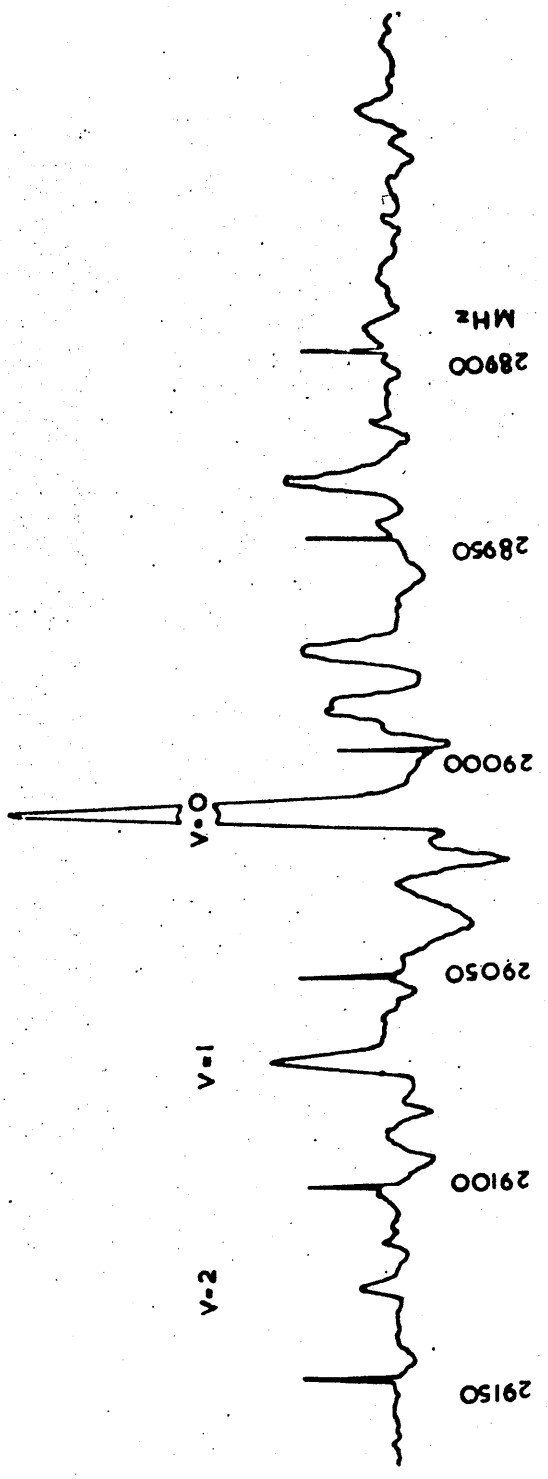

Fig.1(a). The $4_{23} - 3_{22}$ transition of $(CH_3)_2NCN$.

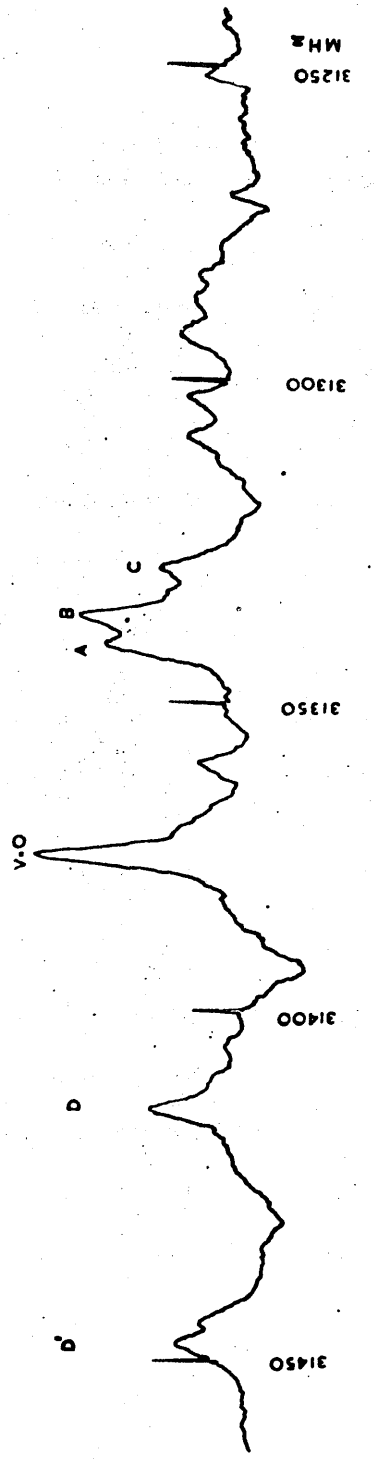

Fig.1(b). The $5_{24} - 4_{23}$ transition of $(CD_3)_2NCN$.

and the strongest satellite line was stronger, relative to the respective ground-states, than that observed in the normal species. To low frequency, a triplet structure could be identified from one ground-state transition to the next. Again, there were weaker satellites to low frequency of the ground-state. Fig.1 shows one of the transitions of simpler appearance of $(CH_3)_2NCN$ and $(CD_3)_2NCN$.

The frequencies and rotational constants of the observed ground-state transitions of $(CH_3)_2NCN$ and $(CD_3)_2NCN$ are given in Table 1 and 2 respectively. A search was made for the J = 1 - 2 μ_c transitions but these were not observed.

In cyanamide the angle ϕ, indicated in the diagram below, has

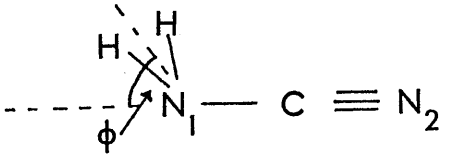

been shown to have a value of 38° 19' (6), and this angle can be taken as an indication of the extent of non-planarity in dimethylcyanamide. The moments of inertia were calculated for dimethylcyanamide by means of three structural models. In each of these the methyl-N distance was taken as 1.47 Å, the methyl groups were assumed to be tetrahedral with a C - H bond distance of 1.09 Å and the remaining bond length values were those of cyanamide (6). The first model was planar and therefore $\phi = 0°$, the second model assumed $\phi = 30°$ and the third model had a tetrahedral configuration for the nitrogen with $\phi = 54° 44'$ The calculated moments of inertia together with the observed are given

Table 1.

The observed transition frequencies and rotational constants for the ground-state of $(CH_3)_2$ NCN.

	observed	$\nu_{obs} - \nu_{calc}$ (MHz)
$3_{03} - 2_{02}$	21083.87	+0.05
$3_{13} - 2_{12}$	19935.79	+0.36
$3_{12} - 2_{11}$	23581.98	+0.03
$3_{22} - 2_{21}$	21893.65	+0.46
$3_{21} - 2_{20}$	22702.43	-0.14
$4_{04} - 3_{03}$	27368.13	-0.09
$4_{14} - 3_{13}$	26381.38	+0.15
$4_{13} - 3_{12}$	31137.15	+0.26
$4_{23} - 3_{22}$	29024.74	+0.02
$4_{22} - 3_{21}$	30845.16	-0.13
$4_{32} - 3_{31}$	29553.59	-0.41
$5_{05} - 4_{04}$	33390.77	-0.33
$5_{15} - 4_{14}$	32711.36	+0.02
$\frac{A+C}{2}$	5962.25	
$\frac{A-C}{2}$	2925.04	
K	-0.58178	
A	8887.29	
B	4260.52	
C	3037.21	
Ia	56.8825	
Ib	118.6548	
Ic	166.4458	
Δ	-9.0915	

Δ = Ic - Ia - Ib.

Ia, Ib, Ic and Δ are in units of a.m.u.Å^2.

Table 2.

The observed transition frequencies and rotational constants for the ground-state of $(CD_3)_2$ NCN.

	observed	$\nu_{obs} - \nu_{calc}$ (MHz)
$3_{12} - 2_{11}$	20762.10	+0.06
$3_{21} - 2_{20}$	20267.84	-0.07
$4_{04} - 3_{03}$	23401.55	-0.12
$4_{14} - 3_{13}$	22804.64	+0.12
$4_{13} - 3_{12}$	27231.29	+0.19
$4_{23} - 3_{22}$	25387.51	-0.06
$4_{32} - 3_{31}$	26081.36	+0.27
$5_{05} - 4_{04}$	28520.54	-0.05
$5_{15} - 4_{14}$	28200.88	+0.06
$5_{14} - 4_{13}$	33223.85	-0.15
$5_{24} - 4_{23}$	31381.16	+0.18
$5_{23} - 4_{22}$	34832.73	+0.04
$5_{33} - 4_{32}$	32627.87	-0.18
$6_{32} - 5_{31}$	33468.30	-0.16
$6_{06} - 5_{05}$	33662.37	-0.14
$6_{16} - 5_{15}$	33516.26	+0.10
$\frac{A+C}{2}$	4658.18	
$\frac{A-C}{2}$	2042.65	
κ	-0.42581	
A	6700.82	
B	3788.39	
C	2615.53	
Ia	75.4431	
Ib	133.4422	
Ic	193.2808	
Δ	-15.6045	

$\Delta = Ic - Ia - Ib.$

Ia, Ib, Ic and Δ are in units of a.m.u.$\AA^2$.

Table 3.

Calculated and observed moments of inertia for dimethylcyanamide (a.m.u.$\AA^2$).

	∠MeNMe	I_a	I_b	I_c	Δ
$\phi = 0^\circ$	120°	57.97	122.26	173.90	-6.33
$\phi = 30^\circ$	114°	56.07	121.97	169.47	-8.57
$\phi = 54^\circ\ 44'$	$109^\circ\ 28'$	55.80	116.45	158.78	-13.47
observed		56.88	118.66	166.45	-9.09

in Table 3. By comparing the values in Table 3 a rough estimation can be made of the configuration of the nitrogen atom. The intermediate configuration ($\phi = 30^\circ$) gives values which closer approximate to the observed. Therefore, the configuration of the nitrogen resembles cyanamide and also shows some involvement of the lone-pair electrons away from the nitrogen.

5-3. Internal Rotation. General Theory.

The restricted rotation of a threefold symmetric top, with respect to the bond it forms with the remainder of the molecule, gives rise to a threefold potential barrier. This potential energy function can be described in terms of the barrier height and the relative angle of internal rotation α. For molecules containing two equivalent methyl internal rotors there is a ninefold potential barrier with ninefold degeneracy in the ground-state in the limit of an infinite barrier.

By means of group theory it is possible to obtain the symmetry species of the various energy levels, their degeneracies, and the selection rules governing the transitions. The general theory for two methyl internal rotational groups, along with the appropriate group theory, has been given by Sage (8) for 2,3- epoxybutane (point group C_S) and by Myers and Wilson (9) for acetone (point group C_{2V}) The Hamiltonian for the two top problem is described in several references eg. (8,9,10,11).

For a C_S molecule with two methyl groups the Hamiltonian is not invariant to a twofold rotation about any of the principal axes, due to changes in α_1 and α_2 (where α_k is the angle of internal rotation for the k th top). The symmetry group under which the Hamiltonian is invariant is generated by the three operations $C_3(1)$, $C_3(2)$ and C_{2b} (8). If, instead of α_1 and α_2, $(\alpha_1 + \alpha_2)$ and $(\alpha_1 - \alpha_2)$ are used

it can be shown that the subgroup $C_3(1)$, $C_3^2(2)$ acts on $(a_1 - a_2)$ only, and the subgroup $C_3(1)$, $C_3(2)$, C_{2b} acts on $(a_1 + a_2)$ and the Eulerian angles. These two groups are C_3 and C_{3V} respectively and give the over-all symmetry group of the molecule as $S = C_3 \times C_{3V}$. The symmetry classes of S can be obtained directly from those of C_3 and C_{3V} and the character table of S can be obtained by a direct product of the character tables of C_3 and C_{3V} (8).

The representations of S are AA_1, AA_2 (one-dimensional), AE (two-dimensional), E_0A_1, E_0A_2 (pseudo two-dimensional) and E_0E (pseudo four-dimensional). The dipole moment is of species AA_2, allowing the transitions $AA_1 \leftrightarrow AA_2$, $AE \leftrightarrow AE$, $E_0A_1 \leftrightarrow E_0A_2$ and $E_0E \leftrightarrow E_0E$ - since the product of the species of two combining levels and A_1A_2 must belong to A_1A_1. For high barriers the zero-order torsional energy levels are ninefold degenerate when $v = v^1$, and eighteenfold degenerate when $v \neq v^1$ (where v^k is the principal torsional number of the k th top). It can be shown (8) that, when $v = v^1$, the nine functions contain the irreducible representations AA_1, AE, E_0A_1 and E_0E and, when $v \neq v^1$, the eighteen functions contain the irreducible representations AA_1, AA_2, E_0A_1 and E_0A_1 once each and AE and E_0E twice each. Thus, in general, the rotational spectrum would consist of quartets for torsional states with $v = v^1$ and octets for rotational states with $v \neq v^1$. While in general the rotational spectra will consist of quartets ($v = v^1$), very often symmetrical triplets are observed. The magnitude of the splitting of the

torsional sublevels increases as barrier height values decrease until the limit of free rotation is reached.

Using a computer program written by Woods (12) for a solution of the n-top problem, the quartet spacings were obtained for several chosen values of barrier height. The method adopted by Woods is an extension of the internal axis method and considers only the ground-state of the molecule. Fig.3 shows the calculated quartet structure for several transitions, each having values of 500, 1000 and 1500 cal/mole for the barrier to internal rotation. The computational input was simplified, without greatly affecting the resultant spacing, by the assumption that dimethylcyanamide is planar. Fig.3 suggests that for a barrier greater than 1500 cal/mole the observed spectrum of dimethylcyanamide would show no quartet or triplet structure in the ground-state.

The values of the barrier height to internal rotation which have been found for several non-planar molecules with two methyl tops are shown in Table 4. It is reasonable to assume that the expected magnitude of the barrier height for dimethylcyanamide (ignoring any reduction in the expected value because of resonance forms of the molecule) would be similar to the values in Table 4 for the molecules in which the central atom is carbon, nitrogen or oxygen. Therefore the expected value would be around 3000 cal/mole. If the fact that dimethylcyanamide is more planar than $(CH_3)_2NH$ produces a lower value, for example 2000 cal/mole, then from Fig.3 no observed splitting would

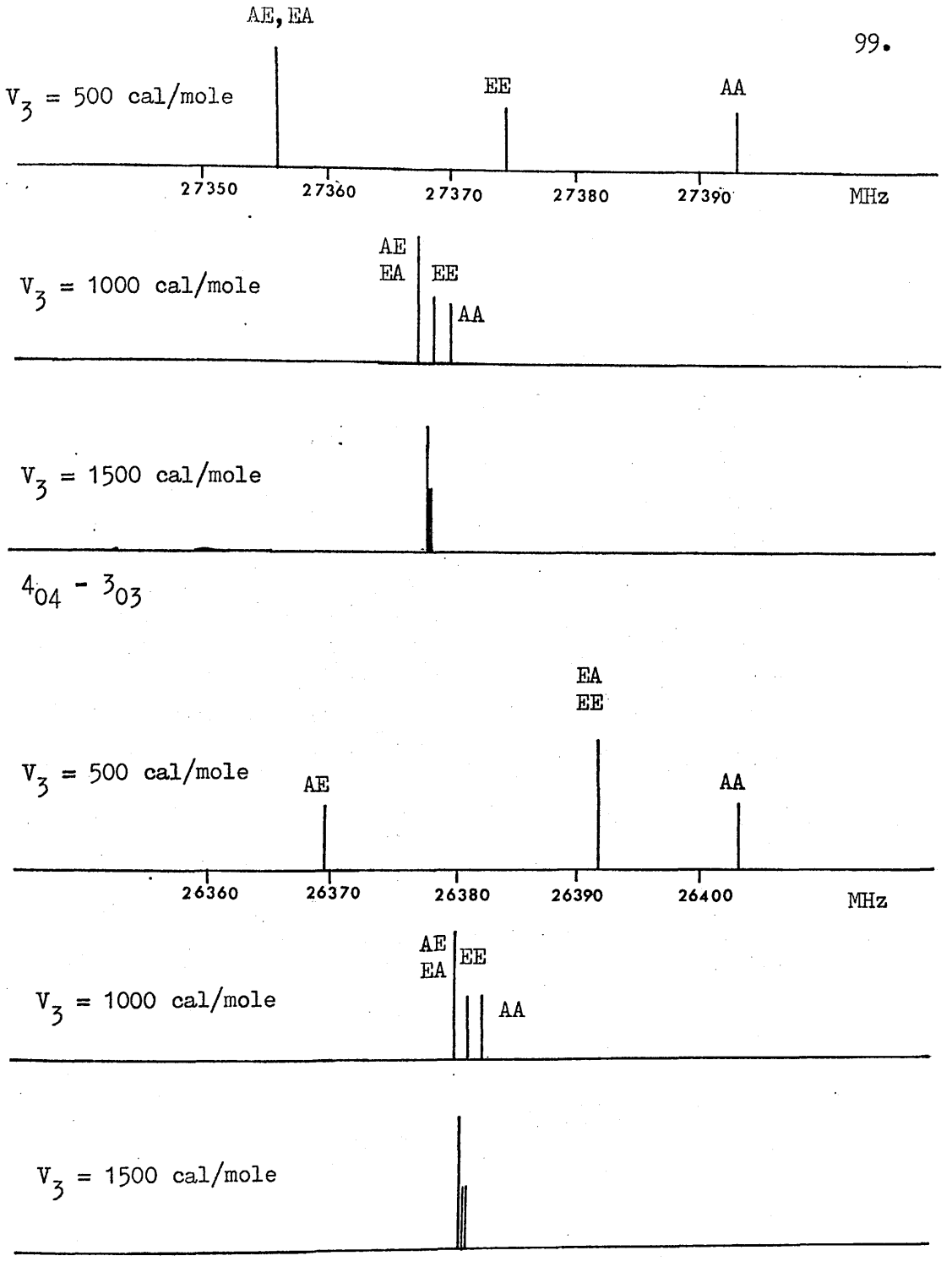

Fig.3. Calculated torsional splittings for various values of V_3 for transitions of dimethylcyanamide.

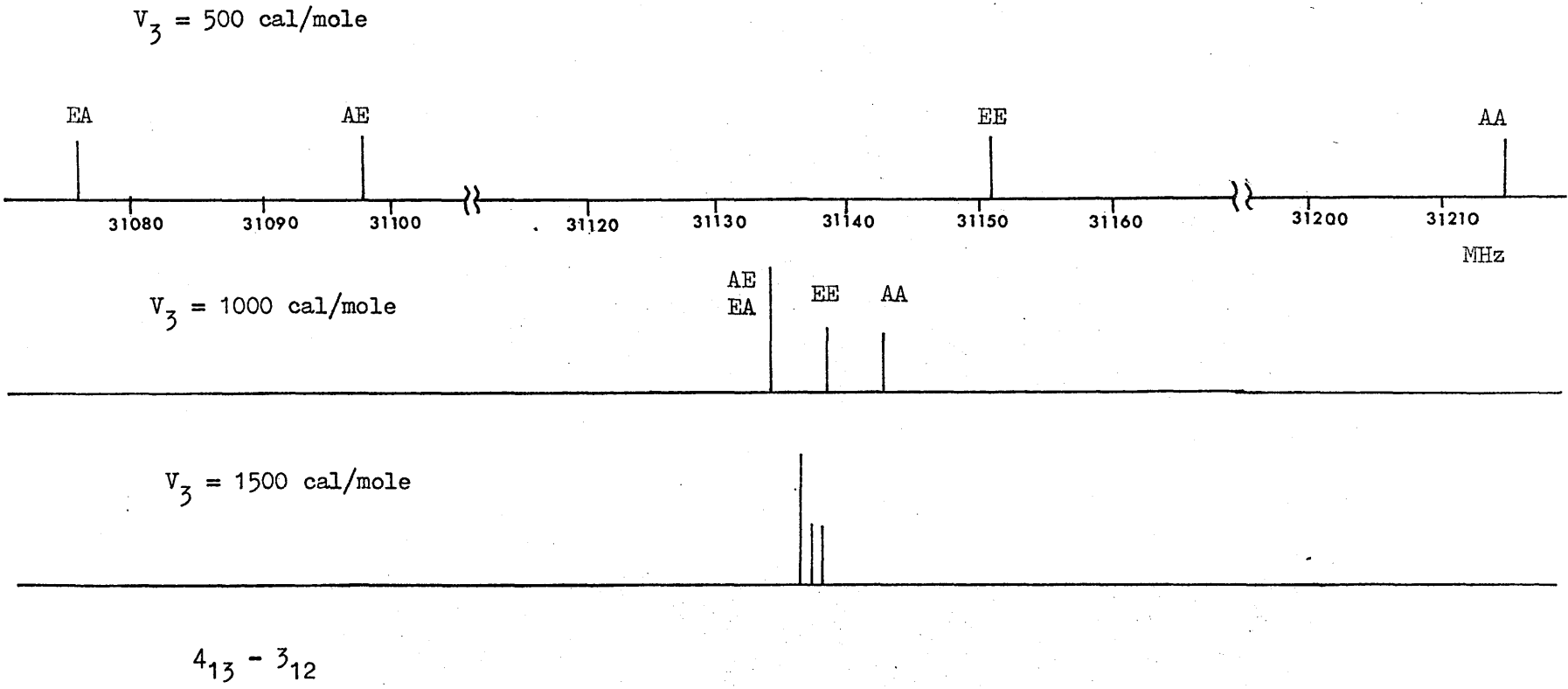

$4_{13} - 3_{12}$

Fig.3. (contd)

Table 4.

Barrier heights to internal rotation in several dimethyl-compounds.

	V_3 (cal/mole)	Ref.
$(CH_3)_2CH_2$	3400	13
$(CH_3)_2SiH_2$	1665	14
$(CH_3)_2NH$	3300	15
$(CH_3)_2PH$	2200	16
$(CH_3)_2O$	2720	17
$(CH_3)_2S$	2118	18

be expected for the ground-state. Since the observed spectrum of the ground-state of dimethylcyanamide showed no quartet or triplet structure, it is concluded that the barrier to internal rotation of dimethylcyanamide is greater than 1500 cal/mole from Fig.3 and probably less than 2500 cal/mole.

As the barrier height to internal rotation could not be obtained from the ground-state (vv = 00) it would have to be obtained from higher torsional states. Rotational transitions for the vv = 11 state of $(CH_3)_2NCN$ would be weak and the torsional sublevels could be widely spread out. $(CD_3)_2NCN$, where internal splittings are reduced from that of $(CH_3)_2NCN$, would perhaps allow for a study of the vv = 11 state. For the symmetrical states (i.e. vv = 00, 11 etc.) for every v there are the four Hamiltonians H_{vv}, one for each of the

torsional sublevels $vv(AA_1)$, $vv(AE)$, $vv(E_0A_1)$ and $vv(E_0E)$, and therefore for the unsymmetrical states (vv = 01, 10, 02 etc.) there would be eight Hamiltonians, one for each of the torsional sublevels. A study of the vv = 01 states may be more applicable for this particular molecule but the work on higher torsional states has not been undertaken here.

5-4. Further Details of the Satellite Transitions Accompanying the Ground-state Transitions of Dimethylcyanamide and Fully Deuterated Dimethylcyanamide.

As mentioned earlier, the accompanying satellite structure appeared more dense and complicated in $(CH_3)_2NCN$ than in $(CD_3)_2NCN$. In the latter there was a closer similarity in the satellite structure of the different transitions.

The vibrational modes with lowest fundamental frequency in dimethylcyanamide will be those associated with the bending vibrations of the CN_1C part of the molecule.

(a) $(CH_3)_2NCN$

In the spectrum of dimethylcyanamide, there were fewer lines to

high than to low frequency of the ground-state transitions, as can be seen from Fig.1. Since the ground-state lines follow rigid-rotor theory, a search was carried out for vibrational satellite lines which exhibited both rigid-rotor behaviour and Stark effects identical to the ground-state transition. Both the first and second excited-state transitions of a vibrational deformation mode, with the above characteristics, were observed to high frequency of each ground-state line (Fig.1). Table 5 records the measured frequencies and rotational constants of this vibrational mode. The J = 1 - 2 group of transitions were studied. A study of the recordings of these transitions did not aid the assignment of the spectra and they were found to be too weak and too broad for accurate oscilloscope measurement.

Double resonance experiments were carried out on a transition of the ground-state spectrum of dimethylcyanamide and on its vibrational satellite to high frequency. Since double resonance effects are observed between two transitions only if they have a common energy level, observation of the effects will help confirm the assignment of both the ground- and first excited-state spectra.

The experiments were carried out on the conventional Stark modulation spectrometer used throughout this work and only the minimum components were added to observe the double quantum transition. Two microwave sources were employed. A klystron produces Q-band power and enabled the $4_{14} - 3_{13}$ transition of dimethylcyanamide to be displayed on the oscilloscope. The pumping radiation was J-band

Table 5.

Measured frequencies and rotational constants (MHz) for the satellite transitions of $(CH_3)_2NCN$ and $(CD_3)_2NCN$.

(a) $(CH_3)_2NCN$.

	v = 1		v = 2	
	observed	νobs- νcalc	observed	νobs- νcalc
$4_{04} - 3_{03}$	27403.82	-0.04	27440.03	-0.12
$4_{14} - 3_{13}$	26409.02	+0.06	26436.62	-0.14
$4_{13} - 3_{12}$	31214.99	+0.05	31292.29	+0.07
$4_{23} - 3_{22}$	29080.97	-0.19	29136.93	-0.07
$4_{22} - 3_{21}$	30924.55	-0.16		
$4_{32} - 3_{31}$	29617.34	-0.01		
$5_{05} - 4_{04}$	33426.66	-0.22	33463.70	+0.06
$5_{15} - 4_{14}$	32742.83	+0.07	32774.60	+0.16
$5_{24} - 4_{23}$	36085.99	+0.37		
$\frac{A+C}{2}$	5987.58		6014.33	
$\frac{A-C}{2}$	2949.59		2975.54	
κ	-0.580813		-0.580147	
A	8937.17		8989.86	
B	4274.41		4288.08	
C	3037.98		3038.79	
Ia	56.5650		56.2334	
Ib	118.2691		117.8922	
Ic	166.4035		166.3593	
Δ	-8.4306		-7.7664	

$\Delta = Ic - Ia - Ib$. Ia, Ib, Ic and Δ are in units of a.m.u.$Å^2$.

(b) $(CD_3)_2NCN$.

D
v = 1

	observed	νobs-νcalc.
$4_{04} - 3_{03}$	23400.19	+0.29
$4_{14} - 3_{13}$	22817.48	+0.22
$4_{13} - 3_{12}$	27273.78	+0.09
$4_{23} - 3_{22}$	25427.44	+0.24
$4_{22} - 3_{21}$	27683.29	+0.10
$5_{05} - 4_{04}$	28518.06	+0.16
$5_{15} - 4_{14}$	28211.36	+0.21
$5_{14} - 4_{13}$	33249.12	-0.13
$5_{24} - 4_{23}$	31419.85	-0.18
$5_{23} - 4_{22}$	34929.15	-0.14
$6_{06} - 5_{05}$	33662.37	-0.22
$6_{16} - 5_{15}$	33524.11	-0.35

$\frac{A+C}{2}$	4639.46
$\frac{A-C}{2}$	2023.54
κ	-0.415006
A	6663.00
B	3799.68
C	2615.93
Ia	75.8714
Ib	133.0455
Ic	193.2513
Δ	-15.6656

(c) $(CD_3)_2NCN$.

	A		B		C	
	observed	νobs- ν calc	observed	ν obs- ν calc	observed	ν obs- ν calc
$4_{04} - 3_{03}$	23369.18	+2.80	23365.25	-0.40	23362.59	+0.48
$4_{14} - 3_{13}$	22774.09	+1.28	22770.59	-0.11	22770.59	+0.40
$4_{13} - 3_{12}$	27206.21	+1.17	27202.87	+0.39	27191.06	-0.46
$4_{23} - 3_{22}$	25364.49	+3.15	25358.67	+0.43	25352.01	-0.44
$4_{22} - 3_{21}$			27574.29	+0.39	27565.76	-0.03
$5_{05} - 4_{04}$	28474.96	-1.61	28474.96	-0.43	28473.14	+0.06
$5_{15} - 4_{14}$	28160.20	+0.23	28157.92	+0.29	28157.92	+0.51
$5_{14} - 4_{13}$	33183.64	-1.55	33183.64	-0.16	33170.24	+0.17
$5_{24} - 4_{23}$	31348.33	+2.46	31343.14	+0.49	31335.36	-0.19
$5_{23} - 4_{22}$	34807.41	-2.58	34803.05	-0.71	34792.11	+0.61
$5_{33} - 4_{32}$			32595.06	+0.31	32586.37	-0.33
$5_{32} - 4_{31}$			33440.97	-0.37		
$6_{06} - 5_{05}$	33607.55	-3.07			33607.55	-0.34
$6_{16} - 5_{15}$			33463.67	+0.02	33463.67	-0.32

(c) $(CD_3)_2NCN$. (contd.)

	A	B	C
$\frac{A+C}{2}$	4648.86	4650.97	4643.77
$\frac{A-C}{2}$	2037.51	2039.89	2032.16
κ	-0.423293	-0.424135	-0.423184
A	6686.37	6690.86	6675.94
B	3786.40	3785.78	3783.80
C	2611.36	2611.08	2611.61
Ia	75.6062	75.5555	75.7244
Ib	133.5123	133.5341	133.6042
Ic	193.5895	193.6096	193.5706
Δ	-15.5289	-15.4800	-15.7580

Ia, Ib, Ic and Δ are in units of a.m.u.$Å^2$.

power from an E.M.I. klystron operating at maximum power level. Radiation from both sources enters the cell via an X-band directional coupler with J-band power entering from the straight arm of the directional coupler to minimise attenuation. Both input arms contain waveguide attenuators to minimise coupling between the two sources. A longer Q-band waveguide than usual was placed before the crystal detector. The essential principle is that the cut-off frequency of the Q-band detector does not pass the strong J-band radiation. This means for the arrangement employed here that there is a band jump between pump and transition frequencies.

The double-resonance experiments on OCS carried out by Cox, Flynn and Wilson (19) were repeated here in order to test the experimental arrangement. For dimethylcyanamide, the $4_{14} - 3_{13}$ transition at 26381.38 MHz was observed and the $3_{13} - 2_{12}$ transition at 19935.79 MHz was pumped. As the J-band klystron was swept through the pump frequency, changes in the line shape of the $4_{14} - 3_{13}$ transition were observed. The double quantum transition was seen to approach, grow stronger and pass across the transition. This experiment was repeated, pumping and observing the high frequency vibrational satellites of the same two transitions. Similar line shape changes, to that described, were observed. The observation of these double quantum transitions acts as further confirmation of the assignments.

(b) $(CD_3)_2NCN$

The $K_{-1} = 2$ transitions of deuterated dimethylcyanamide showed marked similarity in their satellite patterns. Omitting the weaker transitions, this pattern is shown below.

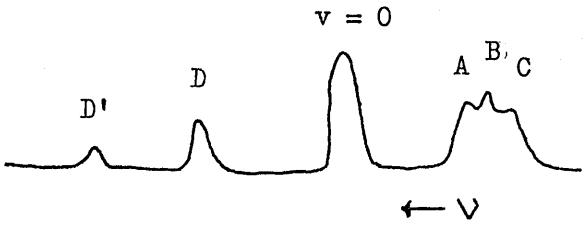

In other transitions, the triplet structure, ABC in the diagram above, was found to be either more spread out or more closely overlapped. Furthermore, for the $K_{-1} = 0$ transitions, the D lines were superimposed on the ground-state transitions. The transitions D and D', shown above, represent the first and second excited-state transitions of a vibrational deformation mode respectively. The D lines were observed to have the same Stark effect as the respective ground-state transitions and were found to display rigid-rotor behaviour. An insufficient number of D' lines were assigned to verify a rigid rotor fit. The lines marked B were observed to be the strongest satellite transitions and, to fit rigid-rotor theory. Satellites with twice the spacings of the B lines from the ground-state were searched for but, although possibilities were found, no definite assignments were made. Of the remaining satellite lines depicted above, rigid-rotor theory was found to apply to the C group of lines, but not to the A group. Table 5 lists the measured frequencies of the satellites and gives rotational

constants obtained from the rigid-rotor least-squares fit. The satellites are listed under the headings A,B,C and D.

Since deuteration occured at that part of the molecule with vibrations of lowest fundamental frequency, it is difficult to correlate the observed skeletal deformation satellites of $(CH_3)_2NCN$ with one of the satellite series of lines A,B,C or D of $(CD_3)_2NCN$. Table 6 shows the collected rotational constants for the excited-state transitions of dimethylcyanamide.

Table 6.

Rotational constants for the ground- and excited-state spectra of $(CH_3)_2NCN$ and $(CD_3)_2NCN$.

	A	B	C		ΔA	ΔB	ΔC	ΔΔ
$(CH_3)_2NCN$								
v = 0	8887.29	4260.52	3037.21	-9.0915				
v = 1	8937.17	4274.41	3037.98	-8.4306	49.88	13.89	0.77	-0.66
v = 2	8989.86	4288.08	3038.79	-7.7664	102.57	27.56	1.58	-1.33
$(CD_3)_2NCN$								
v = 0	6700.82	3788.39	2615.53	-15.6045				
A	6686.37	3786.40	2611.36	-15.5289	-14.45	-1.99	-4.17	-0.08
B	6690.86	3785.78	2611.08	-15.4800	-9.96	-2.61	-4.45	-0.12
C	6675.94	3783.80	2611.61	-15.7580	-24.88	-4.59	-3.92	+0.15
D (v = 1)	6663.00	3799.68	2615.93	-15.6656	-37.82	+11.29	+0.40	+0.06

5-5. Dipole Moment.

Frequency shift measurements on the Stark lobes of several transitions were taken for various voltages of the Stark field. The transitions of dimethylcyanamide studied were $3_{03} - 2_{02}$, $3_{13} - 2_{12}$, $4_{14} - 3_{13}$. The experimental method and calculation of the Stark coefficients were as described in Chapter 2. Stark coefficients were calculated for a molecule with μ_a and μ_c components. The Stark lobes measured were assigned an M value and the expressions for the Stark energies of the transitions are:

	M		
$3_{03} - 2_{02}$	1	$-0.3657\ \mu_a^2 + 0.4865\ \mu_c^2 = -2.054$	
$3_{13} - 2_{12}$	0	$-0.1066\ \mu_a^2 + 0.5056\ \mu_c^2 = -2.027$	
$3_{13} - 2_{12}$	1	$+0.7300\ \mu_a^2 + 0.0550\ \mu_c^2 = +16.28$	...(1)
$4_{14} - 3_{13}$	1	$+0.0347\ \mu_a^2 + 0.1560\ \mu_c^2 = +0.7703$	
$4_{14} - 3_{13}$	2	$+0.3905\ \mu_a^2 + 1.0053\ \mu_c^2 = +8.5184$	

The relative coefficients for the Stark lobes of the $3_{13} - 2_{12}$ and $4_{14} - 3_{13}$ transitions show that certain of the lobes of these two transitions are strongly μ_c dependent. Equations (1) are represented graphically in Fig.4. The fact that there is more than one solution to equations (1) shows that second order perturbation theory is not sufficient to determine the dipole moment from these transitions.

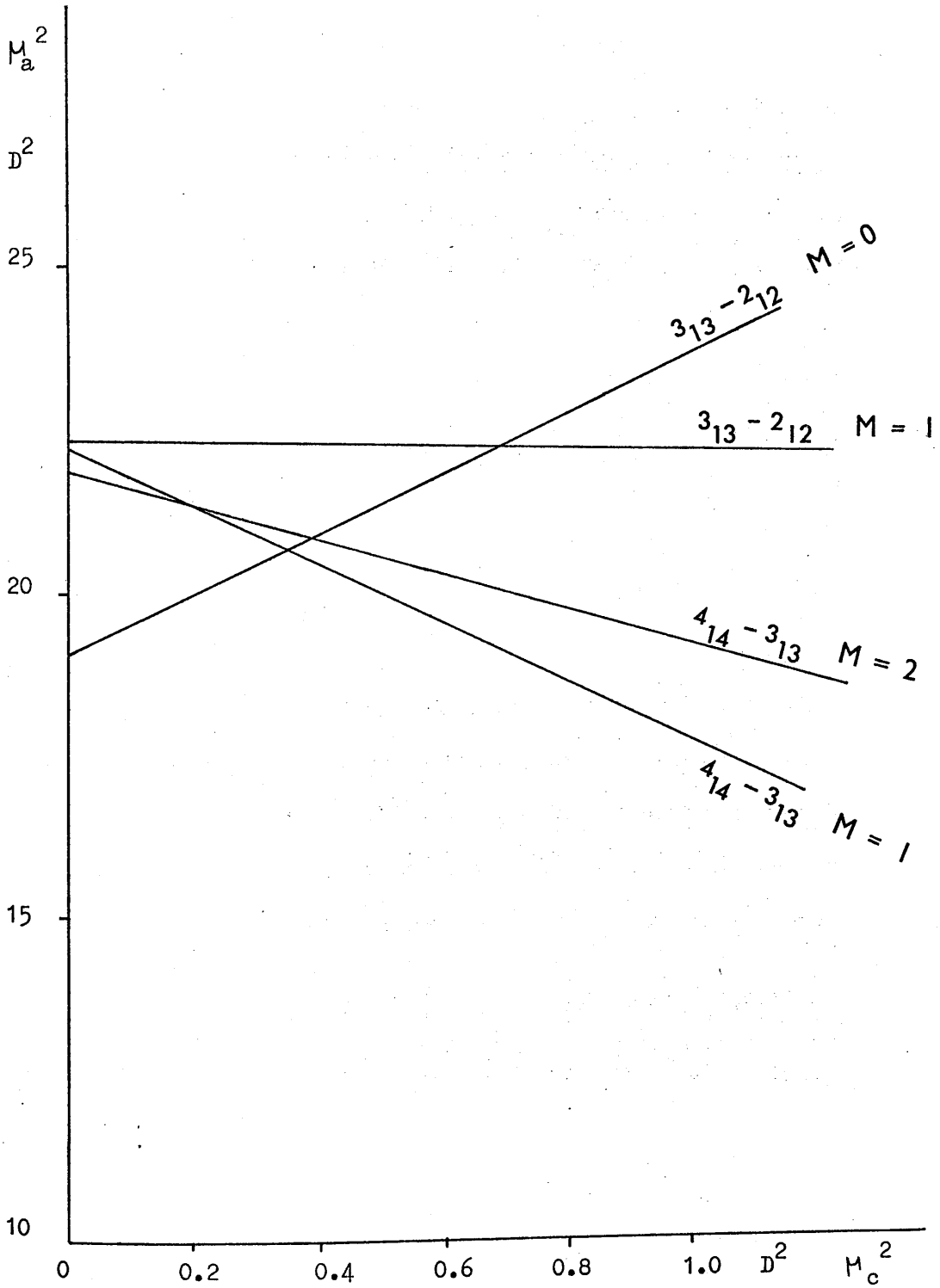

Fig.4. Dipole moment plot of equations (1) for dimethylcyanamide.

The most common reason for the breakdown of second-order perturbation theory is the occurrence of near degeneracy or degeneracy of the energy levels of the transitions studied (20). Fig.5 shows the energy level scheme for dimethylcyanamide and indicates the near degeneracy of the 2_{20}, 2_{21} and 3_{03} levels. The $3_{03} - 2_{02}$ transition is omitted from Fig.4 because of this near-degeneracy. In Fig.4 the $3_{13} - 2_{12}$ M = 0 Stark lobe, which moves to lower frequency on application of a Stark field, appears to deviate the most from the approximate intersection of the other three lines. This Stark lobe is probably affected by the near-degeneracy.

By means of a program written by Macdonald (21) to extend the perturbation treatment of the Stark effect to higher orders, one set of dipole moment components was sought to fit the experimental graphs of frequency shift of the Stark lobe against square of the Stark voltage. Fig.6 shows these graphs, one curve for each of the Stark lobes studied. Each graph shows experimental curve and two calculated curves for each Stark lobe. The best fit to each of the experimental curves was obtained for the following values of the dipole moment components:

$$\mu_a = 4.71 \pm 0.1 \text{ D} \qquad \mu_c = 0 \pm 0.1 \text{ D}$$

When Fig.4 is now consulted three of the Stark equations can be said to agree reasonably well with the above values.

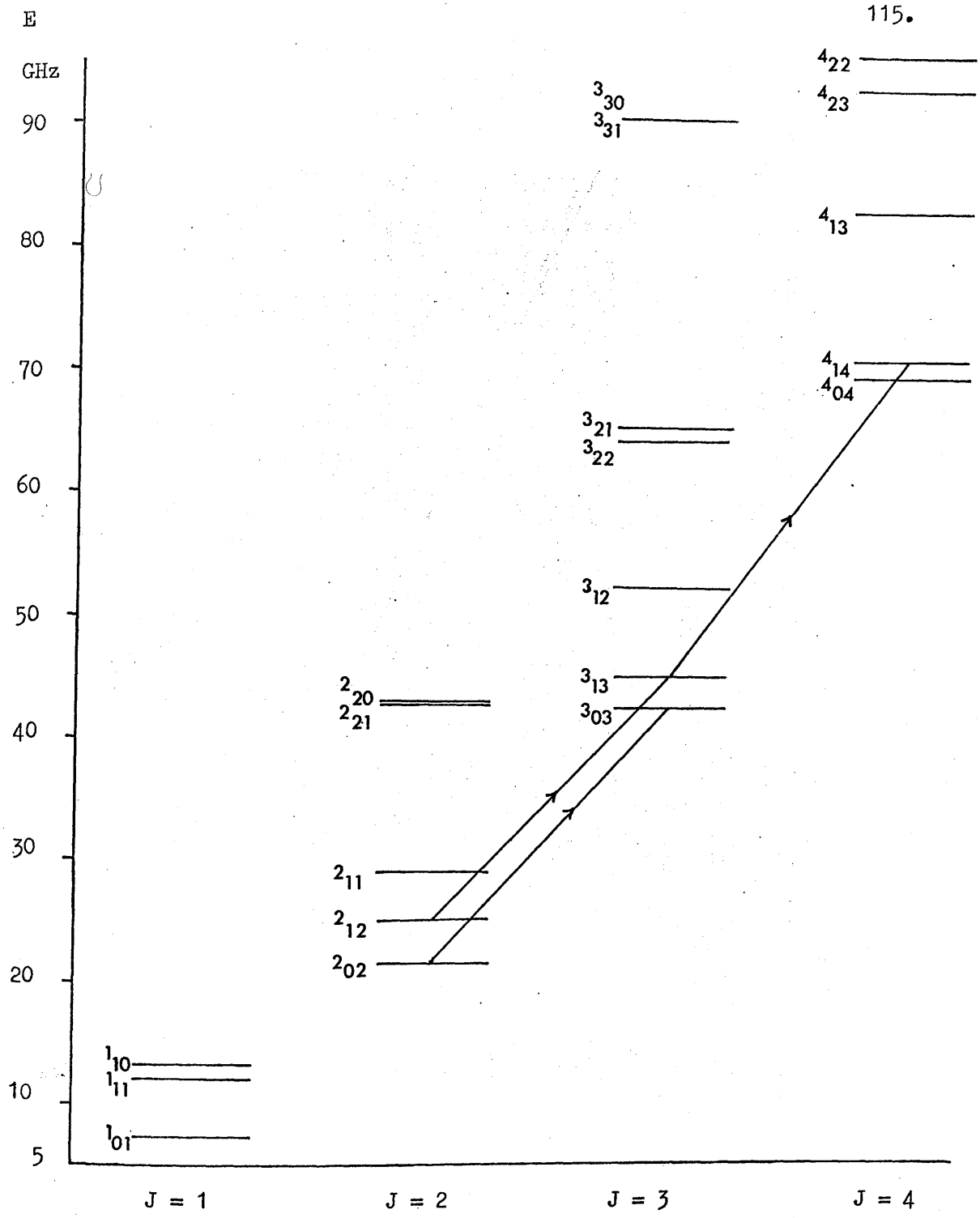

Fig.5. Energy level scheme for $(CH_3)_2NCN$ showing the transitions studied for determination of the dipole moment.

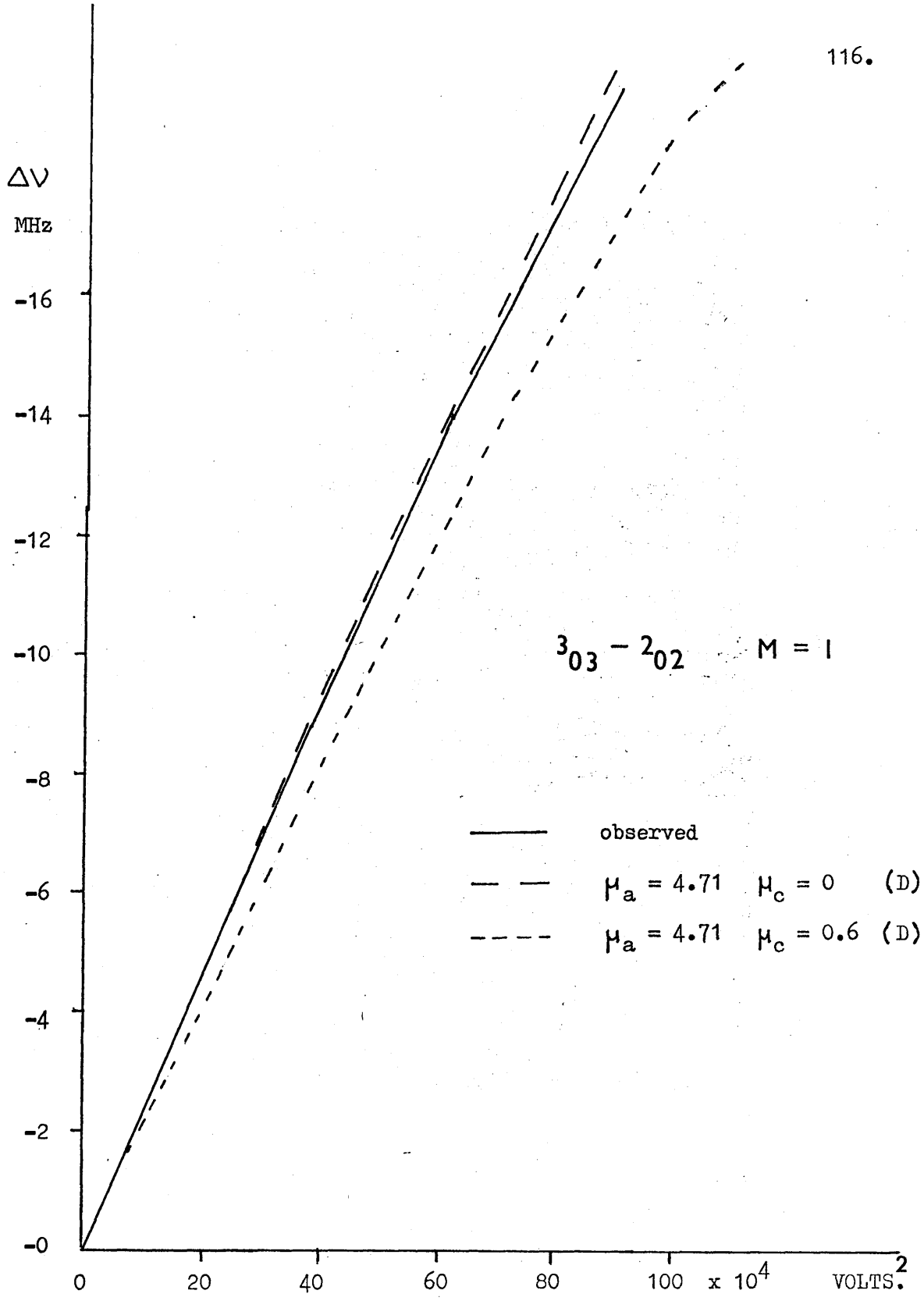

Fig.6. Experimental and calculated Stark effect plots for the $3_{03} - 2_{02}$, $3_{13} - 2_{12}$ and $4_{14} - 3_{13}$ transitions of $(CH_3)_2NCN$.

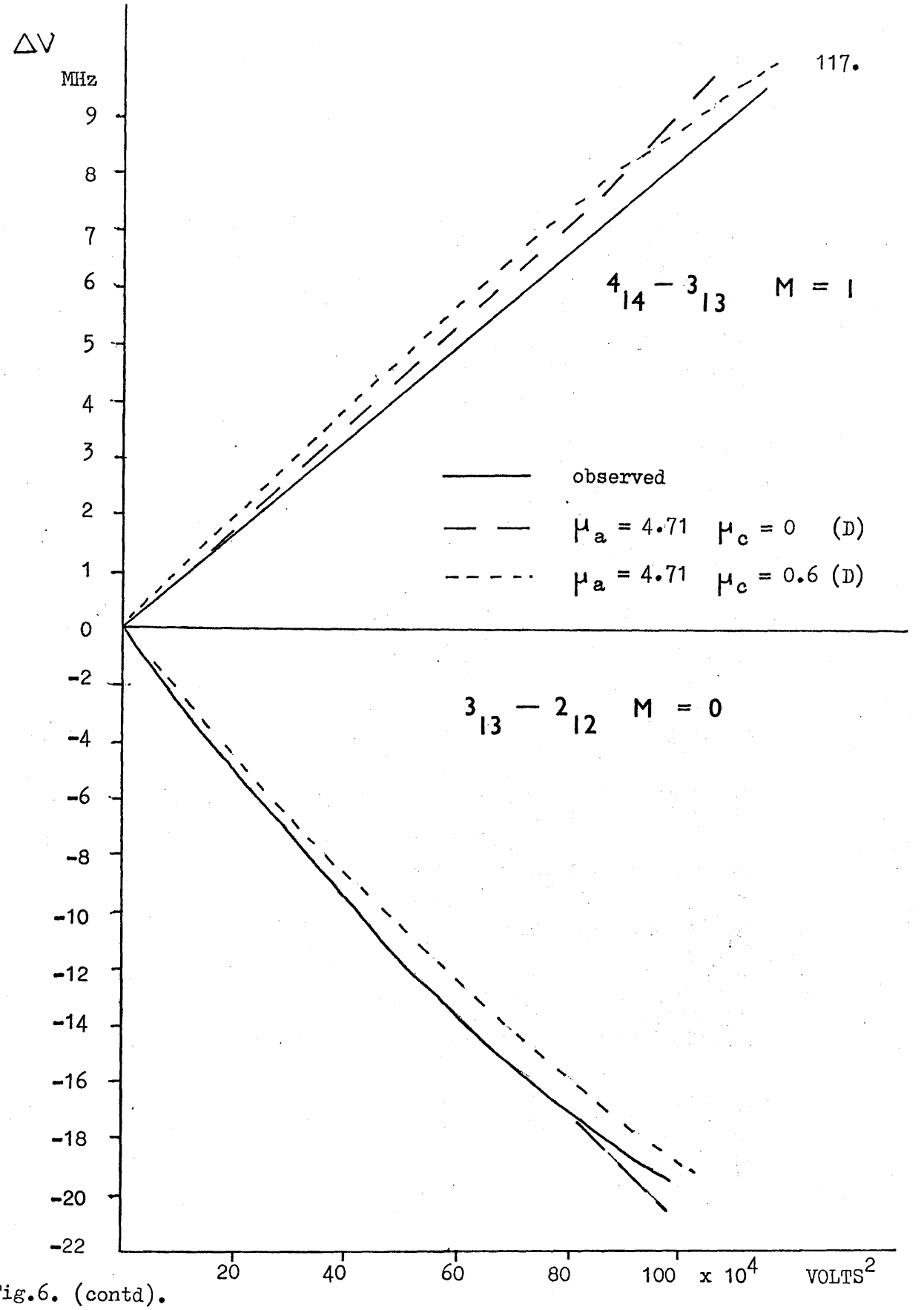
ΔV
MHz
9
8
7
6
5
4
3
2
1
0
-2
-4
-6
-8
-10
-12
-14
-16
-18
-20
-22
20
40
60
80
100
x 10^4
VOLTS^2
4 14 — 3 13 M = 1
observed
μa = 4.71 μc = 0 (D)
μa = 4.71 μc = 0.6 (D)
3 13 — 2 12 M = 0

Fig.6. (contd).

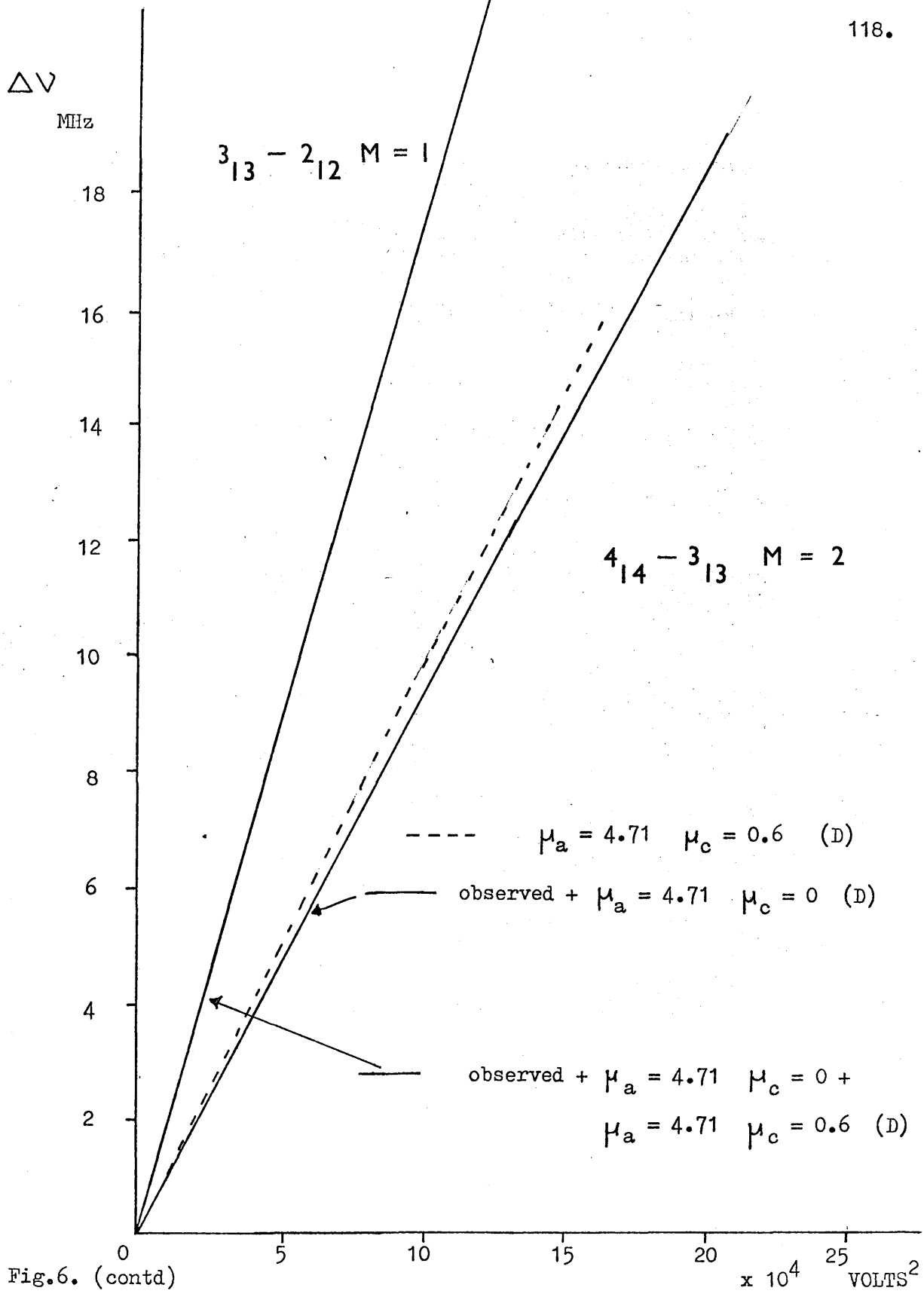
ΔV
MHz
$3_{13} - 2_{12}$ M = 1
$4_{14} - 3_{13}$ M = 2
18
16
14
12
10
8
6
4
2
0
5
10
15
20
25
x 10^4 VOLTS^2
---- $\mu_a = 4.71$ $\mu_c = 0.6$ (D)
observed + $\mu_a = 4.71$ $\mu_c = 0$ (D)
observed + $\mu_a = 4.71$ $\mu_c = 0$ +
$\mu_a = 4.71$ $\mu_c = 0.6$ (D)

Fig.6. (contd)

References.

1. K. V. L. N. Sastry and R. F. Curl, Jr., J. Chem. Phys., 41, 77 (1964).

2. R. F. Curl, Jr., V. M. Rao, K. V. L. Sastry and J. A. Hodgeson, J. Chem. Phys., 39, 3335 (1963).

3. D. R. Lide, Jr. and D. E. Mann, J. Chem. Phys., 27, 868 (1957).

4. B. Bak, J. J. Christiansen, K. Kunstmann, L. Nygaard and J. Rastrup-Anderson, J. Chem. Phys., 45, 883 (1966).

5. M. Davies and W. J. Jones, Trans. of the Farad. Soc., 54, 1454 (1958).

6. J. N. Macdonald, D. Taylor, J. K. Tyler and J. Sheridan, J. Mol. Spec., 26, 285 (1968).

7. "Tables of Interatomic Distances and Configuration in Molecules and Ions", Special Publication No. 11, The Chemical Society (1958).

8. M. L. Sage, J. Chem. Phys., 35, 142 (1961).

9. R. J. Myers and E. B. Wilson, Jr., J. Chem. Phys., 33, 186 (1960).

10. J. D. Swalen and C. C. Costain, J. Chem. Phys., 31, 1562 (1959).

11. L. Pierce, J. Chem. Phys., 34, 498 (1961).

12. R. C. Woods, J. Mol. Spec., 22, 49 (1967).

13. N. W. Luft, Z. Elektrochem., 59, 46 (1955).

14. L. Pierce, J. Chem. Phys., 31, 547L (1959).

15. V. W. Laurie and J. Wollrab, Bull. Am. Phys. Soc., 8, 327 (1963).

16. T. Kojima, E. L. Breig and C. C. Lin, J. Chem. Phys., 35, 2139 (1961).

17. P. H. Kasai and R. J. Myers, J. Chem. Phys., 30, 1096 (1959).

18. L. Pierce, J. Chem. Phys., 34, 498 (1961).

19. A. P. Cox, G. W. Flynn and E. B. Wilson, Jr., J. Chem. Phys., 42, 3094 (1965).

20. S. Golden and E. B. Wilson, Jr., J. Chem. Phys., 16, 669 (1948).

21. J. N. Macdonald, Ph.D. Thesis, University of Glasgow (1969).

CHAPTER 6.

THE MICROWAVE SPECTRUM OF p-CHLOROANILINE.

6-1. Introduction.

This work was carried out primarily to find what influence the introduction of chlorine might have on the NH_2-group in aniline. The fluorine homologue, p-fluoroaniline has been studied previously (1) and, in this case, substituent effects were expected to be maximised for the highly electronegative fluorine.

Of the series of halo-aniline compounds, aniline (2), p-fluoroaniline and now p-chloroaniline have been established as non-planar by microwave spectroscopic analysis. When the lone-pair of electrons are localised on the nitrogen, a nearly tetrahedral configuration of the nitrogen would be expected. In aniline the value of ϕ was determined as being close to 38°, where ϕ is the angle between the HNH plane and the ~~linear~~ NCN$_{\text{bond}}$ extended, and its reduction from the tetrahedral value is accounted for by interaction of the nitrogen lone-pair within the π-system of the benzene ring (2).

In p-fluoroaniline the angle ϕ was determined as 46° and this value was accounted for by involvement of fluorine electrons in the π-system of the molecule reducing the involvement of the nitrogen electrons (1). It was expected that with chlorine in the para position there would be the same effect as that displayed in the fluorine case, though

to a lesser extent. The value of ϕ was determined less accurately in p-chloroaniline than in aniline because of the heavy nature of the molecule. However, its value was nearer that determined for aniline than that determined for fluoroaniline.

6-2. Analysis of Spectra.

A commercially available sample of p-chloroaniline was used and it was not found necessary to purify it further.

Vapour from the sample was streamed through the cell in the normal way but difficulty was experienced in finding spectral lines. It was discovered that this situation could be remedied by initially holding the sample vapour in the cell for a few minutes, under a much higher pressure than used for examining spectra. This was repeated several times using fresh samples before the pressure was reduced to the operating value. The necessity for this procedure is attributed to the adsorption of the sample on the walls of the cell. This process was not repeated in the subsequent study of the sample.

The μ_a R-branch spectrum of the normal species of p-chloroaniline has been analysed and measured by Tyler and Searle (3) and in this work the measurement of the spectrum has been extended. The structural model which aided their initial assignment made use of the known structures of aniline (2) and chlorobenzene (4). In the observed spectrum the transitions appeared as doublets in which the line to higher frequency was assigned to the ground-state and the line to lower frequency to the first excited-state of the inversion motion of the NH_2-group. The observed rotational lines were accurately described by a rigid-rotor analysis and thus the effects of centrifugal distortion are small, as would be expected for a molecule as heavy as chloroaniline. The rotational frequencies were used to compute a refined set of rotational constants and both the frequencies and constants for the ground- and first excited-state spectra are listed in Table 1.

The strongest transitions which were observed were those for $K_{-1} = 2$. This can be explained by the fact that the highest fields which could safely be generated were required to fully modulate these lines and since the $K_{-1} = 0$ and $K_{-1} = 1$ lines require even higher Stark fields they were not fully modulated. This problem of modulation was the main difficulty encountered in the study of the spectrum of p-bromoaniline since, although the $K_{-1} = 2$ transitions could be observed, it resulted in the absence of the $K_{-1} = 0$ and 1 transitions.

Although chlorine has a quadrupolar nucleus no quadrupole structure was observed at the high J value transitions studied. As mentioned,

Table 1.

The transition frequencies and rotational constants of several isotopic modifications of para-chloroaniline.

(a) para-chloroaniline.

	v = 0		v = 1	
	observed	$\nu_{obs} - \nu_{calc}$	observed	$\nu_{obs} - \nu_{calc}$ (MHz)
$12_{111} - 11_{110}$	22263.42	+0.02	22259.92	-0.05
$12_{210} - 11_{29}$	22295.45	+0.25	22291.43	+0.14
$13_{013} - 12_{012}$	22565.33	+0.02	22563.36	+0.06
$13_{113} - 12_{112}$	22316.91	+0.03		
$13_{112} - 12_{111}$	24054.74	+0.02	24051.11	+0.00
$13_{212} - 12_{211}$	23296.81	+0.15	23293.57	-0.10
$13_{211} - 12_{210}$	24210.58	+0.11	24206.12	-0.09
$14_{310} - 13_{39}$	23715.38	+0.09	23711.58	+0.01
$14_{014} - 13_{013}$	24214.83	-0.07	24212.88	+0.07
$14_{114} - 13_{113}$	24003.50	-0.04	24001.56	+0.13
$14_{113} - 13_{112}$	25828.00	-0.02	25824.26	-0.02
$14_{213} - 13_{212}$	25055.60	+0.06	25052.37	+0.00
$14_{212} - 13_{211}$	26121.78	-0.14	26117.20	-0.12
$15_{311} - 14_{310}$	25590.29	-0.03	25586.12	-0.10
$15_{015} - 14_{014}$	25862.55	-0.10	25860.05	-0.43
$15_{115} - 14_{114}$	25686.34	+0.00	25684.38	+0.26
$15_{114} - 14_{113}$	27581.87	+0.07	27578.12	+0.17
$15_{214} - 14_{213}$	26807.56	-0.07	26804.11	-0.18
$15_{213} - 14_{212}$	28026.09	+0.02	28021.27	+0.12
$15_{312} - 14_{311}$	27478.89	-0.16	27474.50	-0.04
$16_{412} - 15_{411}$	27223.72	-0.17	27219.83	-0.05
$16_{016} - 15_{015}$	27510.27	-0.08	27507.98	-0.10
$16_{116} - 15_{115}$	27365.77	+0.05	27363.59	+0.19
$16_{115} - 15_{114}$	29314.96	-0.03	29310.99	-0.07
$16_{215} - 15_{214}$	28552.65	-0.10	28549.38	+0.11
$16_{214} - 15_{213}$	29920.27	+0.20	29915.18	+0.31
$16_{314} - 15_{313}$	29026.65	-0.32		
$17_{313} - 16_{312}$	29381.83	-0.13	29376.91	-0.11
$16_{117} - 15_{116}$	29042.38	+0.27		
$16_{413} - 15_{412}$	29053.76	+0.36		
$16_{412} - 15_{411}$	29080.62	-0.19	29076.31	-0.12

(a) para-chloroaniline. (contd.)

	v = 0	v = 1
$\frac{A-C}{2}$	3215.98	3214.98
$\frac{A+C}{2}$	2384.73	2383.79
κ	-0.939583	-0.939621
A	5600.71	5598.77
B	975.33	975.13
C	831.25	831.20
Ia	90.2620	90.2933
Ib	518.3188	518.4256
Ic	608.1583	608.1971
Δ	-0.4225	-0.5218

Δ = Ic - Ia - Ib.

Ia, Ib, Ic and Δ are in units of a.m.u.Å^2.

(b) ^{37}Cl-para-chloroaniline.

	v = 0		v = 1	
	observed	νobs- νcalc	observed	νobs- νcalc (MHz)
$13_{013} - 12_{012}$	22076.44	-0.04	22074.61	-0.02
$13_{212} - 12_{211}$	22755.37	+0.06	22752.50	-0.00
$13_{311} - 12_{310}$	23014.62	+0.02	23011.64	+0.26
$13_{310} - 12_{39}$	23131.19	-0.03	23127.79	+0.04
$14_{014} - 13_{013}$	23691.51	-0.02	23689.62	+0.00
$14_{114} - 13_{113}$	23471.73	+0.02	23469.90	+0.06
$14_{213} - 13_{212}$	24475.51	-0.04	24472.35	-0.22
$14_{212} - 13_{211}$	25465.06	-0.03	25460.75	+0.03
$14_{312} - 13_{311}$	24789.26	-0.03		
$14_{311} - 13_{310}$	24955.72	-0.01	24951.95	+0.04
$15_{015} - 14_{014}$	25304.22	+0.10	25302.33	+0.19
$15_{115} - 14_{114}$	25118.63	+0.00	25116.67	-0.00
$15_{214} - 14_{213}$	26189.77	+0.18	26186.30	-0.15
$15_{213} - 14_{212}$	27324.60	+0.00	27319.95	+0.05
$16_{313} - 15_{312}$	26562.46	+0.00		
$16_{016} - 15_{015}$	26915.93	-0.17		
$16_{116} - 15_{115}$	26762.24	+0.04	26760.09	-0.06
$16_{215} - 15_{214}$	27897.18	-0.05	27893.82	-0.13
$\frac{A+C}{2}$	3206.79		3205.38	
$\frac{A-C}{2}$	2393.68		2392.31	
K	-0.942625		-0.942657	
A	5600.47		5597.70	
B	950.45		950.25	
C	813.11		813.07	

(b) ^{37}Cl-para-chloroaniline. (contd.)

	v = 0	v = 1
Ia	90.2658	90.3106
Ib	531.8856	531.9953
Ic	621.7222	621.7545
Δ	-0.4292	-0.5514

Δ = Ic - Ia - Ib.

Ia, Ib, Ic and Δ are in units of a.m.u.Å^2.

(c) para-chloroaniline (NHD).

	v = 0		v = 1	
	observed	ν obs- ν calc	observed	ν obs- ν calc (MHz)
$12_{211} - 11_{210}$	20997.32	+0.27	20997.32	-0.17
$12_{210} - 11_{29}$	21704.07	-0.03	21704.07	+0.15
$13_{013} - 12_{012}$	22034.29	+0.10	22035.53	+0.16
$13_{113} - 12_{112}$	21782.61	+0.02	21784.07	+0.13
$13_{112} - 12_{111}$	23454.38	-0.09	23454.38	+0.04
$13_{212} - 12_{211}$	22720.46	+0.27	22720.46	-0.23
$13_{211} - 12_{210}$	23574.52	-0.11	23574.52	+0.24
$13_{311} - 12_{310}$	22982.98	-0.20	22982.98	-0.43
$13_{310} - 12_{39}$	23103.26	+0.11	23103.26	+0.02
$14_{014} - 13_{013}$	23645.71	-0.17	23647.61	+0.39
$14_{114} - 13_{113}$	23429.89	-0.03	23431.58	+0.18
$14_{113} - 13_{112}$	25188.33	-0.06	25188.33	+0.01
$14_{213} - 13_{212}$	24437.40	+0.16	24437.40	-0.41
$14_{212} - 13_{211}$	25437.27	-0.03	25437.27	+0.39
$14_{312} - 13_{311}$	24755.42	+0.11	24755.42	-0.14
$14_{311} - 13_{310}$	24926.45	-0.03	24926.45	-0.08
$15_{015} - 14_{014}$	25255.02	-0.27	25256.90	+0.11
$15_{115} - 14_{114}$	25073.62	+0.03	25075.29	+0.09
$15_{114} - 14_{113}$	26904.41	+0.10	26904.41	+0.08
$15_{214} - 14_{213}$	26148.07	+0.04	26148.07	-0.60
$15_{213} - 14_{212}$	27293.87	-0.12	27293.87	+0.35
$15_{313} - 14_{312}$	26525.85	-0.02	26525.85	-0.28
$15_{312} - 14_{311}$	26762.35	-0.00	26762.35	+0.01
$\frac{A+C}{2}$	3183.20		3181.49	
$\frac{A-C}{2}$	2371.59		2369.80	
K	-0.941876		-0.941885	

(c) para-chloroaniline (NHD). (contd.)

	v = 0	v = 1
A	5554.79	5551.28
B	949.46	949.41
C	811.62	811.69
Ia	91.0081	91.0656
Ib	532.4386	532.4668
Ic	622.8681	622.8108
Δ	-0.5787	-0.7216

Δ = Ic - Ia - Ib.

Ia, Ib, Ic and Δ are in units of a.m.u.$\mathring{A}^2$.

(d) para-chloroaniline (ND_2).

	v = 0		v = 1	
	observed	$\nu_{obs} - \nu_{calc}$	observed	$\nu_{obs} - \nu_{calc}$ (MHz)
$13_{212} - 12_{211}$	22180.72	-0.05		
$14_{114} - 13_{113}$	22892.42	+0.34	22894.56	-0.13
$14_{113} - 13_{112}$	24588.90	+0.21	24590.74	+0.00
$14_{213} - 13_{212}$	23858.56	+0.01	23860.92	+0.08
$14_{212} - 13_{211}$	24799.72	+0.11		
$14_{311} - 13_{310}$	24308.89	-0.10	24311.18	+0.02
$15_{115} - 14_{114}$			24501.97	+0.18
$15_{114} - 14_{113}$	26268.53	+0.03	26270.84	+0.13
$15_{214} - 14_{213}$	25530.36	-0.10	25532.81	-0.12
$16_{016} - 15_{015}$	26257.56	-0.09		
$16_{115} - 15_{114}$	27930.51	-0.03	27932.87	-0.06
$16_{215} - 15_{214}$	27196.02	-0.26	27198.85	-0.08
$\frac{A+C}{2}$	3148.45		3147.71	
$\frac{A-C}{2}$	2355.24		2354.39	
K	-0.94388		-0.94388	
A	5503.69		5502.10	
B	925.39		925.45	
C	793.21		793.31	
Ia	91.8531		91.8797	
Ib	546.2914		546.2568	
Ic	637.3206		637.2393	
Δ	-0.8240		-0.8971	

$\Delta = Ic - Ia - Ib$. Ia, Ib, Ic and Δ are in units of a.m.u.$\AA^2$.

the transitions were observed as doublets and the relative intensity of one member of the doublet to the other was observed to alternate with the odd and even values of K_{-1}.

The satellite members of the doublet were identified as the first excited-state of the inversion motion whereby interconversion occurs between the two equivalent positions which the hydrogen atoms of the nitrogen atom can take on either side of the plane of the benzene ring. There are two stable configurations which the molecule can adopt and these are associated with two equivalent positions, separated by a barrier, at the bottom of a potential well. Inversion can occur by a tunnelling process across the barrier between the two troughs of potential energy. The tunnelling splits what would otherwise be two-fold degenerate levels, one for each of the equivalent N positions, and the magnitude of this split is strongly dependent on, and decreases as with, the height of the barrier hindering inversion. The inversion vibration is, therefore, strongly anharmonic.

Since there is only a small separation in energy between the ground- and first excited-state of the inversion vibration, the relative intensities of the two states are not greatly altered by the Boltzmann factor. The relative intensities of the states in p-chloroaniline are determined by the nuclear spin statistical weight effects. In p-chloroaniline there are three pairs of equivalent hydrogen atoms and, since the hydrogen atom obeys Fermi-Dirac statistics, an interchange of either one or three pairs of nuclei will result in a

change in sign of the total wave function.

$$\Psi_{total} = \Psi_V \times \Psi_{J_{K-1\ K+1}} \times \Psi_N \qquad \ldots(1)$$

where Ψ_{total} is the product of vibrational, rotational and nuclear spin functions. For n pairs of equivalent nuclei the ratio of the number of symmetric spin functions to antisymmetric spin functions is given by

$$n_s : n_a = \left[\prod_{i=1}^{n}(2I_i + 1) + 1\right] : \left[\prod_{i=1}^{n}(2I_i + 1) - 1\right] \qquad \ldots(2)$$

From (2) it was found that for p-chloroaniline

$$n_s : n_a = 9 : 7$$

and, from (1) and (2), for rotational lines with

$$K_{-1} \text{ even} \quad (v = 0) : (v = 1) = 7 : 9$$

and for

$$K_{-1} \text{ odd} \quad (v = 0) : (v = 1) = 9 : 7$$

By means of their relative intensities, the members of the doublet transitions of p-chloroaniline were assigned to the ground- or the first excited-state.

The isotopic samples prepared and studied were ^{37}Cl-, NHD- and ND_2- p-chloroaniline. ^{37}Cl- was studied in natural abundance (~25%). The observed transition frequencies and rigid-rotor constants for the ground- and first excited-state of the isotopic species studies are given in Table 1.

The search for ^{37}Cl transitions was undertaken for J = 13 - 14,

as these were the strongest group of transitions available as a result of modulation difficulties for high J. A rough prediction of the ^{37}Cl transition frequencies was sought. The symmetric top centres of ^{37}Cl and ^{35}Cl, with the correct relative intensities, were easily observed and the difference between the two was found to be 580 MHz. For an asymmetric top the symmetric top centre is given approximately by $(J + 1)(B + C)$ and hence the difference by $(J + 1)(\Delta B + \Delta C)$. Since $\Delta B = \Delta C$, the observed difference between the symmetric top centres was used to obtain values of B and C for the ^{37}Cl spectrum. Difficulty was experienced in assigning lines to ^{37}Cl using the predicted transition frequencies obtained from the calculated constants. The $14_{114} - 13_{113}$ transition was observed to be 100 MHz above the predicted frequency. A more accurate set of predicted transition frequencies were later obtained from the following expression.

$$^{37}Cl\ \nu_1 + {}^{35}Cl\ \nu_2 - {}^{35}Cl\ \nu_3 = {}^{37}Cl\ \nu_4$$

where ν_1 is the frequency of the transition predicted by the model (3)

ν_2 is the frequency of the observed symmetric top centre

ν_3 is the frequency of the symmetric top centre calculated from the model

and ν_4 is the calculated frequency of the transition.

This proved to give calculated transition frequencies for ^{37}Cl only several MHz from the observed lines. In the spectrum of ^{37}Cl- p-chloroaniline the members of the doublet lying to high frequency were

assigned to the ground-state.

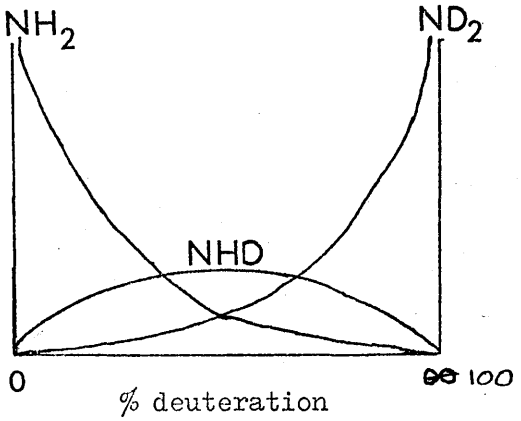

Fig.1. The relative concentrations of deutero-species of p-chloroaniline with the % deuteration of p-chloroaniline.

On a first study of the spectrum of NHD- p-chloroaniline, the preparation involving 50/50 H_2O/D_2O appeared to have failed since the symmetric top centre of J = 13 - 14 of the NHD species was not observed. The preparation was repeated with 100% D_2O and the ND_2 symmetric top centre was observed in the region predicted. On searching for the NHD centre (since it must now be present as shown in Fig.1) it was observed to be coincident with the ^{37}Cl centre. The intensities of the coincident centres were compared with that of the normal species centre and showed the expected relative intensity of $1\frac{1}{2}$: 1.

R-branch transition frequencies were calculated for the NHD species of p-chloroaniline using the observed moments of inertia of the normal species as described in Chapter 2. The ND_2 sample spectrum was calculated twice, firstly by using the observed moments of inertia of the normal species and secondly by using those of the NHD species.

The doublet splitting was found to be reduced in the NHD species from that obtained for the normal species. Only $K_{-1} = 0$ and the lower $K_{-1} = 1$ lines showed any splitting, the intensities of the doublet lines being approximately equal. In the ND_2 species doublets were again observed with the member to low frequency assigned to the ground-state. In the case of the ND_2 species the relative intensities are for transitions with the characteristics of

K_{-1} even $(v = 0) : (v = 1) = 13 : 11$

and K_{-1} odd $(v = 0) : (v = 1) = 11 : 13.$

6-3. Calculation of the Geometry of the NH_2-group in p-Chloroaniline.

The observed moments of inertia and inertial defects for all isotopic samples of p-chloroaniline are given in Table 2. As in

Table 2.

Ground-state moments of inertia of p-chloroaniline (a.m.u.$Å^2$).

	I_a	I_b	I_c	Δ
p-chloroaniline	90.2620	518.3188	608.1583	-0.4225
^{37}Cl - "	90.2658	531.8856	621.7222	-0.4292
NHD- "	91.0081	532.4386	622.8681	-0.5787
ND_2- "	91.8531	546.2914	637.3206	-0.8240

$\Delta = I_c - I_a - I_b$.

the previously studied molecules, aniline and p-fluoroaniline, the large negative value of Δ for p-chloroaniline and its behaviour on deuteration confirms the non-planarity of the molecule.

The following Kraitchman's equations (5) were used for the location of the atoms isotopically substituted in p-chloroaniline. The hydrogen coordinates can be located independently from the moments of inertia of NHD- and ND_2- p-chloroaniline in conjunction with the moments of inertia of p-chloroaniline itself.

$$a^2 = \frac{1}{2\mu}(\Delta I_c + \Delta I_b - \Delta I_a)\left[1 + \frac{\Delta I_a + \Delta I_b - \Delta I_c}{2(I_a - I_c)}\right]\left[1 + \frac{\Delta I_a + \Delta I_c - \Delta I_b}{2(I_a - I_b)}\right] \quad \ldots(3)$$

where a, b, c are the coordinates of the substituted atom relative to the principal axes of the molecule and the b, c coordinates are

obtained by cyclic permutation of the subscripts. The coordinates obtained are given in Table 3.

Table 3.

The substitution coordinates of p-chloroaniline relative to the principal axes (Å).

	a	b	c
Cl	-2.6261 ± 0.003	0	0
H (from NHD-data)	3.7465 ± 0.005	±0.8308 ± 0.008	0.2844
H (from ND_2-data)	3.7427 ± 0.005	±0.8311 ± 0.008	0.3267

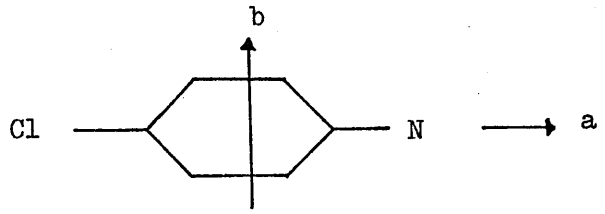

The a and b coordinates obtained from the mono- and di-deutero species show the expected variations from zero-point vibrational effects. However, from Table 3 it can be seen that the c_H coordinate must contain a large error to account for the two determined values and that, consequently, the value of the angle between the plane of the benzene ring and the HNH plane, denoted ϕ, will be poorly defined.

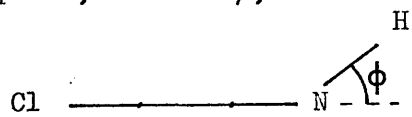

Furthermore, the error in the value of c_H is larger than would be expected for this near-axis coordinate (5). The difference between the two values of c_H can be accounted for by the fact that the error in

c_H results from the $(\Delta I_a + \Delta I_b - \Delta I_c)$ term in equations (3). The other two terms in equation (3) are approximately unity. This term was found to have a value of 0.1561 for the NHD data and 0.4014 for the ND_2 data and will contain a large percentage error resulting from the addition and subtraction operations. The c_H value has been more accurately determined in aniline (2) and, for comparison, the moments of inertia and the coordinates of the amino-hydrogen atoms of aniline are given in Table 4. Thus, it can be seen that the variation in the values of the term $(\Delta I_a + \Delta I_b - \Delta I_c)$ is directly related to the variation in the values of c_H. In the heavier molecule, p-chloroaniline, the individual moments of inertia will have a larger error than in aniline and this introduces a larger error in the term and hence in the value of c_H.

Table 4.

Moments of inertia (a.m.u.$\mathring{A}^2$) and amino-hydrogen atom coordinates ($\mathring{A}$) for aniline (2).

	I_a	I_b	I_c	$(\Delta I_a + \Delta I_b - \Delta I_c) \approx 2\mu c^2$
aniline	89.9938	194.8968	284.4792	
NHD- "	90.7277	202.7314	292.8747	0.1730
ND_2- "	91.5871	210.3096	301.0849	0.4004

	a	b	c
NHD- "	2.7801	0.8352	0.3016
ND_2- "	2.7770	0.8320	0.3305

The inertial defect of the $Cl.C_6H_4N.$ fragment was calculated using the coordinates given in Table 3 and was found to be -0.0913 a.m.u.$\AA^2$. Similar values were found of -0.0034 a.m.u.$\AA^2$ in aniline and $+0.1589$ a.m.u.$\AA^2$ in p-fluoroaniline. All three values are good evidence for the planarity of the benzene ring fragments.

The $\angle HNH$ in p-chloroaniline is given by $HNH = \sin^{-1} 2z_H$ for an assumed value of r(N - H) of 1.00$\AA$. The following outlines the calculation of ϕ and the diagram helps to define the notation.

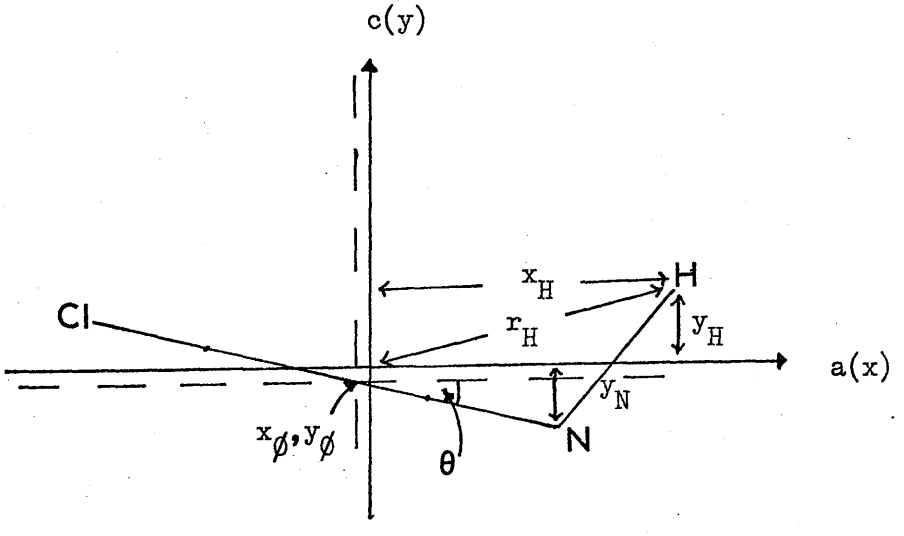

The angle θ, shown in the diagram, is given by

$$\theta = \sin^{-1} \frac{2m_H \, x_H \, y_H \left(1 + \frac{2m_H}{M\phi}\right)}{I_b - \mu r_H^2} \qquad \ldots(4)$$

where m_H = mass of the hydrogen atom,

x_H, y_H = coordinates of the hydrogen atoms relative to the

principal axes of the molecule,

r_H = distance of the hydrogen atoms from the centre of mass of the molecule,

$M\phi$ = mass of $Cl.C_6H_4N$.,

I_b = principal moment of inertia about the b-axis of the molecule,

and $\mu = \dfrac{(\text{M.W. of p-chloroaniline})\ (-2m_H)}{(\text{M.W. of p-chloroaniline}) + (-2m_H)}$.

Also, y_N as shown in diagram is given by

$$y_N = y_\phi + r_N \sin\theta \qquad \ldots(5)$$

where y_ϕ = y coordinate of the centre of mass of $Cl.C_6H_4N$.

and r_N = distance of N from centre of mass (x_ϕ, y_ϕ) of $Cl.C_6H_4N$.

It follows that,

$$y = y_N + y_H \qquad \ldots(6)$$

and $$\theta' = \sin^{-1}\frac{y}{l} \qquad \ldots(7)$$

where $$l = \cos^{-1}\frac{\angle HNH}{2}$$

$$\underline{\phi = \theta + \theta'} \qquad \ldots(8)$$

In order to calculate r_N in equation (5), a structural model is necessary for $Cl.C_6H_4N$. The model, (which is that used throughout this work) used the C - Cl bond length value determined for chlorobenzene (4) and assumed a regular hexagon for the benzene ring. All the

remaining bond lengths were taken from those determined for aniline (2). The model is therefore, in Å

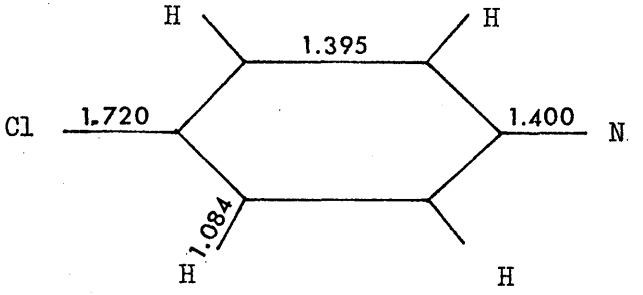

The calculated values of HNH angle and ∅ are compared with those of aniline and p-fluoroaniline in Table 5.

Table 5.

The geometry of the NH_2-group in p-chloroaniline, aniline and p-fluoroaniline.

	HNH	∅
p-chloroaniline (from NHD data)	112° 22' ± 30'	33° 22'
" (from ND_2 data)	112° 24' ± 30'	39° 12'
aniline	113° 16'	37° 39'
p-fluoroaniline	111° 52'	46° 22'

(the method of calculation is the same for all three molecules)

Variation of the N - H bond distances by ±0.01 Å results in changes in the region of ±2° in NHN angle and ∅.

As shown from the values of ϕ in Table 5 no conclusions can be drawn from the poorly defined angle ϕ when comparing p-chloroaniline and aniline. However, the value of ϕ in chloroaniline more closely approximates that determined for aniline than that determined for fluoroaniline. The HNH angle can be directly compared between the three molecules as the method of calculation is the same and the intermediate value determined for chloroaniline suggests that the chlorine electrons are involved in the π-system of the ring, but to a lesser extent than the fluorine electrons.

References.

1. A. Hastie, D. G. Lister, R. L. MacNeil and J. K. Tyler, Chem. Comm., 108 (1970).

2. D. G. Lister, Ph.D. Thesis, University of Glasgow, (1968).

3. V. J. Searle, B.Sc. Thesis, University of Glasgow, (1970).

4. R. L. Poynter, J. Chem. Phys. 39, 1962 (1963).

5. J. Kraitchman, Am. J. Phys., 21, 17 (1953).

CHAPTER 7.

CHEMICAL PREPARATIONS

In this chapter details are given of the methods of preparation of the compounds whose microwave spectra have been studied in this thesis.

7-1. (a) Pyran-4-thione.

Pyran-4-thione can be prepared very simply from pyran-4-one (1). For the preparation of pyran-4-one (2) a 1 : 2 weight/weight mixture of dry chelidonic acid and dry precipated black copper powder was dry distilled in a retort from a Wood's metal bath. The temperature of the metal bath was raised to 340°C over a period of $1\frac{1}{4}$ hours. Care had to be taken to ensure that the temperature of the pyran-4-~~thi~~one was sufficiently reduced for collection as a liquid (m.p. 31°C), otherwise the yield is reduced by a loss of gaseous sample through the outlet of the apparatus. The crude distillate was then refluxed in benzene for 46 hours in a Dean and Stark apparatus to remove traces of water. After removal of the benzene under vacuum the residue was distilled at 108°C/12m.m. of mercury to give a clear liquid which, on cooling, crystallises to a white crystalline solid (yield 33%). Pyran-4-one is highly deliquescent and must be stored under vacuum in a desiccator.

A solution of pyran-4-one in dry toluene was refluxed with excess P_2S_5 for thirty minutes. After filtering hot, the residue was extracted with hot toluene. The extractions were dried over anhydrous magnesium sulphate and the toluene removed under reduced pressure. The resultant red oil crystallised when cold to give orange crystals (m.p. 48 - 50°C yield 70%).

(b) 3,5 d_2- pyran-4-thione.

3,5 d_2- pyran-4-one was prepared as described in (3,4,5) by a direct exchange of the 3,5 hydrogen atoms with deuterium oxide.

0.4 g. of pyran-4-one were added to 2.4 g. of 98% enriched D_2O and the solution made slightly acidic (pH $\sim$ 6 - 7) with dilute hydrochloric acid. The solution was refluxed for 36 hours at 95°C. The pyran-4-one is extracted into ether, the solution dried over anhydrous magnesium sulphate and the ether removed (yield 50%). Only the di-deutero species was observed in the microwave spectrum. The 3,5 d_2- pyran-4-one was treated with P_2S_5 as described in (a).

(c) 2,6 d_2- pyran-4-thione.

The preparative method of Lord and Phillips (3) used here makes use of the difference in ease of exchange of the 3,5 and 2,6 hydrogen atoms in pyran-4-one.

Chelidonic acid was recrystallised several times from water and finally from D_2O. The sample was dried at 110° for 24 hours in an atmosphere of nitrogen. 10 g. of this material were dissolved in 150 g. of 98% D_2O in a closed system under a positive pressure of nitrogen. The resulting solution was warmed for 72 hours at 85°C. The D_2O was then removed by vacuum distillation and the residue obtained dried at 100°C in a stream of nitrogen to give d_4- chelidonic acid (yield 95%).

The fully deuterated chelidonic acid was then pyrolised to give d_4- pyran-4-one by the method in (a).

0.037 moles of d_4- pyran-4-one were then heated with one equivalent of water for 24 hours at 95°C. This replaced the deuterium atoms α to the carbonyl group by hydrogen atoms (yield 50%). The 3,5 d_2- pyran-4-one was then converted to 3,5 d_2- pyran-4-thione.

(d) ^{18}O- pyran-4-thione.

The preparation of ^{18}O- pyran-4-one is described in (3).

0.234 g. pyran-4-one is dissolved in 1 g. of 62% enriched $H_2{}^{18}O$ and dilute hydrochloric acid added until pH ~ 3. The solution was refluxed for 26 hours at 98°C. The work-up is as described for the deuterated species. The product is treated with P_2S_5 to give ^{18}O- pyran-4-thione.

7-2. NF_2CN.

The experimental method was based on that given in (6). NF_2CN is prepared by elemental fluorination of phosphate buffered aqueous NH_2CN. The fluorine was obtained from a fluorine cell and the cyanamide from Cyanamid Co. Ltd.

The apparatus employed for the experiment is shown in Fig.1. Joints and stopcocks were lubricated with Kel. F. No. 90 grease. The two traps were incorporated in case of suck-back and an exit bubbler containing Kel. F. oil was connected to the last trap.

A slurry of 6.5 g. of $Na_2HPO_4 \cdot 7H_2O$, 10 g. of $Na.H_2PO_4 \cdot H_2O$ and 10 ml of deionized water was mixed with 35 ml of a 50% aqueous cyanamide solution. The mixture was poured into a 250 ml round-bottomed flask surrounded by an ice-bath. A gas stream consisting of a mixture of nitrogen (550 c.c./min.) and fluorine (30 c.c./min.) was passed through the system. The solution became yellowish and then dark orange as the run progressed. After one hour the gas stream was stopped. The material in the -196° trap was isolated from any liquid fluorine by means of a vaccuum line and then allowed to expand into a glass bulb.

Optimum yields were obtained with solution temperatures of $5^{\circ} - 9^{\circ}$. High gas flow rates and no mechanical stirring are recommended. Deviation from these conditions resulted in lower F_2NCN production and extensive HNF_2 and CO_2 formation.

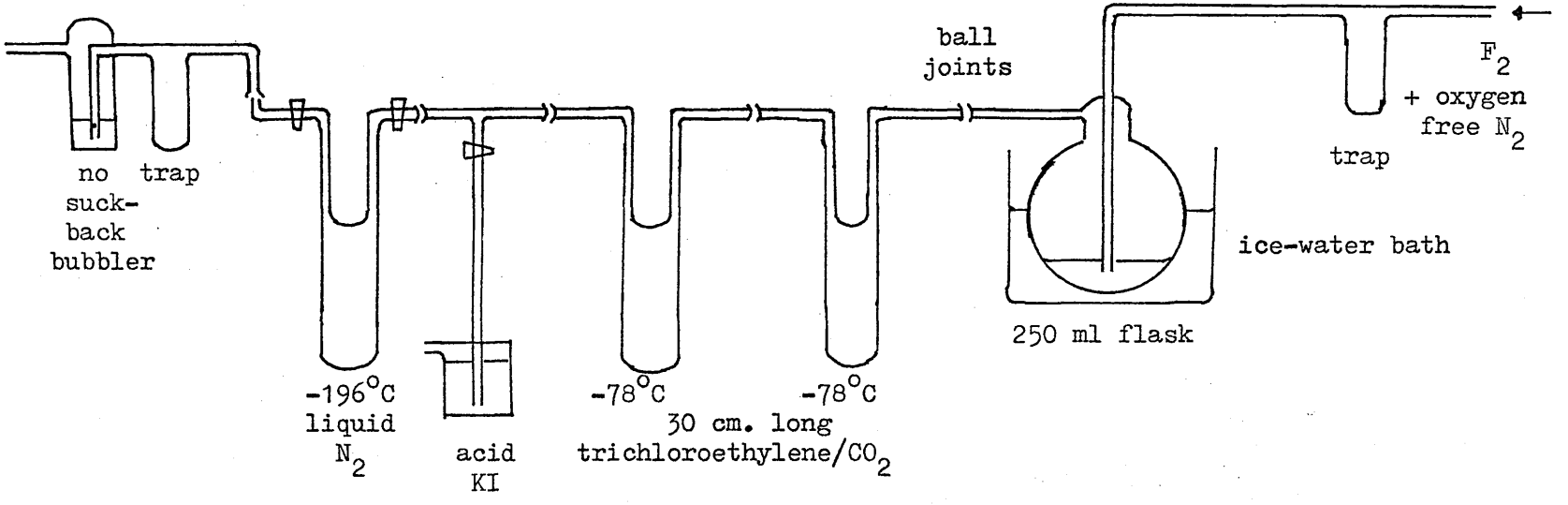

Fig.1. The experimental apparatus for the preparation of NF_2CN.

Impurities derived from the experiment include CO_2, H_2O, HCN, N_2F_4, HNF_2 HNCO and N_2O. Of these HNF_2 (b.p. -27°, m.p. -116°) is highly explosive as a solid. Therefore, when manipulating NF_2H the main points are the exclusion of all air, oxygen or oxidising material and the avoidance of any chance of solidification. The necessity for care in handling NF_2H accounts for the following precautions being carried out. The nitrogen was ensured oxygen free by passing the gas through alkaline pyragellol and the apparatus was purged with nitrogen for several hours before the fluorine gas was admitted to the reaction vessal. Although U-tubes were used to trap the NF_2H, below is shown a more efficient method and ensures that the NF_2H remains a liquid. The NF_2H was rendered harmless by reaction

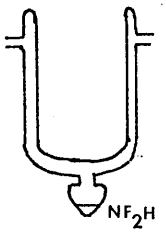

with acidified KI. If possible a safety shield should be used but here it was found an incumbrance. The safety apparel which is essential for the experiment includes face shield, ear-muffs, chrome-leather coat, apron and gloves. The ear-muffs are required to protect the ear-drums from the shock-waves generated by an unexpected detonation, and chrome-leather clothing is necessary for protection against flying glass or metal.

NF_2CN (b.p. -61°, m.p. -196°) was stored with no apparent deterioration for several months at room temperature in a glass bulb.

7-3. (a) $(CH_3)_2NCN$

The experimental method was as described in (7).

9 g. of finely powdered sodium cyanamide were added to 100 c.c. of absolute alcohol and the mixture was stirred to ensure that the sodium cyanamide remained finely divided in the alcohol. 28.4 g. of methyl iodide were added and the mixture refluxed. The alcohol is removed by distillation and the residue extracted with boiling absolute ether. The ether and the remaining alcohol were distilled off and the 163° fraction contained mainly dimethylcyanamide (yield 60%).

(b) $(CD_3)_2NCN$.

The following describes the HI method of preparation (8). 10 g. (13 ml) of deuterated methanol were mixed with 250 g. (145 ml) of constant boiling point hydroiodic acid (57%) in a 250 ml flask fitted with a condenser for distillation. The rate of distillation was kept at 1 - 2 drops per second and when about half the liquid had distilled over, the distillation was stopped. The lower layer of crude iodide was separated, washed with an equal volume of concentrated hydrochloric acid, then successively, with water, 5% sodium carbonate solution and water. The iodide sample was then dried with anhydrous calcium chloride and redistilled.

The deuterated methyl iodide was then converted to deuterated

dimethylcyanamide by the method described in (a).

References.

1. A. Hantzsch, Ber., 52, 1535 (1919).

2. J. N. Macdonald, Ph.D. Thesis, University of Glasgow (1969).

3. P. Beak and G. A. Carls, J. Org. Chem., 29, 2678 (1964).

4. R. C. Lord and W. D. Phillips, J. Am. Chem. Soc., 74, 2429 (1952).

5. D. W. Mayo, P. J. Sapienza, R. C. Lord and W. D. Phillips, J. Org. Chem., 29, 2682 (1964).

6. M. D. Meyers and S. Frank, J. Inorg. Chem., 5, No. 8, 1455 (1966).

7. W. Traube and A. Engelhardt, Ber., 44, 3149 (1911).

8. Vogel, "Practical Organic Chemistry", Longmans Third Edition P. 285.